Parametrized Salt Intrusion in Navigation Locks, an Improved Analytical Description

A master thesis by Jelle Blom

For the degree of Master of Science in Civil Engineering at Delft University of Technology

Supervisors: Dr.ir. J.D. Pietrzak

Dr.ir. W.S.J. Uijttewaal

Dr.ir. R.J. Labeur

ir. O.M. Weiler

ir. A.J. van der Hout

ir. M.F.E. Wauben

Conducted at Witteveen+Bos Raadgevende ingenieurs B.V. under supervision of Marcel Wauben.

Preface

This document is a thesis for the degree of Master of Science in civil engineering at Delft University of Technology. The subject of this study is ensued from a proposal by Otto Weiler, who has made major contributions to the development of the ZSF on behalf of the Dutch knowledge institute: Deltares. Especially in view of the current climate changes, the future will bring many surprises that must be solved together. I would therefore call it a privilege to be able to contribute, albeit a small one, to the preparations for climate change. The research was supervised by Marcel Wauben from Witteveen+Bos, to whom I would like to express my gratitude. Furthermore, I would especially like to thank Arne van der Hout, who has been able to help me time and again. Finally, I would like to thank Martin Magnus from Rijkswaterstaat, who went with me to the Krammer locks for a very interesting outing.

Jelle

List of Symbols

A_c	Channel cross-section	[m^2]
$A_{primary,s}$	Area of the saline part of the return current distribution	[m^2]
A_s	Ship cross-section	[m^2]
A_{saline}	Top view area of undisturbed saline water volume in a lock	[m^2]
A_{valves}	Combined flow area of lock valves in a single lock gate	[m^2]
c	Propagation speed of wave	[m/s]
c_i	Initial propagation speed of wave	[m/s]
c_{th}	Propagation speed of wave (estimate from Stevin Locks experiments)	[m/s]
$c_{th,0}$	Propagation speed of wave from lock to lake	[m/s]
$c_{th,z}$	Propagation speed of wave from sea to lock	[m/s]
d	Water depth	[m]
d_0	Water depth at lakeside	[m]
d_{int}	Interface depth	[m]
d_{int}^+	Increment to the interface depth	[m]
$d_{int,0}$	Interface depth at t= 0	[m]
$d_{int,new}$	New interface depth after changes	[m]
d_s	Ship draught	[m]
d_z	Water depth at seaside	[m]
Δd	Differences in water depth	[m]
Δ_{model}	Differences in computed salt intrusion between modelling approaches	[kg]
Δ_M^*	Nondimensionalized form of Δ_{model}	[-]
f_{exit}	Recommended ZSF ΔM-factor for exiting of ships (see: ΔM)	[-]
f_{level}	Recommended ZSF ΔM-factor for levelling (see: ΔM)	[-]
g	Gravitational acceleration constant	[m/s^2]
h	Height of water column	[m]
h_0	Height of water column at t= 0	[m]
h_{int}	Interface height	[m]
h_{lock}	Height of water column in lock	[m]
J	Nondimensionalization factor	[kg]
l	Lock length	[m]
l_s	Ship length	[m]
μ	Contraction coefficient of lock valves	[-]
M	Suspended salt mass	[kg]
M_0	Initial suspended salt mass in lock	[kg]
ΔM	Amount of salt intrusion in lakeside	[kg]
$\Delta M_{2L\Delta t}$	Amount of salt intrusion according to this study	[kg]
ΔM_{th}	Amount of salt intrusion (estimate from Stevin Locks experiments)	[kg]
ΔM_{ZSF}	Amount of salt intrusion according to the ZSF	[kg]
n	Simulation step	[-]
Q	Discharge	[m^3/s]
Q_{lvl}	Levelling discharge	[m^3/s]
q	Specific discharge per meter width	[m^2/s]

q_r	Specific discharge of return current per meter width	[m^2/s]
ρ	Density	[kg/m^3]
ρ_0	Boundary condition of density at lakeside	[kg/m^3]
ρ_{mix}	Average/mixed lock density	[kg/m^3]
ρ_z	Boundary condition of density at seaside	[kg/m^3]
$\Delta\rho$	Difference in density	[kg/m^3]
S	Salinity	[kg/m^3]
S_0	Salinity at lakeside	[kg/m^3]
S_{lvl}^*	Average salinity of levelling discharge over a levelling phase	[kg/m^3]
$S_{primary}^*$	See $\overline{S_x}$	[kg/m^3]
$\overline{S_x}$	Average return current salinity of the conceptual model during t_{pass}	[kg/m^3]
S_z	Salinity at seaside	[kg/m^3]
S_{mix}	Average salinity over lock volume	[kg/m^3]
ΔS	Differences in salinities	[kg/m^3]
t	Duration	[s]
t_{door}	Duration between opening of the lock gates and ship movement	[s]
t_{LE}	Theoretical duration of a lock exchange	[s]
t_n	Time at simulation step: n	[s]
t_{open}	Duration of lock gates being open	[s]
t_{pass}	Sailing duration through a single lock gate	[s]
t_{wait}	Duration between consecutive ship movements	[s]
Δt; dt	Model step size	[s]
U	Relative lock exchange `	[-]
u_L; u_{limit}	Limiting speed of propagating ship in channel	[m/s]
u_r	Return current velocity	[m/s]
u_s	Sailing velocity	[m/s]
V	Lock volume	[m^3]
V_{box}	Volume of schematized expelled water	[m^3]
V_{fresh}	Fresh water volume	[m^3]
V_{lvl}	Levelling volume	[m^3]
$V_{lvl,HT}$	Levelling volume during high tide	[m^3]
$V_{lvl,LT}$	Levelling volume during low tide	[m^3]
$V_{primary}$	Volume of return current	[m^3]
V_s	Ship volume	[m^3]
V_{saline}	Saline water volume	[m^3]
V_U	Relative lock exchange volume	[m^3]
w	Width of lock	[m]
w_{free}	Width of uninterrupted lock	[m]
w_s	Width of ship	[m]
$\bar{z}$	Depression	[m]
z_{bv}	Bottom level of lock valves	[m]
z_{tv}	Top level of lock valves	[m]

Table of Contents

Summary

The Netherlands is susceptible to salt intrusion from the North Sea, which is especially evident at sea locks. Given the complexity related to saline flows in such locks, a suitable method to quantify the salt intrusion is with the use of a parametrized salt intrusion model. The current model from Deltares is the ZSF. This thesis aims to improve the accuracy of the salt intrusion calculations of the ZSF by refining two assumptions whose physical representations are questionable: the assumption of instantaneous shipping, and the assumption of homogeneous lock density. For this purpose, a return current distribution according to the continuity method and a stratified salt distribution inside the lock are assumed. These descriptions are subsequently applied to a newly developed conceptual lockage model based on the algorithm of the ZSF. An additional assumption is called for which describes the simultaneity of the processes. For this, the time scale is discretised into time steps (Δt) after which the relevant hydraulic processes to salt intrusion (i.e. return currents and the lock exchange) are applied alternately. This assumption makes it possible to include the influence of the return current on the lock exchange. The combination of these assumptions in this study is referred to as the $2L\Delta t$ assumptions. Upon validating the conceptual model to the Stevin Locks experiments, it was found that $2L\Delta t$ assumptions reproduce the results of the experiments with more accuracy than the ZSF assumptions. Furthermore, it has been established that completely pushing back the exchange flow by return currents while a ship is moving towards lakeside overestimates the influence of the return current on the lock exchange. This effect may be caused by the propeller jet on the lock chamber.

In quantitative terms, an analysis is carried out on the discrepancies of the model approaches by setting up analytical formulations of shipping contributions to salt contribution. Initially, the lock exchange was neglected. The formulation is then made nondimensional using a nondimensionalisation factor J. Regardless of the used shipping class, discrepancies followed a parabolic curve with a peak at approximately 16% around h_0/d equal to 0,5. After reintroducing the lock exchange, the outputs are now also dependent on the duration of the lockage, expressed in t_{door} and t_{wait}. To ensure that the lock exchange has a similar magnitude for different initial salinity conditions, the lockage durations are divided by the theoretical duration of a lock exchange (t_{LE}). It was found that larger discrepancies are obtained for more saline locks, shorter waiting periods before exiting the lock after opening the lock gates (t_{door}/t_{LE}), and longer lockage durations. These observations can be explained by the influence of the return current on the lock exchange when exiting the lock compared to entering the lock, the latter being smaller due to the present lock exchange. This finding suggests that generally a lower amount of salt intrusion is calculated by shipping for the $2L\Delta t$ assumptions. When the computational parameters that lead to the largest discrepancies are applied over the full navigation phase, a final maximum discrepancy of about 11% of the total amount of salt intrusion is found. During realistic (i.e. using realistic values for computational parameters) and consecutive lockages, generally less salt intrusion is accounted for the $2L\Delta t$ assumptions with respect to the ZSF assumptions during high tide. For low tide, almost no differences can be seen between computed amounts of salt intrusion between both model approaches. Another finding is that the contribution of return currents to salt intrusion is greater at low tide than at high tide. This is because the differences between the effects of the return current on the current lock exchange between exiting the lock and entering the lock are greater at low tide, as the lock has less salt water when entering the lock.

Therefore, a model factor (f_{exit}) can be used which reduces the contribution of return currents on salt intrusion inversely proportional based on the salt mass present in the lock and lockage duration. This follows from the finding that generally less salt intrusion is obtained for higher saline lock volumes because of pushing back the exchange flow. The validation step showed, however, that the salt tongue should not be pushed back entirely as this resulted in discrepancies with the Stevin lock experiments. The factor (f_{exit}) should be applied to the total amount of salt intrusion over the navigation phase. Regarding its magnitude, it was seen that by using the parameters that lead to the biggest discrepancies, a total f_{exit} of $883/985 \approx 0{,}89$ was required. As the validation chapter shows that the pushback contribution is overestimated in the $2L\Delta t$ model relative to values seen in practice, the value of f_{exit} of $0{,}89$ can be interpreted as its lower bound, while the upper limit for f_{exit} is equal to $141/122 \approx 1{,}16$. This limit is of considerably less importance because the increased salt intrusion for the $2L\Delta t$ assumptions only occurs at very small lockage durations compared to the salt intrusion calculated by the ZSF (navigation phase of less than 5 minutes). It is estimated that an f_{exit} of around 0,9 is applicable for realistic lockages. In addition, the ZSF should include a levelling factor (f_{level}), based on the usage lock valves and stratification. This levelling factor is to be proportional to the amount of salt mass in the lock. It is stated with certainty that this factor is never to be below 1,0. Having a fully fresh lock after having levelled to seaside (thus using saline water for levelling upwards) is impossible, hence the lower bound of f_{level} being 1,0.

Finally, it is recommended that more research is done into the contribution of the propeller jet on the flow pattern during a lockage. Both during the passage of ships in and out of the lock, as the created flow pattern by the acceleration and deceleration in the lock. Furthermore, it is recommended to do more research on the levelling factor (f_{level}) as proposed in this study, to determine its size and dependency.

1 Introduction

1.1 Problem of Salt Intrusion

Having sufficient fresh water is vital for a country to function properly, not only for personal use but also for industrial purposes. The Netherlands is prone to salt intrusion from the North Sea. This negatively affects the amount of fresh water available for agricultural and industrial purposes, drinking water, and negatively affects the water quality for ecological reasons. Intrusion of salt water in fresh waterbodies is therefore highly undesired.

Salination of the waterbodies in the Netherlands is expected to increase in relevance in the coming years. First, sea levels are rising because of global warming. This promotes salt intrusion through coastal seepage and exchange flows in estuaries and shipping locks. Also, the low-lying nature of the Netherlands causes salt wedges to reach further land inwards. Second, because of global warming the discharge of the river Rhine is expected to decrease in the coming years. This will reduce the supply of fresh water, which is commonly used for mitigating salt intrusion by flushing locks. Finally, because of the growing economy larger ships and more frequent lockages are expected, adding to the salt intrusion through navigation locks. Navigation locks play a large role in the salt intrusion of the Netherlands. Hence, there is a need to actively counteract salt intrusion here.

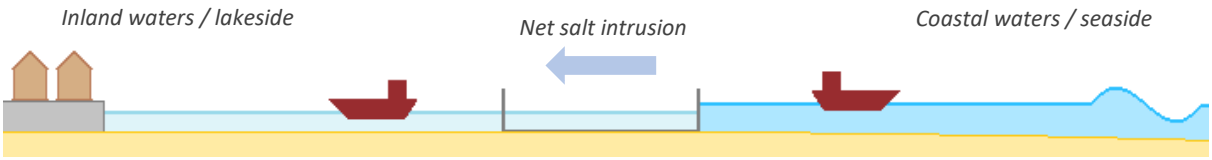

Figure 1.1: Schematization of a lock between fresh and saline waterbodies during high tide. The lockages (i.e. the passage of a lock by a ship) bring forth a net amount of salt intrusion.

1.2 Salt Intrusion Model

Combating salt intrusion in locks calls for a parametrized salt intrusion model. Such a model is useful as it can provide an estimate of the amount of salt intrusion of multiple lockage scenarios based on lockage parameters. In contrast, more advanced models, such as CFD models, are not always able to provide a solution due to the large amounts of data they rely on. The current model of Deltares, named Zeesluisformulering (ZSF, translated: sea-lock formulation) offers a good solution to this need.

The project of the ZSF was established with the aim of developing a generic salt intrusion model for locks. The formulation to be prepared had to contain the essential lockage parameters of the salt intrusion process which were by Deltares determined to be: the salinity and water level differences over the lock, the dimensions of the lock, the locking operation and corresponding durations, and the implementation of salt mitigation measures [1]. Tests of the model showed promising results, although some elements required extra attention. Two specific point of attention are the implementation of shipping in the ZSF [2][3], and the usage of a homogeneous lock density. These points will be at the base of this thesis.

To motivate the aim of this study, the implementation of shipping should first be explained briefly. In the ZSF, the return currents are modelled by instantaneously replacing a ship with water of the ship's destination. This can be explained from the diagram in Figure 1.2. When a ship sails from location A to location B, a similar volume of water is transported in the opposite direction. This implementation of navigation can be considered rather coarse. In addition, it is assumed that the lock density during lockage is homogeneous.

Because the ZSF is a parametrized lockage model, having assumptions that are coarse is not necessarily unjust, as such a model is aimed at providing a reliable estimate of the amount of salt intrusion in practice. However, both assumptions are at the base of the determination of the salt intrusion from shipping. Moreover, the density distribution in the lock plays a major role in the determination of salt intrusion by levelling, which means that this process will largely be influenced by the density assumption. This raises the question of whether optimized assumptions can increase the accuracy of the parametrized estimate.

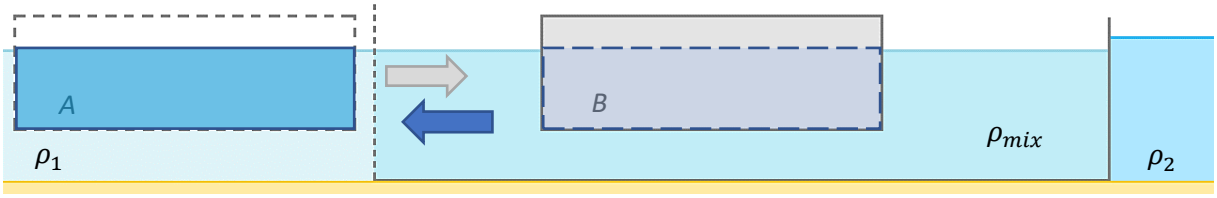

Figure 1.2: Schematization of instantaneous shipping in combination with a homogeneous lock density; $\rho_2 > \rho_{mix} > \rho_1$.

1.3 Research Problem

Due to the increasing relevance of salt intrusion projected in the coming years, a general intrusion model is desired for estimating the salt intrusion for lockages in the Netherlands. The ZSF is a suitable model for this purpose but uses two assumptions of which the physical representation can be optimized. To contribute to the development of salt intrusion control practices, this thesis will examine if improving the assumptions of the ZSF holds improving the accuracy of the parametrized salt intrusion estimate. Moreover, this will examine to what extent the simplified assumptions lead to deviations with salt intrusion in practice and optimistically propose alternative descriptions of these assumptions. This is formulated as the following research problem:

To what extent can the accuracy of the salt intrusion estimate of the ZSF be improved by replacing the assumptions of homogeneous lock density and instantaneous shipping with assumptions of greater physical representativeness?

1.4 Methodology and Research Questions

To answer this research question, a causal-comparative method is chosen where the influences of spatial lock density and - shipping contributions on the salt intrusion are investigated. A combination of a literature review, a sensitivity analysis and a case study is pursued. The research is subsequently formulated in threefold:

- What is a more realistic description of the return current and density distribution in the lock based on literature?
- What is the impact of the new implementations of shipping and density distribution in the lock on the computed salt intrusion as compared to the ZSF?
- For what range of applicability do the new assumptions provide an improvement to the parametrized salt intrusion estimate?

First, the relevant hydraulic processes that occur in practice during a lockage are investigated by means of a literature study. Based on this analysis, an optimized analytical description of the contribution of shipping to salt intrusion and the density distribution in the lock will be explored. Second, the new descriptions will be tested in a reconstruction of a conceptual, systematic lockage model in Python. The model will be validated using experimental data from the Stevin Locks experiments [6]. Third, a sensitivity analysis and case study will be carried out using the conceptual model. This is used for finding the conditions under which the new assumptions improve the salt intrusion estimate in a sensitivity analysis. Moreover, this will allow for quantifying the impact of the new assumptions on the parametrized salt intrusion estimate. Last, it will be concluded whether the new assumptions have led to an improvement in the estimate of salt intrusion, and if so, under what conditions these assumptions lead to improvements.

1.5 Outline

This research will start with a literature review in chapter 2. Here, two elements are addressed. First, a lockage in practice will be studied. Next, the underlying algorithm and assumptions of the ZSF will be studied. In Chapter 3, an analytical representation of a lockage will be constructed in a conceptual model in Python based on the findings of the literature study. Next, a validation study in Chapter 4 will test whether the conceptual model with the refined assumptions is a step forward compared to the ZSF. Chapter 5 will focus on a sensitivity analysis. The first part attempts to establish conditions for the extent to which the current assumptions of the ZSF lead to discrepancies, and the new descriptions provide improvements. The second part aims at providing insight in the differences of the parametrized salt intrusion estimates between the models by carrying out a case study. This will be on data from the Krammer locks which are depicted in Figure 1.3. This is followed in Chapter 6 by the discussion of this study in which the uncertainties are brought forward. The conclusion of the study is drawn up in Chapter 7. Based on the case study and the sensitivity analysis, recommendations are then made in Chapter 8 as to whether better estimates of the parametric salt intrusion have been obtained, and what follow-up studies are proposed.

Figure 1.3: Aerial photo of the Krammer locks in Zeeland, the Netherlands. Photo taken by Siebe Swart, 23 November 2013.

2 Existing Descriptions of Salt Intrusion in Locks

This literature study will focus on a lockage in practise and how a lockage is represented in the ZSF. Based on these two aspects, the author aims to explain the possible inaccuracies brought forward with the current assumptions in the ZSF and propose refined assumptions. The findings will then be summarized in a preliminary conclusion.

2.1 Lockage in Practice

Locks are used for increasing navigability for ships in canals and waterways by bridging hydraulic heads. This is being done by closing the lock gates and filling and emptying of the lock, which is also referred to as levelling. They are often found near the coastline where they serve a secondary function, namely separating fresh and salt water. As the focus of this research is on salt intrusion, only locks situated in between fresh and saline waterbodies will be considered. Such sea locks can reach lengths of up to 500 meters and widths of 70 meters (*Zeesluis IJmuiden*). Data from Deltares [4] from 2018 shows that 13,9 lockages per day is a representative frequency of use at IJmuiden. The Stevin - and Lorentz locks at the IJsselmeer have a daily average of 11,0 and 12,5 lockages per day respectively [5], which are at the slightly less used waterways for comparison. The Krammer locks have a representative use of about 36 passages per day for its four locks.

A lockage cycle can be regarded as a series of lockage phases, containing several hydraulic processes. These processes originate from having either one lock gate opened, for entering or exiting the lock with a ship, or having both gates closed, for levelling of the lock. Since some processes therefore only occur during a certain phase of the lock cycle, it is practical to divide the lock into levelling phases and navigation phases. The different hydraulic processes that can be distinguished during these phases are *levelling*, *lock exchange*, and *shipping disturbances*. These hydraulic processes will be introduced in this paragraph.

Lockage phases:

1. *Levelling to lakeside.*
2. *Navigation at lakeside.*
3. *Levelling to seaside.*
4. *Navigation at seaside.*

A schematization of the phases is shown in Figure 2.1. Although shipping is not included in this image, it gives a clear view on the operation of levelling and the presence of the lock exchange. It also shows that the levelling process takes place in phases 1 and 3, and the lock exchange and shipping displacements take place in phases 2 and 4. An overview of the lockage cycle and where the processes are present in the lockage cycle is given in Figure 2.2. The naming convention of parameters and quantities in this chapter is based on an axis system in the lock whereby lakeside and seaside are

regarded as the beginning and end of the x-axis, therefore respectfully denotated by the suffixes *0* and *z*. The direction in the vertical is denoted by the z-axis. Furthermore, the bottom levels of the lock heads, the lock and the waterbed are all at the same height such that bottom variations can be neglected.

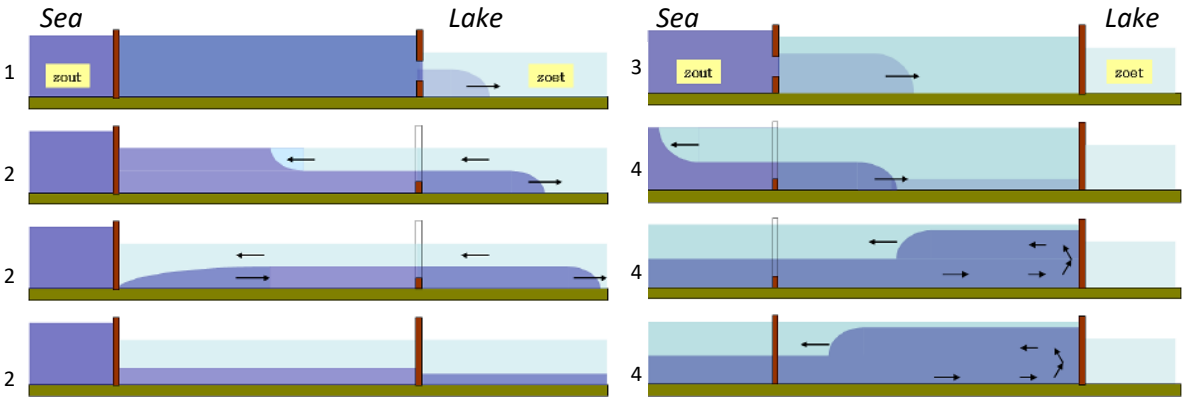

Figure 2.1: Schematization of a lockage cycle during high tide. Seaside is shown on the left of the lock, lakeside on the right. The numbers in front of the image correspond to lockage phases, denoting: 1) levelling to lakeside, 2) navigation at lakeside, 3) levelling to seaside, 4) navigation at seaside. [6]

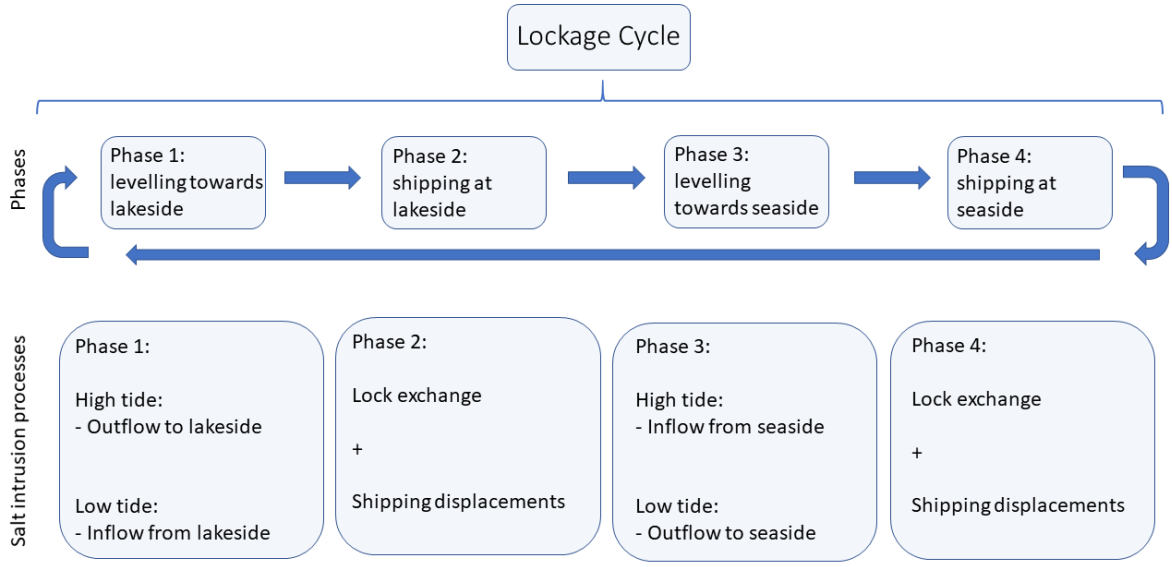

Figure 2.2: Overview of where the different hydraulic processes contributing to salt intrusion take place during a lockage cycle.

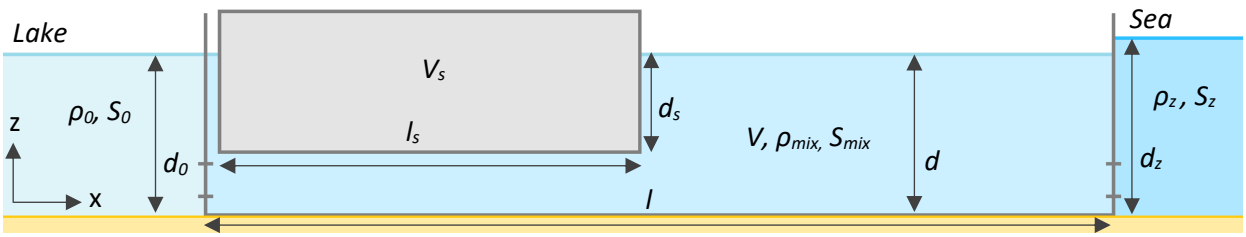

Figure 2.3: Free body diagram of a schematized lock during high tide with a present ship with width dimensions in y direction perpendicular to the image. Both lock gates are closed, and the lock level is at lake level. The magnitudes of the given densities read $\rho_z > \rho_{mix} > \rho_0$.

It has proven to be convenient to take water depths, given by d, positive in the negative z-direction. Furthermore, lengths are given by l, widths by w, water densities by ρ and salinities by S, defined as the amount of salt mass per cubic meter water. To familiarize the reader with the naming convention, a free body diagram of a lock is shown in Figure 2.3. From the dimension of Figure 2.3, the volume of the lock and the volume of the ship volume follow.

$$V = l * w * d, \qquad V_s = l_s * w_s * d_s \tag{2.1 \& 2.2}$$

2.1.1 Levelling

During the process of levelling, the lock gates are closed such that the water level within the lock can change. This is generally achieved by opening of the lock valves located at the bottom of the lock gates which allows a free-flowing current. These valves are shown in the lock gates in Figure 2.3, which have a flow area of A_{valve}. The volume required for levelling (V_{lvl}) can be determined using continuity (2.3) based on the water level differences over the lock gates, or Δd. For the flow through the valves, Torricelli's formula (2.4) can be used where μ represents the contraction coefficient of the flow.

$$V_{lvl} = l * w * \Delta d \tag{2.3}$$

$$Q_{lvl} = \sqrt{2g\Delta d} * A_{valve} * \mu \tag{2.4}$$

Throughout the duration of the levelling process, the differences in water levels (Δd) reduce, resulting in a reduction of discharge through the lock valves. This is explained by the relation between (2.3) and (2.4), given by differentiating (2.3) which results in (2.5).

$$Q_{lvl} = l * w * \Delta d/dt \tag{2.5}$$

The salt transports accompanied by the process of levelling can be obtained by the product of the levelling volume and the differences in salinity. Regarding sea locks, the saline side is commonly subjected to tidal forcing. As a result, the water level on seaside varies during the tidal cycle, so that the sea level generally fluctuates above and below the water level on lakeside. Consequently, different water conditions and discharge directions hold for levelling throughout the day. Therefore, the explanation of levelling will be subdivided into separate tidal phases of high tide and low tide.

2.1.1.1 High Tide

High tide is generally characterized by a higher sea water level in relation to the water level at lakeside. For high tide, upward levelling is achieved by the inflow of water from seaside. This increases the average salinity within the lock. The increase in the salt concentration in the lock poses a threat to the salinity on lakeside. As the lock is levelled downwards, the residual lock volume is discharged on lakeside and the previously accumulated salt concentration in the lock contributes to the salt intrusion. The levelling process during high tide is illustrated in Figure 2.4.

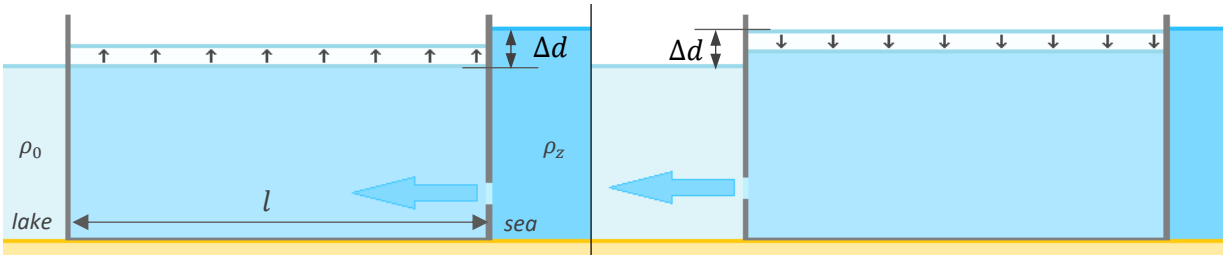

Figure 2.4: Schematization of levelling during high tide.

2.1.1.2 Low Tide

During low tide, the water level at lakeside is generally lower than the water level at seaside. This holds that for upward levelling the lock is filled with fresh water, thus reducing the average salinity within the lock. For the duration of downward levelling, the water is here discharged on seaside, as opposed to high tide. It can already be seen from the schematization that the low tide situation brings about less salt intrusion than the high tide situation, as no arrows are directed towards lakeside. This is schematized in Figure 2.5.

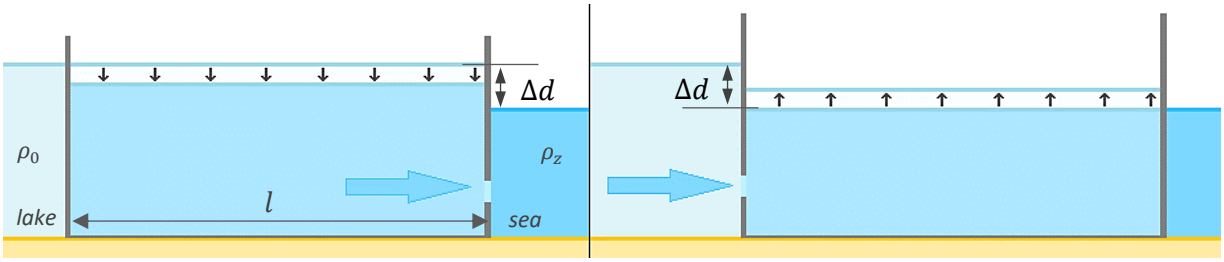

Figure 2.5: Schematization of levelling during low tide.

2.1.2 Lock Exchange

As the lock gates are opened at either side for ships to pass, the lock volume is exchanged with the adjacent water due to exchange flows. This is being referred to as the lock exchange. The differences in densities between the lock volume and the neighbouring water brings forth a difference in potential energy, which is converted to kinetic energy by an internal pressure gradient. The result of this are two opposing flows over the vertical at location of the lock gates. This process is shown schematically in Figure 2.6. To determine the salt intrusion by exchange flows, a description is needed for the propagation of the salt front. Therefore, the literature will be consulted first on an analytical solution.

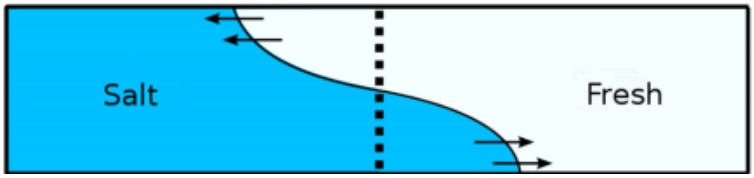

Figure 2.6: Schematic illustration of lock exchange [7].

The full analytical solution of the propagation of exchange flows can be obtained by solving for the Navier-Stokes equations. However, this comprises of accounting for complex phenomena such as wall stresses, fluid stresses and diffusion of the fluids [8]. Instead, numerous examples in literature have found ways of describing laboratory experiments of exchange flows using the two-layer shallow water equations (2LSWE, see Appendix A) (Rottman & Simpson, 1983; Shin et al., 2004; Lowe et al., 2005; Rotunno et al., 2010). This model has proven to offer a simplified approach in comparison to the full analytical solution for obtaining propagation characteristics, such as layer heights and velocities, of the exchange flow in a general sense. Although the 2LSWE has been used in numerous examples, a general analytical solution for the propagation of lock exchange currents cannot be found due to the previously mentioned neglected effects [8].

Instead, the empirical relative lock exchange formulation (2.6) as proposed by V.d Burgh & De Vos (1962) and Van der Ven et al. (2018) can be a practical alternative for describing the lock exchange. This relation, given by U in (2.6), presents the ratio of exchanged water volume (V_U) over the total volume of the lock (V) in time. To obtain the transported volume from the relative lock exchange, U must therefore be multiplied with the total lock volume.

The relative lock exchange formulation is a fit of lock exchange experiments, where the total amount of salt intrusion is expressed as a function of elapsed time (t) relative to the total theoretical time scale of a lock exchange (t_{LE}). This allows for calculating the total amount of exchanged water volume instantly from the lockage duration. The theoretical duration of a lock exchange is defined as the time it takes for the salt wedge to travel to the other side of the lock and back by reflection, given by (2.7). This reflection phenomenon can clearly be seen in lockage phase 4 of Figure 2.1. In this formulation, c_i is the initial propagation speed of the exchange flow as applied by V.d. Burgh and De Vos.

$$U = \tanh\left(\frac{t}{t_{LE}}\right) = V_U/V \tag{2.6}$$

$$t_{LE} = \frac{2l}{c_i}, \qquad c_i = \frac{1}{2}\sqrt{g\frac{\rho_z - \rho_0}{\rho_0}d} \tag{2.7 \& 2.8}$$

Experiments from 1962 and 1973 show a similar course of lock exchange as the relative lock exchange formulation, shown in Figure 2.6. Recent field and scale experiments in IJmuiden confirmed the time scales of the hyperbolic tangent formulation as well (A.J. van der Hout, Deltares, personal communication, May 26, 2021). Therefore, it can be assumed with reasonable certainty that the relative lock exchange formulation describes the lock exchange with acceptable accuracy.

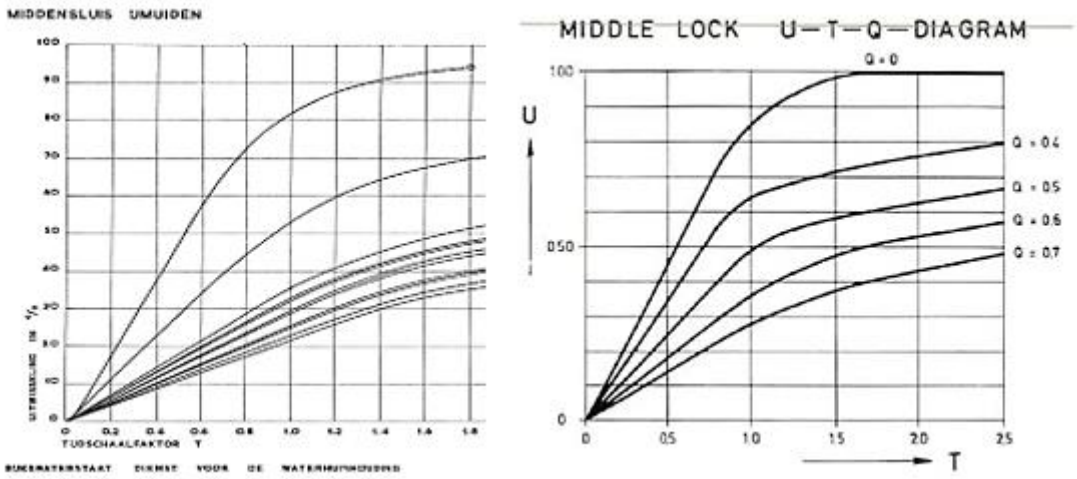

Figure 2.7: Lock exchange measurements from 1962 (left) and 1973 (right), set out with duration t/t_{LE} on the x-axis. The measurements correspond with the tanh formulation, having a constant gradient between $0 < t_{open}/t_{LE} < 1$ and approaching U= 100% with increasing durations. The top plot are experiments with an undisturbed lock; lower plots represent experiments with bubble screens. [9][10]

2.1.3 Shipping Displacements

Formerly described by Deltares [6], water displacements by shipping can be subdivided into two components: static – and dynamic displacements. First, the static water displacements and their effect on the lock chamber will be discussed.

The static displacements are characterized by the influences of a stationary ship on the lock volume during a lockage cycle. Due to the presence of a ship the available volume in the lock, and thus the water volume, is reduced. As a result, the inflow of saline water will result in faster salinization of the lock chamber. Moreover, more inflow of water to the lock will take place when the ships depart. This is considered numerically by adjusting the equation of (2.1) to include a present ship, given by (2.9).

$$V = l * w * d - V_{ship} \tag{2.9}$$

According Vrijburcht [11], a second contribution to the static displacement can be seen in the blocking of the lock exchange by the presence of a ship. The reduction of the hydraulic perimeter at location of the present ship results in a reduction of the propagation speed of the salt wedge. This brings forth an uneven salt distribution in the lock during levelling, as shown in Figure 2.7. This image is constructed from observations from a hydraulic scale model. Unfortunately, no closures could be found for this contribution and will therefore not be regarded further.

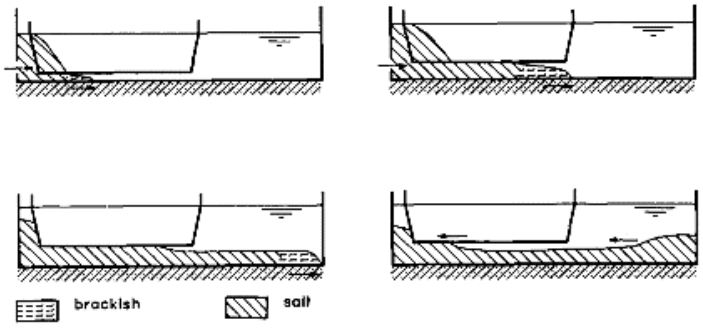

Figure 2.7: Filling of a fresh lock with saline water and a large ship blockage. [11] The levelling process is done via the lock valves. Attention is directed towards the observed salt by Vrijburcht.

The second set of shipping contributions to the salt intrusion can be found in the dynamic water displacements. These contributions originate from ship movement and can be further subdivided in contributions by the return current, shipping waves, and by thrust from the ship's propeller. The return current and propeller jet will now be further examined.

2.1.3.1 Return Current

In practice, water is repressed in front of the ship and a void is formed behind the ship as it propagates. The excess water from the bow flows to the stern which is being referred to as a primary wave or return current. A depression in water level occurs next to the ship from the increment in hydraulic head relative to the pressure head resulting from this current. Both the depression and the return current are dependent on the propagation velocity of the ship and can be approximated by making use of the theory by Schijf [12].

Return currents of ships in channels with finite dimensions have been studied extensively and can be determined with Schijf's theorem, or his corresponding diagram (see Appendix B). The basis of this theorem is a combination of the mass balance and Bernoulli's equation based on a free-body diagram like Figure 2.8. The return current velocity (u_r) then follows iteratively based on the depression ($\bar{z}$, written with an overbar to avoid confusion with z-axis), and is furthermore dependent on the cross-sectional areas of the channel and ship (respectively A_c, A_s) and the velocity of the ship (u_s). The formulation of Schijf's theorem is given by (2.8). According Schijf, the return current distribution over depth can then be determined by multiplying u_r with the available free width of the lock. This is a function representing the width of the lock over depth (vertical in z-direction) minus a present ship, given by (2.10). This results in a volume flux distribution shape as depicted in Figure 2.9.

It should be noted that the total water displacement from Schijf's return current theorem approximates the volume of the ship for low sailing speeds. This is shown in Figure 2.10 where Schijf's diagram is used according to Appendix B to determine the total volume of the primary wave of four shipping classes, of which the dimensions are given in Table 2.1.

$$\frac{u_r}{\sqrt{gd}} = \left[\frac{1}{\left(1-\frac{A_s}{A_c}\right)-\frac{\bar{z}}{d}} - 1\right] * \frac{u_s}{\sqrt{gd}} \tag{2.8}$$

$$\bar{z} = \frac{u_s^2 - (u_s + u_r)^2}{2g} \tag{2.9}$$

$$w_{free}(z) = \begin{cases} w - w_s, & 0 \geq z > -d_s \\ w \quad , & -d_s \geq z \end{cases} \tag{2.10}$$

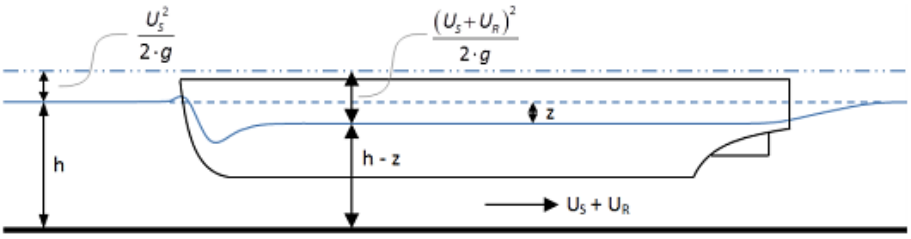

Figure 2.8: Free-body diagram of a passing ship through a channel. [13]

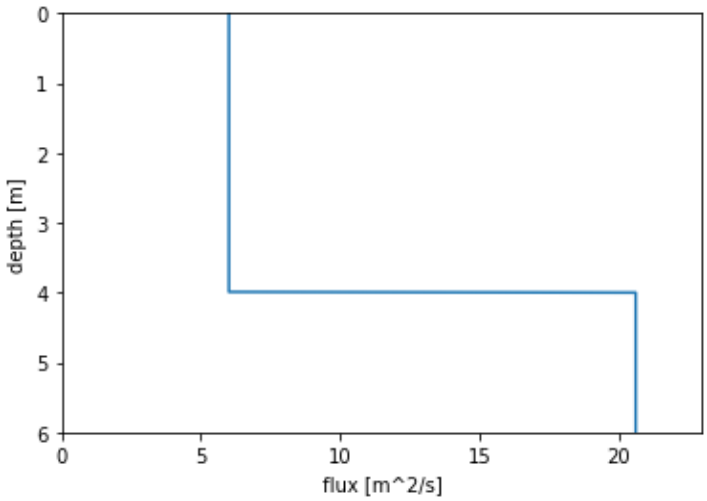

Figure 2.9: Volume flux distribution over depth according Schijf's return current theorem for shipping class CEMT: VIa, sailing at 0,6 times the limiting speed.

Table 2.1: Dimensions of CEMT classes [14] *used for Figure 2.10.*

CEMT class	d_s/d [-]	A_s/A_c [-]	U_{limt} [m/s]
IIIa	*0,42*	*0,14*	*3,84*
IVa	*0,50*	*0,21*	*3,38*
Va	*0,58*	*0,29*	*2,61*
VIa	*0,66*	*0,47*	*1,61*

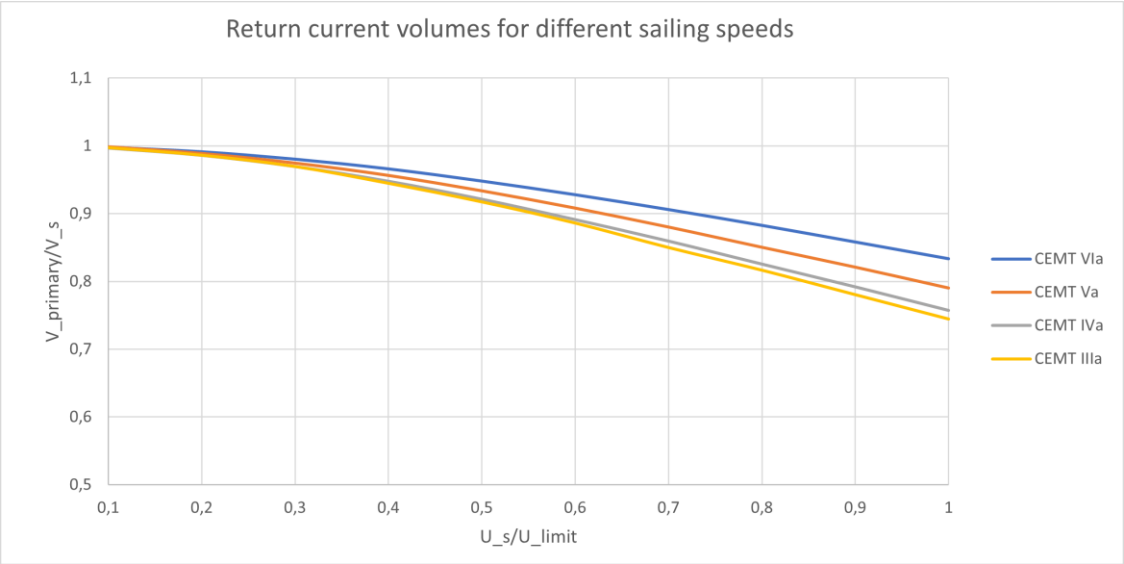

Figure 2.10: Volume of water displaced by return current according Schijf's theorem for different shipping sizes and sailing speeds. It is seen that smaller ships and faster sailing accounts for relatively less water displacement. The x & y-axis show resp. the primary wave volume over the ship's volume and the ship's speed over the limiting speed according Appendix B.

2.1.3.2 Propeller Jet

The effects of the propeller on the lock volume and salt intrusion are complex due to the large spatial variability of the flow that is accompanied. The reason for this is as follows. In addition to the translation of the ship, which moves the propeller along the length of the lock, water from the vicinity of the propeller is transported into the jet stream. Also, the direction of the propeller jet varies during navigation through the lock. Vessels use their propellers to slow down by reversing them when they are at the end of the lock, causing the jet to point in the direction of the ship's bow.

The influence of propeller jets on the salt intrusion was included in the scope of research of the Stevin Locks experiments in 2010. According to findings by Groenenboom (2010) [15], it was found the propeller jet displaces a total water mass of the same magnitude as the mass of the ship, sometimes even twice its mass. Reliable results regarding the long-term behaviour of salt intrusion by propeller jets in locks could not be found in this study, or in literature. Therefore, they will not be dealt with any further.

2.1.4 Density Distribution

Now that all the relevant hydraulic processes during a lock passage have been addressed, more insight is needed into the distribution of suspended salt in the lock. During a lock passage in practice there are several processes that can influence the overall distribution. In addition, hydraulic processes may locally cause a variation in lock density due to mixing and inflow or outflow to adjacent waters.

Salt water is heavier than fresh water, which causes the salt water to sink to the bottom when fresh and saline waters are mixed. As shown in Figure 2.1, 2.4, 2.5, and 2.6, during levelling and lock exchange, salt water enters the lock at the bottom. Levelling in practice is achieved by opening lock valves which are at the bottom of lock gates to minimize the forcing on present ships; salt wedges travel over the bottom of the lock. Given that the volume is insufficiently disturbed, this salt water will therefore remain on the bottom of the lock. Moreover, experiments from the Stevin Locks [6], depicted in Figure 2.11, show that the density distribution during these processes in a lock has a stratified character.

Before anything can be said about the applicability of a stratified salt distribution in practice, the contributions of shipping to the salt distribution must be considered. Uittenbogaard and Cornelisse [6] have found in their study on the experiments at the Stevin locks that although the propeller jet induces turbulence, the presence of the salt wedge is hardly influenced by it: a significant salt wedge was still present in the lock after subsequent lockages. Partly based on the previous observation, this study assumes that a layered salt distribution is a representative approximation of the actual distribution in the lock. Unfortunately, no measurements could be found on this exact matter.

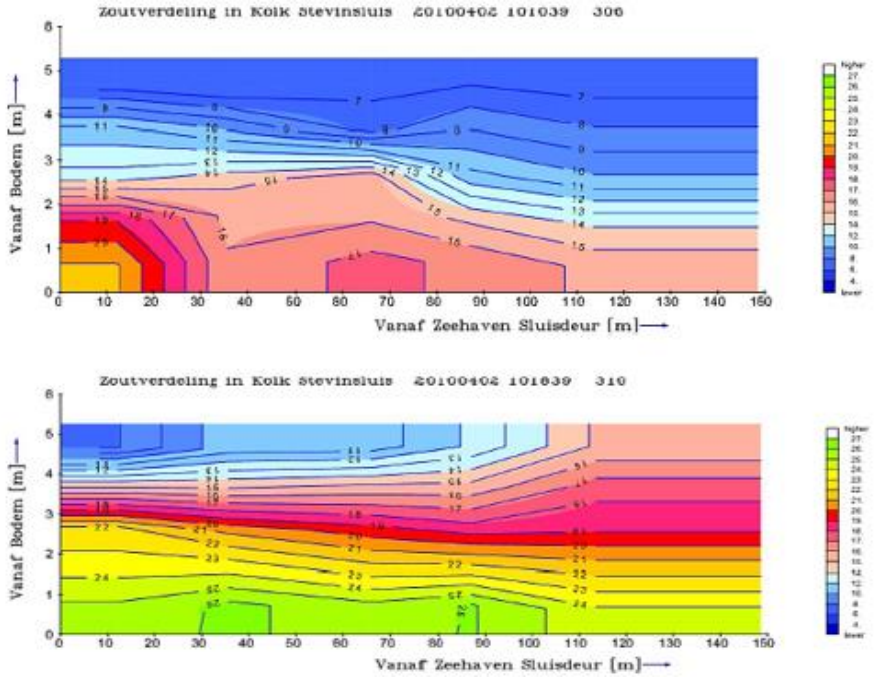

Figure 2.11: Salt distribution from Stevin Locks experiments [6] of lock exchange by opening of the gate at seaside, after 1 minute (top) and 9 minutes (bottom). The colours represent salinity, ranging from 4 (blue) to 27 (green) g/kg.

2.2 Lockage in the ZSF

To elaborate on the motivation for this research, a clear image of the representation of a lockage in the ZSF will now be given. The ZSF is a parametrized model which is used to estimate the total amount of salt intrusion during a lockage. This is done by simulating a lock with water volume V, separated by fresh and saline waterbodies with constant densities. This water volume is then subjected to several hydraulic processes.

Like a lockage in practice, a single lock passage in the ZSF can be divided into several phases, where a distinction is made between levelling phases with closed doors (phases 1 and 3) and navigation phases with open doors on one side (phases 2 and 4). In addition to the previously mentioned phases in Paragraph 2.1, the ZSF makes an additional division in the navigation phases, distinguishing between individual shipping displacements and the lock exchange. This is because these processes are carried out in the ZSF in turn, whereas in practice they occur simultaneously.

Lockage phases:

1	*Levelling to lakeside.*
2.a	*Exiting ship from lock to lakeside.*
2.b	*Lock exchange at lakeside.*
2.c	*Entering ship in lock at lakeside.*
3	*Levelling to seaside.*

4.a Exiting ship from lock to seaside.
4.b Lock exchange at seaside.
4.c Entering ship in lock at seaside.

The hydraulic processes included in the ZSF that contribute to salt intrusion are *levelling*, *lock exchange*, and *shipping disturbances*. In this chapter, the implementations of these processes will be laid out. The formulas in this paragraph will be denoted by the lockage phases of the ZSF listed above.

The dimensions in this paragraph denote either no suffix, representing lock dimensions, and suffixes *s, 0, z, U*, and *lvl*, denoting ship, lakeside, seaside, lock exchange, and levelling respectively. The water volume within the lock can be calculated using (2.9). Furthermore, Figure 2.3 is reproduced for the convenience of the reader in Figure 2.12. The implementations of the processes will be addressed according to a similar structure as Paragraph 2.1, starting with the process of levelling, lock exchange, shipping disturbances, and followed by the density distribution. Finally, a brief schematic of an entire lockage according the ZSF is given at the end of this paragraph.

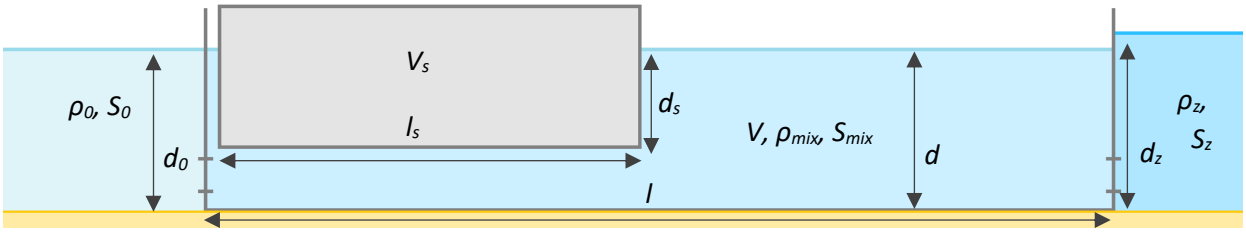

Figure 2.12: Initial situation of the simulation at t=0 with width dimensions in y-direction perpendicular to the image.

2.2.1 Levelling

For the implementation of levelling in the ZSF, a distinction is made between the separate tidal phases by using separate quantities for levelling during each phase.

$$LT: \quad V_{lvl,LT} = l * w * (d_0 - d_z), \qquad V_{lvl,HT} = 0 \tag{2.11}$$

$$HT: \quad V_{lvl,LT} = 0, \qquad V_{lvl,HT} = l * w * (d_z - d_0) \tag{2.12}$$

The amount of transported salt mass to the lock (ΔM) accompanied by levelling is then calculated by multiplying the levelling volume ($V_{lvl,LT}$ or $V_{lvl,HT}$) with the water density. Because this density contains a volumetric part water, it is of convenience to work with the salinity (S) instead.

$$LT: \quad 1: \quad \Delta M = V_{lvl,LT} S_0 \tag{2.13 \& 2.14}$$

$$3: \quad \Delta M = -V_{lvl,LT} S_{mix}$$

$$HT: \quad 1: \quad \Delta M = -V_{lvl,HT} S_{mix} \tag{2.15 \& 2.16}$$

$$3: \quad \Delta M = V_{lvl,HT} S_z$$

2.2.2 Exchange Flow

The lock exchange in the ZSF is approximated by making use of the relative lock exchange formulation, given by (2.6). To calculate the total salt transport, U must be multiplied with the lock volume and the differences in salinity.

$$\Delta M = \Delta S V U = \Delta S V_U \tag{2.17}$$

$$2.b: \quad \Delta M = -(S_{mix} - S_0) V_U \tag{2.18}$$

$$4.b: \quad \Delta M = (S_z - S_{mix}) V_U \tag{2.19}$$

2.2.3 Shipping Displacements

As mentioned in the beginning of this paragraph, the shipping process in the ZSF is carried out separately from the lock exchange. This implementation of the navigation process will now be dealt with further. From section 2.1 it was shown that shipping can physically be divided into static - and dynamic contributions. In the ZSF, only the return current of the dynamic contributions is implemented. Moreover, changes to the lock volume and salt intrusion because of navigation are applied instantaneous [3]. This has been adopted as follows.

First, a present ship in the lock is exchanged with a water volume of lake- or seaside in phases $2.a$ and $4.a$ respectively. Second, the lock exchange is carried out in phases $2.b$ and $4.b$, based on the total nondimensional duration t/t_{LE} as explained in section 2.1.2. Finally, a ship enters the lock by exchanging it with a water volume from inside the lock in respectively phases $2.c$ and $4.c$. The total contribution of shipping to the salt intrusion in the ZSF can thus be seen in the differences of the displaced water density between exiting and entering of the lock. This can be summarized into the following equations per navigation phase.

$$2.a: \quad \Delta M = V_s S_0 \tag{2.20}$$

$$2.c: \quad \Delta M = -V_s S_{mix} \tag{2.21}$$

$$4.a: \quad \Delta M = V_s S_z \tag{2.22}$$

$$4.c: \quad \Delta M = -V_s S_{mix} \tag{2.23}$$

A discrepancy is expected to occur between the computed salt flux and practice by using a salinity equal to that of lake side, seaside, or the lock in $(2.20 - 2.23)$. By doing so, no account is taken of dynamicity of return current density during the entry and exit of ships, because of the lock exchange. Moreover, a return current in practice has a larger volume flux underneath the ship than next to it, following from Schijf's theorem. In combination with the applicable stratification in a lock, as was shown in section 2.1.4, it is therefore expected that this combination results in a larger salt mass flux than is currently implemented in the ZSF.

In addition to the direct discrepancies expected with instantaneous shipping, a second aspect of this is questioned. In the ZSF, it is also assumed that the salt intrusion due to shipping in a single lockage phase can be approximated by having a ship exit the lock at the beginning of the phase and enter at the end. If the average salinity in the lock was linear with time, this would give an accurate approximation of the salt intrusion by shipping. However, Figure 2.6 shows that the course of salt flux in time by lock exchange, and thereby the course of the salinity in the lock, is only linear for the duration of once the theoretical lock exchange duration (t_{LE}). In practice, lockages may last longer. Furthermore, there is the return current which may or may not affect the salt tongue during the entry and exit of ships, which further raises the question of whether the course of the lock density over the cycle is linear and hence motivates the question of applicability of instantaneous shipping.

For the convenience of the reader, a schematic of the lockage phases of the ZSF is given in Figure 2.13. When a navigation phase 2 (at lakeside) or 4 (at seaside) starts, a ship is immediately exchanged with an adjacent water volume, represented by phases $2.a$ and $4.a$. After this phase, the lock exchange is performed in a single computation step according to (2.6) using the lockage duration. When this duration ends, a ship enters the lock in phases $2.c$ and $4.c$.

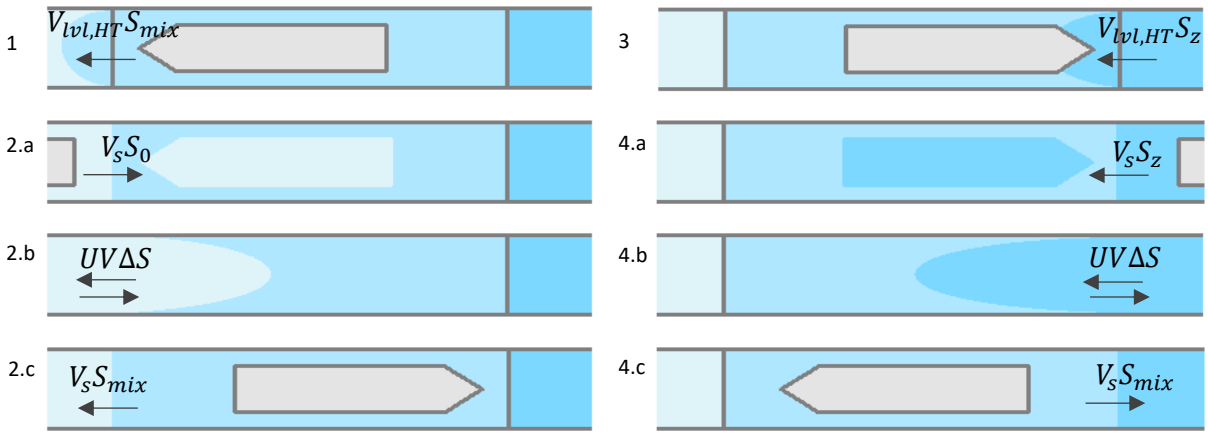

Figure 2.13: Schematization of top view of the lockage phases and transports in the ZSF during high tide. The arrows denote salt mass transports per phase, the colours denote different salinities where a darker colour represents more saline water.

2.2.4 Density Distribution

As mentioned in paragraph 1.2, the lock volume in the ZSF is assumed to be homogeneously mixed throughout the lockage simulation. This is done by determining the average salinity in the lock and adjusting this after each process that influences it. This can be explained by the illustration of the lock phases in Figure 2.13. Between each schematized lockage phase a new salinity in the lock is determined by dividing the present salt mass in the lock over the present water volume in the lock. This assumption is, together with the implementation of shipping, at the base of this research.

In the motivation of this research in paragraph 1.2, the expected underestimation of the combination of instantaneous shipping and a homogeneous lock density was already briefly presented. This can now be further motivated. From section 2.1.3 it followed that in practice, a return current has a larger volume flux underneath the ship than next to it. In combination with a larger density near the bottom due to stratification, this results in a larger salt mass flux as a result from the return current. In addition, the usage of a homogeneous density influences the levelling processes in phases 1 and 3 too. As previously stated, levelling is done by opening lock valves located at the bottom of the lock. This means that during downward levelling, i.e. discharging residual water from the lock, a larger portion of the saline layer will be extruded in comparison to the fresh layer. This is seen as a second underestimation from the usage of a homogeneous density.

The use of a homogenous density also implies a physical discrepancy: energy is constantly being added to move the suspended salt in the vertical direction upwards. Physically, this can be interpreted as having a mixer in the lock that continuously adds kinetic energy to the lock volume. As previously stated, because the ZSF is a parametrized model, this is not necessarily unjust. However, in a future when the knowledge of salt intrusion in locks develops in such a way that more dynamic contributions from shipping can be added to the ZSF, such as propeller jets, this could be a problem as the mixing character of the propeller jets cannot be added to a fully mixed lock. This will however not be addressed in this study and will only serve as further motivation for the use of a two-layer system.

2.3 Preliminary Conclusion

The ZSF contains two assumptions that can be considered coarse in practice according to the description of a lockage in practice: the homogeneous lock density, and instantaneous shipping displacements. The refinements to these assumptions follow from the literature study as presented in this chapter.

Two-Layer Model

To test the influence of a homogeneous lock assumption on salt intrusion, a new representation of a lock passage is set up with a more realistic density distribution. Based on the findings presented in this paragraph, this research proposes an unmixed salt distribution in the lock also known as a two-layer model or two-layer system. This is based on observations from the literature (Vrijburcht [11] observed stratification in his hydraulic scale model shown in Figure 2.7; Cornelisse and Uittenbogaard [6] found turbulence by shipping does not disturb the presence of a significant salt wedge; experiment data from the Stevin Locks experiments [2] show a clear stratification during lock exchange in Figure 2.11). Despite the applicability of stratification being mentioned in several studies [2][6][11], there are no examples in the literature of parametrized stratified lockage models. Furthermore, this assumption will test the other end of the mixing spectrum in terms of a homogeneous distribution.

The use of this assumption, together with a refinement of the return current, will cause differences in the determination of salt transport by the return current and levelling. Furthermore, it is expected that the actual salt distribution is somewhere in between the fully mixed and fully stratified situations. Therefore, it is relevant to consider the salt intrusion during a completely unmixed situation.

Continuity Method

A refined implementation of shipping will be proposed according to the return current distribution of Schijf [12], where a greater volume flux near the bottom is considered. Furthermore, shipping will also be modelled gradually. By applying this approach, the lock conditions are allowed to vary during sailing of which it is expected the result will be a more realistic description of salt intrusion by return currents.

For the combined effect of this refinement and the density distribution, the attention is pointed towards Figures 2.14 and 2.15. Figure 2.14 shows how shipping is currently implemented in the lockage cycle of the ZSF. It exchanges a ship volume with a mixed lock volume. The refinements according to literature are depicted in a schematization in Figure 2.15, where the blue distribution represents the volume flux from the return current.

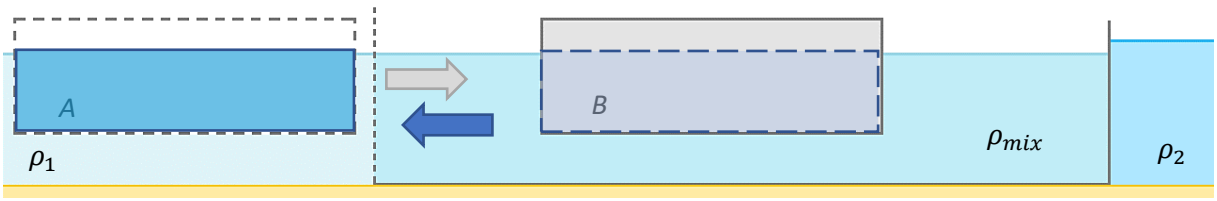

Figure 2.14: Schematization of instantaneous shipping in combination with a homogeneous lock density; $\rho_2 > \rho_{mix} > \rho_1$. Volumes A (fresh water) and B (ship) are swapped. The ship moves from lakeside to the lock (grey arrow) whereas the water volume is transported from the lock to lakeside.

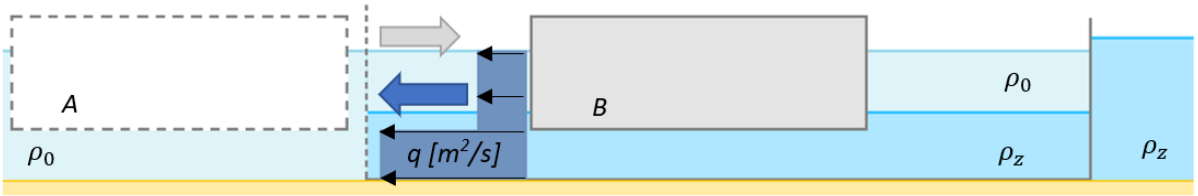

Figure 2.15: Schematization of a return current volume flux distribution according Schijf in combination with a stratified lock density; $\rho_z > \rho_0$. The transition of the ship from A to B is gradual.

3 Conceptual Model

Literature has been addressed for optimized descriptions of water displacements by sailing and the density distribution. Next, steps can be taken towards the conceptual lockage model. This chapter sets out the set-up of the model, the assumptions it relies upon, and the implemented processes and related equations. Instead of a homogeneous lock density, the conceptual model will make use a two-layer system. In addition, shipping will be applied gradually instead of instantaneous and will include the return current of the theory by Schijf. As will become clear, depression is neglected from Schijf's theorem, hence the implementation of sailing will be according to the continuity approach.

In the first part of this chapter, the set-up of the model is shown. Here, the focus will be on the lockage phases, the modelling domain, and water level variations due to tidal forcing. Next, the impact of the new descriptions of return currents and density distribution will be laid out in Paragraph 3.2. After this is covered, a short paragraph will follow which shows the implemented hydraulic processes in the conceptual model according to a similar structure as was applied in Chapter 2. This chapter then concludes with a descriptive schematization and outputs of the conceptual model.

3.1 Set-Up and Domain

To get the most reliable answer on the influence of the refined assumptions, the other aspects of the ZSF algorithm will be reproduced as much as possible. The principle behind the conceptual model is therefore like the ZSF: it simulates a lock volume and over the duration of a tidal cycle this volume will be subjected to different hydraulic processes. These processes affect the total amount of suspended salt in the lock and thereby the salt intrusion at lakeside. The lockage cycle is also divided into separate phases but does not include a separate lock exchange phase. This process will be carried out at the same time as the ship movements in lockage phases 2 and 4.

Lockage phases:

1	*Levelling to lakeside.*
2.a	*Exiting ship from lock to lakeside.*
2.b	*Entering ship in lock at lakeside.*
3	*Levelling to seaside.*
4.a	*Exiting ship from lock to seaside.*
4.b	*Entering ship in lock at seaside.*

Before going into the lockage phases, the domain of the model should first be described. As previously stated in Chapter 1, the case study of this research will be on the Krammer locks, depicted in Figure 1.2. This lock size will be the default for the conceptual model. It has dimensions of 280 metres in length, 24 metres in width and 6 metres in depth. The maximum ship class that can make use of this lock are ships of CEMT class: VIa, with dimensions of 135 meters in length, 18 meters in width, and 4 meters in draught. The water level at lakeside will remain unvaried at NAP+0,00m.

Figure 3.1 shows a schematization of the modelling domain of the conceptual model. As the conceptual model will make use of stratified lock, an initial condition for the interface depth (d_{int}) or interface height (h_{int}) must be specified. The gradient of this interface will be modelled linearly and horizontally throughout the lockage. This considerably reduces the complexity of the determination of the salt intrusion: the position of the interface over the lock and thus the density of discharged water will only depend on continuity of the saline and fresh volumes. The initial water volume in the lock is calculated according (2.9). The initial layer volumes of the two-layer system then follow according to the interface depth and the dimensions of the lock and the present ship, given by (3.2 & 3.3).

$$d_{int} + h_{int} = d \tag{3.1}$$

$$V_{fresh} + V_{saline} = V - V_s \tag{3.2}$$

$$V_{fresh} = \begin{cases} l * w * d_{int} - l_s * w_s * d_{int}, & d_{int} \leq d_s \\ l * w * d_{int} - V_s, & d_{int} > d_s \end{cases} \tag{3.3}$$

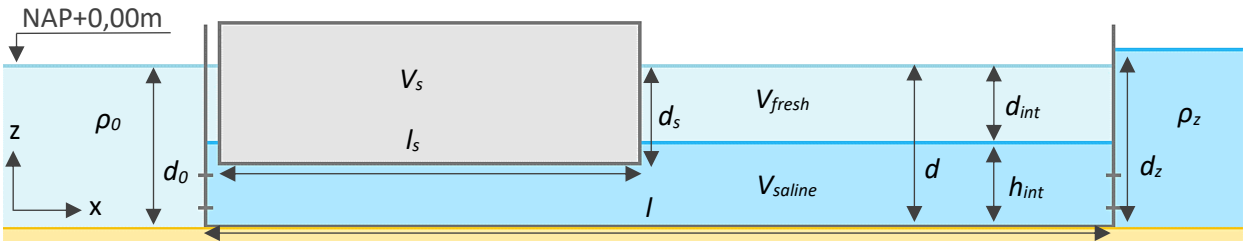

Figure 3.1: Initial situation of the simulation at t=0 with width dimensions in y-direction perpendicular to the image.

The axis-system depicted in Figure 3.1 will be used throughout this chapter. Here, the z-axis represents the vertical and the level $z = 0$ is set at water level at lakeside. Depths, given by d, will be calculated from NAP+0,00m ($z = 0$) downwards, thus positive depths are directed in the negative z-direction. The x-axis is parallel to the sailing direction. Because the axis system will mostly be used for describing the sailing process, the positive direction for the x-axis is ideally equal to the direction of the return current. Therefore, the orientation of the x-axis is chosen in such a way that it is opposite to the sailing direction and therefore changes with each sailing movement. This will be specified clearly for every equation provided throughout this chapter.

To include the tidal cycle, the water level for the lockage phases at seaside will be varied for consecutive lockages. This will be done by discretizing a sinusoidal curve over the amount of lockages per tidal cycle, as shown in Figure 3.2 for 10 lockages. The taken amplitude for the tidal cycle equals 1,5 meters. These values correspond to the Krammer locks.

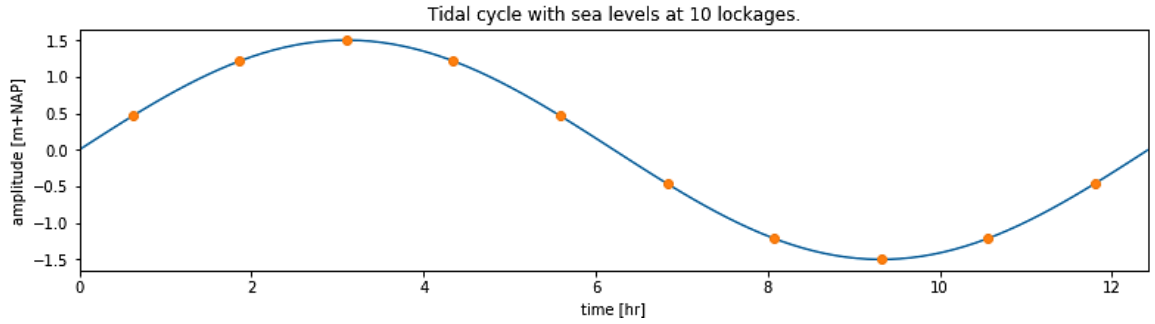

Figure 3.2: Tidal cycle discretized in several lockages equally far apart. The orange dots represent the water levels for consecutive lockages used for the conceptual model and the ZSF.

3.2 Implementations of New Descriptions

The $2L\Delta t$ assumptions will bring forth differences in the determination of the salt intrusion for all phases compared to the ZSF. For the levelling phases (*1 and 3*) this involves the influence of the stratification on the levelling process, whereas for the navigation phases (*2 and 4*) this is the contribution of shipping in a two-layer system. The changes in the determination process for levelling will now be addressed.

3.2.1 Two-Layer System

There are two distinct cases in the levelling process: high tide and low tide. During low tide, discharges are carried out towards seaside, whereas during high tide they are carried out to lakeside. Since the interest in this section lies in the influences of the two-layer model on levelling, it is convenient to consider separate cases of water entering and exiting the lock instead of the tidal phases. Therefore, the division in this section is made based on levelling up- and downwards.

3.2.1.1 Upward Levelling

During upward levelling, the incoming water is transported directly to the layer of corresponding density because of the two-layer model. During low tide, this holds that the interface height (measured from bottom to interface) remains unchanged, but both the interface depth and the lock depth increase. Similarly, during high tide the interface depth remains unchanged, and the interface height and the lock depth increase. This process is schematized in Figure 3.3 for both tidal phases.

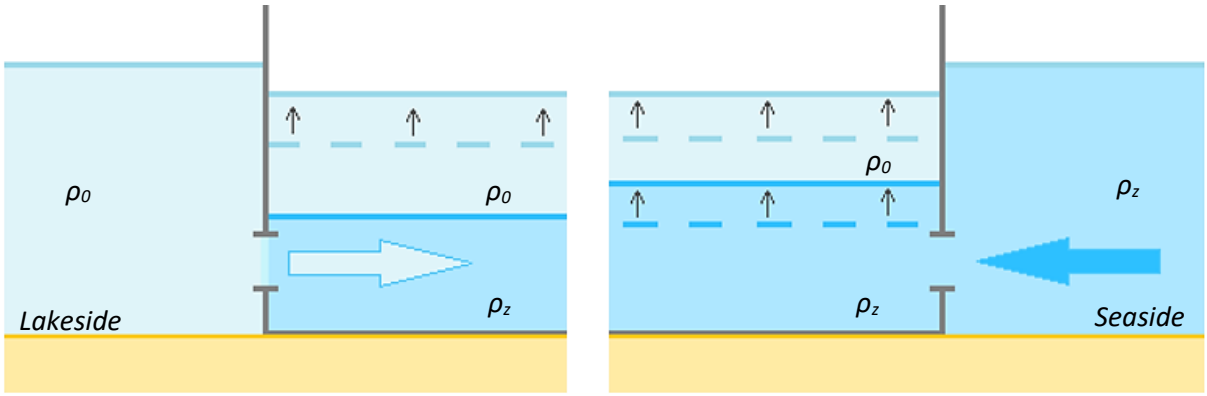

Figure 3.3: Schematization of upward levelling using a two-layer system during low tide: phase 1 (left) and high tide: phase 3 (right).

When the levelling process starts, the initial discharge (Q_{lvl}) is determined according (2.4). This discharge is then applied to fill the lock for a duration of Δt. After this duration, the model reevaluates the lock level and calculates a new discharge Q_{lvl}. This is reiterated until the lock reaches the appropriate level.

$$V_{lvl} = Q_{lvl} * \Delta t \tag{3.4}$$

The equations below list the changes to the lock volume in the conceptual model for each step size Δt for the cases of upward levelling shown in Figure 3.3. The accompanied amounts of salt intrusion can be calculated according (2.13 & 2.16).

$$LT: \quad 1: \quad d_{new} = d + \frac{V_{lvl}}{lw} \tag{3.5 \& 3.6}$$

$$1: \quad d_{int,new} = d_{int} + \frac{V_{lvl}}{lw}$$

$$HT: \quad 3: \quad d_{new} = d + \frac{V_{lvl}}{w * l} \qquad (3.7 \ \& \ 3.8)$$

$$3: \quad h_{int,new} = h_{int} + \frac{V_{lvl}}{lw}$$

3.2.1.2 Downward Levelling

During downward levelling, the density of the discharged volume follows from the implication of the two-layer model and the use of the lock valves. The amount of fresh and saline water that is discharged is determined by the depth of the interface and the elevation of the lock valves. The density of the discharged water is fully saline if the interface level is above the top of the lock valves, denoted by z_{tv} from 'top valve'. If the interface level reaches the bottom level of the valves, the discharged water is fully fresh, denoted by z_{bv} from 'bottom valve'. Between these two bounds, the ratio varies linearly between a fully fresh and saline density, as shown schematically in Figure 3.4. The attention is directed to the *black node* on the interface between the fresh and saline layers, which follows the green plot as the interface falls. This plot belongs to an axis system in which the discharge density plotted against the interface height.

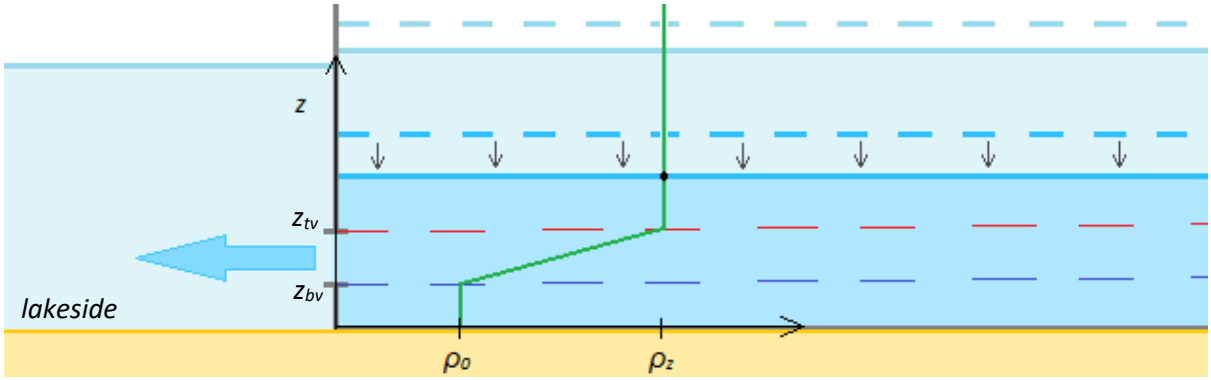

Figure 3.4: The bounds for determination of the discharge density during high tide: phase 1. As the interface falls, the green line shows the density of the discharged volume. The discharged water is fully saline for as long as the interface height remains above the top (z_{tv}) of the lock valves. Between the two valve bounds, the discharge will vary linearly between fully saline and fully fresh.

In the conceptual model downward levelling is implemented iteratively per step size Δt, likewise as the upward levelling process. The process is dependent on the values of z_{tv}, z_{bv}, and h_{int} (or $d - d_{int}$). The amount of salt mass intruded in lakeside (ΔM) per Δt then follows by multiplying the levelling volume and the salinity (3.11 & 3.13).

$$HT: \quad 1: \quad d_{new} = d - \frac{V_{lvl}}{lw} \qquad (3.9)$$

$if\ h_{int} > z_{tv}$:

$$HT: \quad 1: \quad h_{int,new} = h_{int} - \frac{V_{lvl}}{lw} \qquad (3.10 \ \& \ 3.11)$$

$$1: \quad \Delta M = V_{lvl} S_z$$

$if\ z_{tv} > h_{int} > z_{bv}$:

$$HT: \quad 1: \quad h_{int,new} = h_{int} - \frac{h_{int} - z_{bv}}{z_{tv} - z_{bv}} \frac{V_{lvl}}{lw} \qquad (3.12 \ \& \ 3.13)$$

$$1: \qquad \Delta M = V_{lvl}\left(\frac{h_{int} - z_{bv}}{z_{tv} - z_{bv}} S_z + \frac{z_{tv} - h_{int}}{z_{tv} - z_{bv}} S_0\right)$$

$if\ z_{bv} \geq h_{int}$:

$$HT: \qquad 1: \qquad h_{int,new} = h_{int} \tag{3.14}$$

It should be noted that this above section should not be employed during levelling phase 3 during low tide. In the model presented in this thesis, no account has been taken for the changes to the lock head densities because of levelling discharges (thus outside of the lock). This holds that for low tide, the discharged water on seaside (phase 3) does not contribute to the salt intrusion process (e.g., due to the pushing back of the discharged levelling volume at location of the lock heads by exiting ships). Only downward levelling during high tide, shown in Figure 3.4, plays a role in the amount of salt intrusion.

Other accompanied differences in computed salt intrusion using the two-layer system are found in the navigation phases. These will be explained in the next section together with the implementation of gradual sailing and the return current.

3.2.2 Gradual Shipping: Static Water Displacement

As was previously mentioned, shipping contributions can be divided in static and dynamic water displacements. Before going into the dynamic water displacement, (i.e. return currents), the static water displacement will be addressed. The implementation of gradual sailing, in combination with a two-layer system from this study brings forth an extra contribution to the static water displacement.

To explain the changes to the static water displacement, an entering ship in the lock will be considered here. As a ship enters the lock, water is repressed in front of the ship. If the draught of the ship is bigger than the depth of the interface, partially saline water is repressed. This water is redistributed over the saline layer of the lock. Local interface height variations are not considered as the interface is modelled horizontally as was brought up in Paragraph 3.1. This will eventually lead to a loss of continuity and therefore internal consistency.

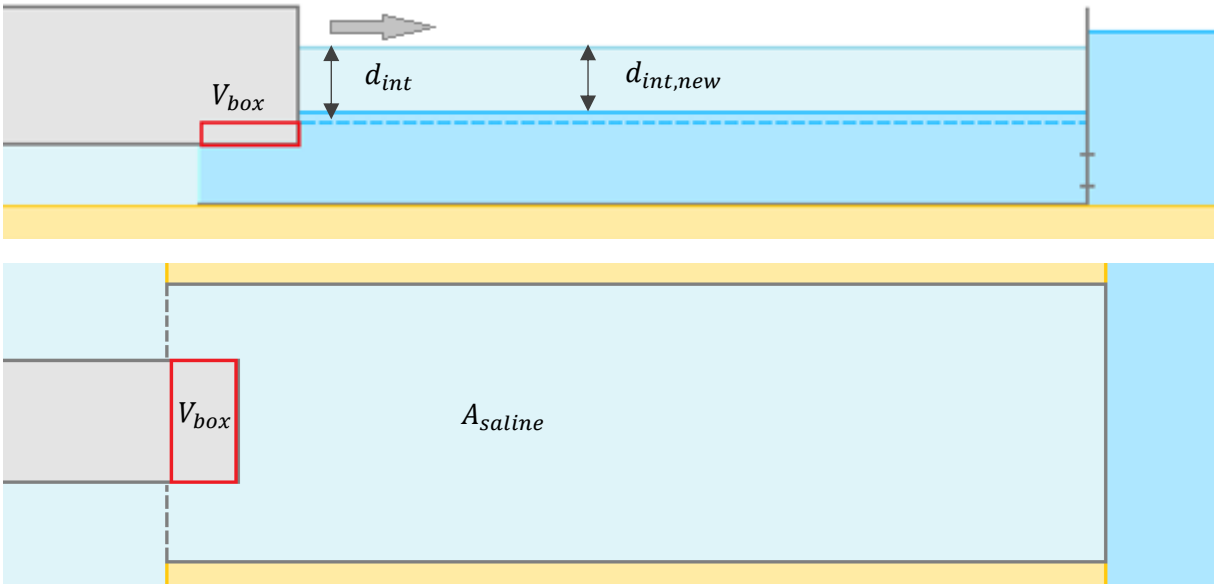

Figure 3.5: Schematization of interface increment or reduction during navigation. The top figure shows a ship entering the lock with a draught deeper than the interface. The bottom figure shows the same situation from a top view. The red box represents a volume V_{box} of saline water that is expelled by the presence of an incoming ship. The area of this saline layer is given by $A_{saline}(t)$.

To take this into account, the interface depth must be adjusted if the draught is deeper than the interface depth. For ships exiting the lock, the interface falls. Similarly, for ships entering the lock, the interface rises. These equations are determined based on Archimedes' principle and Figure 3.5. For ships entering the lock, equations $(3.15 - 3.17)$ are used. For ships exiting the lock, $(3.18 - 3.20)$ are applicable. h_{lock} in these equations represents the water level in the lock in meters above NAP. The factor $(d_s - d_{int} - h_{lock})$ is the part of the draught of the ship in the saline layer of the lock.

$$V_{box}(t) = (d_s - d_{int} - h_{lock}) * \left(\frac{t}{t_{pass}}\right) * (l_s * w_s) \tag{3.15}$$

$$A_{saline}(t) = (l * w) - \left(\frac{t}{t_{pass}}\right) * (l_s * w_s) \tag{3.16}$$

$$d_{int,new} = d_{int} - \left(\frac{V_{box}(t_n) - V_{box}(t_{n-1})}{A_{saline}(t_n)}\right) \tag{3.17}$$

V_{box} represents the volume in the saline layer that is expelled by an incoming ship. This volume needs to be redistributed over the remainder of the saline layer, of which the horizontal area is given by A_{saline}. The increment to the interface height is then determined by the difference in the volume of V_{box} between two consecutive modelling steps according (3.17). After the increment has been determined, other processes can influence the saline volume within the lock, for instance lock exchange. Therefore, (3.15) needs to be re-evaluated in each modelling step of the conceptual model.

For ships exiting the lock, $(3.18 - 3.20)$ are used.

$$V_{box}(t) = (d_s - d_{int} - h_{lock}) * \left(1 - \frac{t}{t_{pass}}\right) * (l_s * w_s) \tag{3.18}$$

$$A_{saline}(t) = (l * w - l_s * w_s) + \left(\frac{t}{t_{pass}}\right) * (l_s * w_s) \tag{3.19}$$

$$d_{int,new} = d_{int} + \left(\frac{V_{box}(t_n) - V_{box}(t_{n-1})}{A_{saline}(t_n)}\right) \tag{3.20}$$

It should be noted that these formulas also apply to boundary layers that only interfere with the draught of a ship halfway through the sailing process. This is due to the iterative natures of $(3.17\ \&\ 3.20)$, and the fact that V_{box} can only be positive. In this way, the utilization of $(3.17\ \&\ 3.20)$ is determined by the point in time when the interface level is above the ship's draught.

In addition to the adjustments in this section regarding the static water displacement for the navigation phases, an additional contribution to the rising and falling interface during levelling with fresh water is required as well. This can be explained with the help of Figure 3.6, which shows the lockage phase '*levelling to lakeside'* during low tide. As the lock is filled with fresh water, the ship is lifted from the interface layer. This results in an increment of the interface depth in case the draught of the ship (d_s) is greater than the height of the freshwater layer within the lock ($h_{lock} - d_{int}$), given by (3.21). This increment is not required for the other levelling processes, even for levelling to lakeside during high tide. This is because for all other levelling processes salt water is either removed or added to the lock, which results in the interface level rising or falling with an equal amount as the lock level, and thus the ship and its part in the saline water layer.

$$d_{int,new} = d_{int} + \frac{\frac{V_{lvl}}{lw} * l_s w_s}{lw - l_s w_s} \tag{3.21}$$

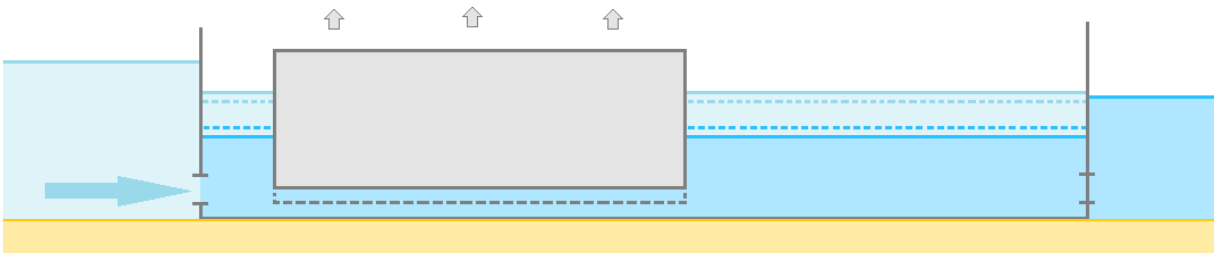

Figure 3.6: Schematization of levelling to lakeside. As the lock is being filled with fresh water, the ship rises with the water level such that the interface level falls.

In (3.21), the volume $\frac{V_{lvl}}{lw} * l_s w_s$ represents the volume that is created in the saline layer from lifting or lowering the ship over a duration of Δt. Subsequently, this volume needs to be filled with the surrounding saline water. Hence, the volume needs to be divided over the difference in area of the lock and the present ship ($lw - l_s w_s$).

3.2.3 Gradual Shipping: Dynamic Water Displacement

As will become clear in this section, the use of gradual navigation for application of the return current has an implication, namely the lock change must also be performed gradually. Therefore, when describing the implementation of the return current by Schijf, a short detour in this section must be made in subsection 3.2.3.3, which explains the gradual lock change. In order not to confuse the reader, an overview of this entire section will first be given.

First, in 3.2.3.1 the determination of the volume flux by return currents will be explained. Second, the distribution of salt mass flux by return currents for a ship entering from the lakeside will be explained in subsection 3.2.3.2. Third, a short break is required where the gradual lock exchange is described in 3.2.3.3 before the exiting of ships can be addressed. Finally, the resulting salt mass flux distribution by return currents for exiting ships is explained in subsection 3.2.3.4.

3.2.3.1 Volume Flux Distribution

The sailing of the ships is accompanied by a return current of which the magnitude can be determined by the theory of Schijf. To explain the effects of the implementation of Schijf's return current, the determination of the flux distribution must first be addressed. From subsection 2.1.3.1 it followed that the determination of the return current velocity (u_r) requires an iterative process, from its interdependence to the depression ($\bar{z}$). To be able to fully implement the determination of u_r in the conceptual model, the model must be able to perform this iteration with any combination of ship size, depth and sailing speed. This has proven to be a rather complicated process.

To simplify the determination process of the return current velocity in the conceptual model, the occurrence of depression next to the ship is neglected. By neglecting depression, the method by which Schijf defines the return current simplifies to the continuity equation which allows to determine the velocity noniteratively.

For explaining the derivation of this method, the axis system from Figure 3.1 will be used. The reader is reminded that depths are taken positive and $z = 0$ equals water level. The formulation of u_r (2.8) from Schijf is reproduced here for convenience.

$$\frac{u_r}{\sqrt{gd}} = \left[\frac{1}{\left(1 - \frac{A_s}{A_c}\right) - \frac{\bar{z}}{h}} - 1\right] * \frac{u_s}{\sqrt{gd}} \tag{3.22}$$

After assuming the depression ($\bar{z}$) equals zero and multiplying by $\sqrt{gd}$, (3.22) can be written as the following.

$$u_r = \frac{A_s}{A_c - A_s} * u_s \tag{3.23}$$

The specific discharge over depth by the return current then follows from multiplying the return current velocity (u_r) with the free width, defined by (3.25).

$$q_r(z) = u_r * w_{free}(z) \tag{3.24}$$

$$w_{free}(z) = \begin{cases} w - w_s, & 0 \geq z > d_s \\ w \quad , & d_s \geq z \end{cases} \tag{3.25}$$

To test if this description holds, continuity must be ensured. This is demonstrated by first integrating the return current distribution over the depth to obtain the magnitude of the full discharge distribution (Q). Because $w_{free}(z)$ is not continuous, (3.24) cannot simply be integrated. Therefore, this is determined according to an analytical process given by (3.27). The formulation can then be rewritten according (3.28) using algebra.

$$Q = \int_{-d}^{0} q_r(z)\, dz \tag{3.26}$$

$$Q = u_r * (w - w_s) * d_s + u_r * w * (d - d_s) \tag{3.27}$$

$$Q = u_r(A_c - A_s) \tag{3.28}$$

Multiplication of the total discharge with the passage time results in the total volume by the return current, also named primary wave, $V_{primary}$. By combining (3.23) with (3.28), it follows that the total volume is equal to the ship volume, thus indicating that continuity holds.

$$V_{primary} = Q * t_{pass} \tag{3.29}$$

$$t_{pass} = \frac{l_s}{u_s} \tag{3.30}$$

$$V_{primary} = A_s * l_s = V_s \tag{3.31}$$

3.2.3.2 Salt Mass Flux Distribution: Entering Ship

So far, this approach has only resulted in formulating a return current distribution, whereas the interest lies in the determination of the salt intrusion. To determine the salt mass transported by the return current, a description of the salinity over depth is required. For this, the layer height distribution of the two-layer model will be used. The left picture of Figure 3.7 helps in explaining this determination process for the conceptual model. This figure shows the two processes that are present during the lockage phase 2. *b: entering ship at lakeside*. The left picture shows the displacement of a ship into the lock for a duration Δt, resulting in a displacement Δx of $u_s \Delta t$. The return current from the ship's movement is shown by the flux distribution at location of the lock gate. For the determination of the transported salt mass, it is assumed that the part of the volume flux distribution which is in the saline layer is completely saline and therefore contributes to the salt intrusion. To ensure continuity using this assumption, the interface depth must be adapted according to the removed saline water volume (ΔV_{saline}) according (3.32 & 3.33).

$$\Delta V_{saline} = \int_{-d}^{-d_{int}} q_r(z) \Delta t\, dz \tag{3.32}$$

$$d_{int,new} = d_{int} + \frac{\Delta V_{saline}}{lw} \tag{3.33}$$

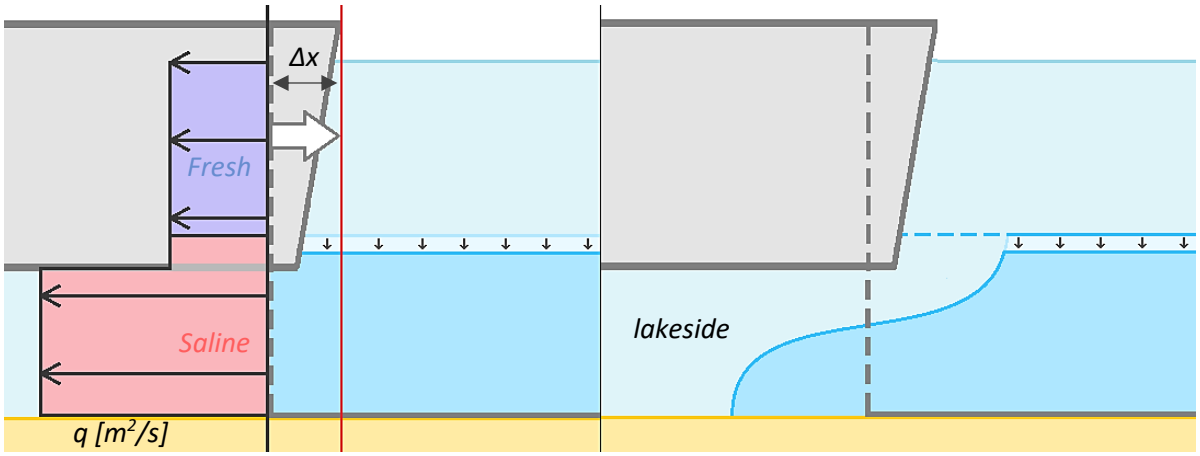

Figure 3.7: Schematization an entering ship from lakeside, with contributions to the salt intrusion by primary waves (left) and lock exchange (right). The displacement of the ship (left) is given by the white arrow, whereas during the lock exchange (right) the ship remains stationary. The distribution on the left represents the return current volume flux with saline flow (red) and fresh flow (blue) according to the interface depth.

Because the saline layer has a constant density, multiplication of ΔV_{saline} with the salinity of the saline layer (S_z) results in the intruded salt mass in lakeside.

$$\Delta M = \Delta V_{saline} S_z \tag{3.34}$$

After the duration Δt, the ship is displaced again whereby the new interface depth will be used to determine the new amount of salt intrusion. Before explaining the other direction of sailing, which is the exiting of a ship from the lock, it is important to consider the presence of the lock exchange.

3.2.3.3 Alternating Displacements Assumption

The total lock exchange cannot be calculated with one calculation step as in the ZSF, as this will result in large jumps in the salt mass present in the lock, and thus in large jumps in the interface depth. To take this into account, the lock exchange must be applied gradually as well. This subsection will focus on how this is carried out.

The lock exchange can be described using the relative lock exchange formulation, given by (2.6) and reproduced here for convenience (3.35). To be able to approach the lock exchange gradually according to this formulation, the time scale of the lock exchange must be discretized in individual computation steps of duration Δt (3.36).

$$U = \tanh\left(\frac{t}{t_{LE}}\right) \tag{3.35}$$

$$t_n = n * \Delta t \tag{3.36}$$

$$U_n = \tanh\left(\frac{t_n}{t_{LE}}\right) - \tanh\left(\frac{t_{n-1}}{t_{LE}}\right) \tag{3.37}$$

The amount of salt mass that is transported by the lock exchange must be removed from the lock to preserve continuity. This results in the new interface depth after duration Δt.

$$d_{int,new} = d_{int} + \frac{U_n V}{lw} \tag{3.38}$$

The gradual lock exchange, including the adapted interface depth, is shown on the right side of Figure 3.7. Both salt intrusion processes are dependent on the interface depth. Therefore, the processes must be applied in turn. This concept of applying a lock exchange and shipping displacements in turn will be referred to in this study as the *alternating displacements assumption*. This assumption holds that for the duration of sailing, the effects of lock exchange and return currents are applied alternately. As will become clear when describing the exiting of a ship from the lock in the next section, this assumption has a major influence on the calculated saline mass flux due to return currents.

3.2.3.4 Saline Mass Flux Distribution: Exiting Ship

The saline mass flux by return currents from a ship exiting the lock is dependent on the alternating displacements assumption. This can be explained according to the schematization of Figure 3.8. The saline volume flux in the right picture is obtained by assuming the part of the return current that is in the salt wedge, prior to the shipping displacement Δx, is fully saline. This salt wedge is shown in the left picture of Figure 3.8. It is assumed the height of the salt wedge, measured from the bottom, is approximately half the height of the saline layer, which equals $(d - d_s)/2$. By doing so, the effect of pushing back the salt tongue can be included in the determination of salt intrusion.

It should be noted, however, that the amount of salt being propelled back to the lock can never be greater than the amount of salt that entered lakeside by lock exchange prior to shipping. In the conceptual model, a limit is therefore imposed on the amount of transported saline volume to the lock ΔV_{saline}.

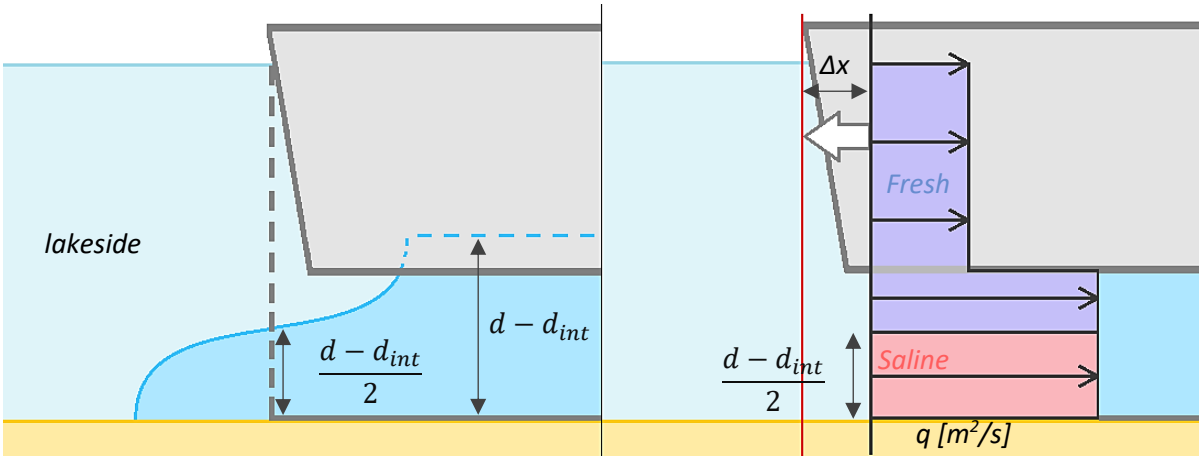

Figure 3.8: Schematization an exiting ship to lakeside, with contributions to the salt intrusion by lock exchange (left) and primary waves (right). The saline volume flux is determined according to the preceding lock exchange step.

$$\Delta V_{saline} = \int_{-d}^{-d+\frac{d_{int}}{2}} q_r(z)\Delta t \, dz \tag{3.39}$$

$$U_n V \geq \Delta V_{saline} \tag{3.40}$$

If the amount of transported saline volume is bigger than the volume of the salt wedge given by $U_n V$, the value for ΔV_{saline} will be limited to $U_n V$. Physically, this can be interpreted as having the entire salt wedge transported back to the lock by return currents. During sailing to seaside, the same principle is applied only this time it affects the extruded freshwater wedge near the top, shown in Figure 3.9.

$$\Delta V_{saline} = \int_{-\frac{d_{int}}{2}}^{0} q_r(z)\Delta t \, dz \tag{3.41}$$

$$U_n V \geq \Delta V_{fresh} \tag{3.42}$$

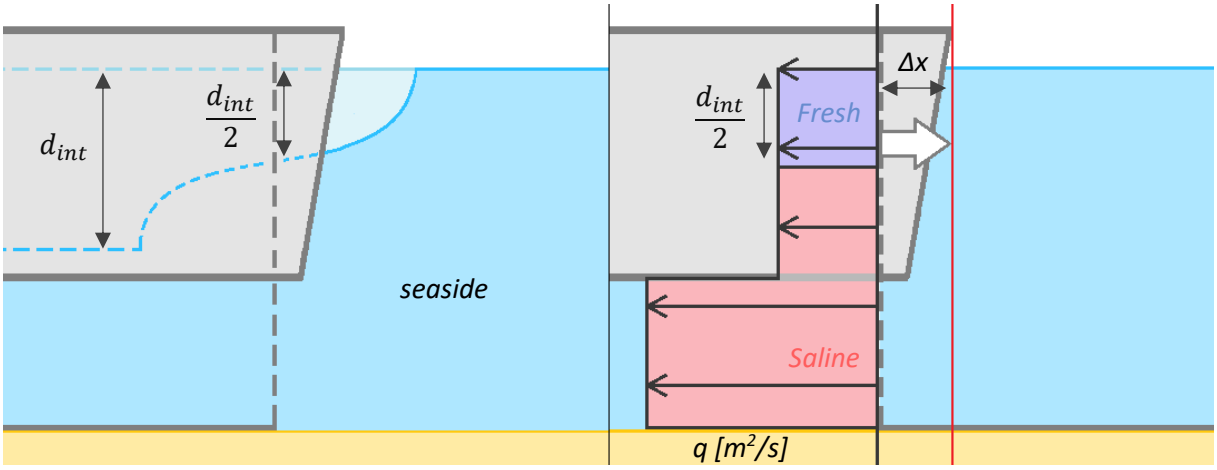

Figure 3.9: Schematization an exiting ship to seaside, with contributions to the salt intrusion by lock exchange (left) and primary waves (right). The saline volume flux is determined according to the preceding lock exchange step.

3.3 Outline of Computation

The previous paragraph has shown the implications of the new descriptions for the return current and the lock density on the computed salt intrusion. This paragraph summarizes the equations of the hydraulic processes and assumptions of the model in a similar structure as was used in Chapter 2. In addition, an overview of the model and lockage phases is provided at the end of this paragraph.

3.3.1 Hydraulic Processes

The processes that are relevant to this study are *levelling*, *lock exchange*, and *shipping displacements.* Levelling is carried out using the two-layer system and lock valves, and by using the assumption of alternating displacement, the return current can affect the salt tongue.

3.3.1.1 Levelling

The full levelling process can be explained according $(3.4 - 3.14)$ and (3.21).

3.3.1.2 Lock Exchange

According to the literature review, the hyperbolic tangent formulation is an accepted description of the lock exchange. To get a better understanding of the influences of the assumptions focused on in this study, the same formulation will be applied for lock exchange in the conceptual model, given by $(2.6 - 2.8)$. Following from subsection 3.2.2.3, this will be carried out gradually according $(3.35 - 3.38)$.

3.3.1.3 Shipping Displacements

In sections 3.2.2 and 3.2.3 the contribution of the return current to the salt intrusion has been covered thoroughly. For navigation, the gradual shipping implementation entails that the interface depth must be adapted according $(3.15 - 3.20)$. For a ship entering the lock, the changes to the lock volume and salt intrusion can be determined according $(3.32 - 3.34)$. For a ship exiting the lock, $(3.39 \,\&\, 3.40)$ are used for changes to the lock volume at lakeside and $(3.41 \,\&\, 3.42)$ are used for changes to the lock volume at seaside.

3.3.2 Assumptions

The key assumptions used for the conceptual model are all mentioned in this section. They can be divided in assumptions regarding the modelling domain, stratification, and shipping.

Assumptions regarding the domain:

- Water from seaside and lakeside outside of the lock have constant densities.
- The bottom levels of the lock heads and the lock are horizontal.
- Wind forcing and seaside wave forcing will be neglected.

Assumptions regarding shipping:

- Ship dimensions are based on CEMT shipping classes and taken rectangular with no slant hull.
- Ships sail with a constant speed of 60% of their limiting speed in the lock (see Appendix B).
- Only primary waves (return currents) regarding the movements of ships are considered.
- The velocity of the primary wave is constant over the depth according Schijf, resulting in a larger flux underneath the ship than next to the ship.
- The ship's return current is determined without accounting for depression, resulting in the continuity balance. According Schijf's diagram a depression of approximately 2,5% of the depth is present (see Appendix B).
- The salt mass flux by shipping is determined on the layer heights and flux distribution over depth in the two-layer system.
- Shipping is carried out gradual and alternately with the lock exchange.

Assumptions regarding stratification:

- Stratification is stable and no mass transfer between layers can occur.
- The pressure within the lock is hydrostatic because of the two-layer model.
- The densities of the layers in the lock are constant.
- The density of discharged water out of the lock during levelling will vary linearly between fully fresh and saline, as a function of the position of the lock valves and the depth of the interface.
- The interface between the layers is modelled linear and horizontal.
- The lock exchange is carried out gradually and according to the relative lock exchange.

3.3.3 Model Schematization

To show all modelling phases and processes, a schematization of the model is presented in a similar fashion as the ZSF in Figure 2.13, where the black arrows denote salt mass transports. Because it is complex to write a formulation for the salt intrusion by the new levelling implementation, the levelling salinity is here shown as S^*_{lvl} which is defined as the average salinity of the levelling volume over the duration of levelling. Likewise, the salinity $S^*_{primary}$ is defined as the average salinity of the transported volume by the primary wave for the duration of sailing. High tide and low tide situations are schematized in respectively Figures 3.10 and 3.11. Furthermore, in the navigation phases 2 and 4, the direction of sailing is indicated by the grey arrows.

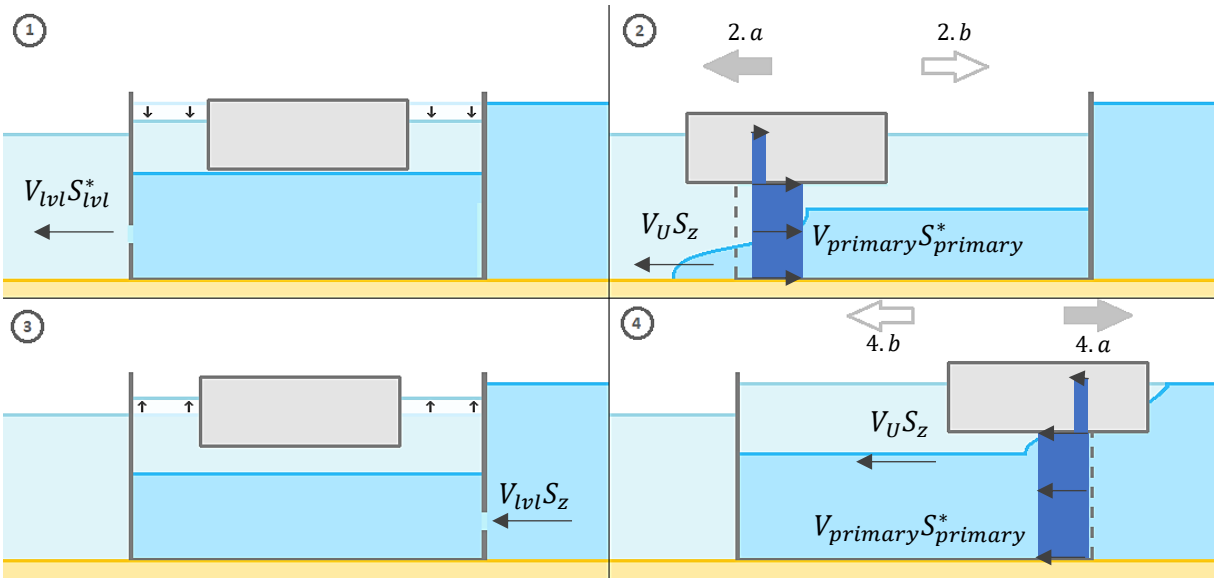

Figure 3.10: Schematization of the steps in the conceptual model during high tide. Salinities with an asterisk are to be determined iteratively with the conceptual model as no straightforward formulations can be set-up. Variations to the interface are not drawn in to promote readability.

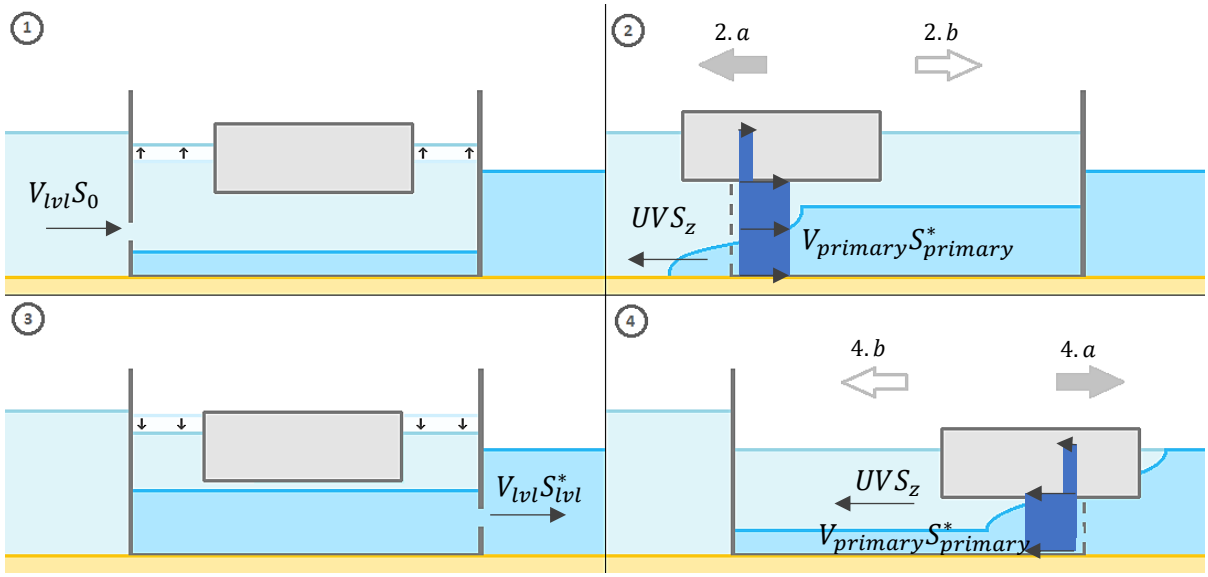

Figure 3.11: Schematization of the steps in the conceptual model during low tide.

The outputs and the assumptions of this study will from here on forward be referred to as $2L\Delta t$. The $2L\Delta t$ outputs are included in Appendix A.

4 Validation

To check whether the new assumptions have led to significant improvements in the accuracy of the ZSF, validation of the conceptual model is required. Unfortunately, validation data of salt intrusion from ships during lockages is scarce in literature. The focus of salt intrusion in locks in literature is strongly on the lock exchange. However, shipping was included during the experiments of the Stevin Locks [6] carried out in 2010, which is the only experiment found in the literature on shipping contributions to salt intrusion in locks. Although these were only measurements of a few ship movements, this chapter attempts to make a statement about improvements to the current formulation based on this experiment.

The first part of this chapter deals with the set-up and method of the experiment at the Stevin Locks. The second part of the chapter deals with the experiment data and its interpretation. The third part is devoted to the analysis of the experiment results. The aim here is to find the parameters needed to perform calculations with the conceptual model. Examples include sailing durations, ship dimensions, and initial conditions of salt masses in the lock. Finally, the experiment data will be reproduced using both the $2L\Delta t$ assumptions and the ZSF assumptions. This will then be used to determine whether the refined assumptions of this study have led to a significant improvement in the accuracy of parametrized salt intrusion.

4.1 Experiment Set-Up

During the experiments in 2010, the Stevin Locks were equipped with 25 salinity sensors in the same vertical plane. There are five sensors paired on vertically suspended strings, where the top three sensors are connected to floatation devices and the bottom two are connected to the lock bottom, shown in Figure 4.1 This creates a depth profile of the salinity represented by five sensors. The sensors then measure salinity variations over time. An estimate of the salt mass in the lock is obtained by multiplying the average salinity of all the sensors by the volume of the lock. The amount of transported salt mass in and out of the lock is then obtained from observed changes in salinity measurements for the time that either lock gate is open.

Similar strings were placed at location of the lock heads on either side, which allowed for measuring the salinity of outer waters as can be seen in Figure 4.2. This figure shows a measurement of the so-called steady state condition (i.e. prior to any activity) from which the boundary conditions of the densities can be read. Salinity measurements from this figure show that salinity differences over the lock are approximately 25 parts per thousand, or 25 kilograms per cubic meter.

$$V = 148{,}6 * 4{,}7 * 14{,}0 = 9778\ m^3 \tag{4.1}$$

As can be seen from Figure 4.1, the length of the lock is 148,6 meters and the water depth is 4,7 meters at NAP+0,0m. The width of the lock is 14,0 meters at location of the lock heads [6].

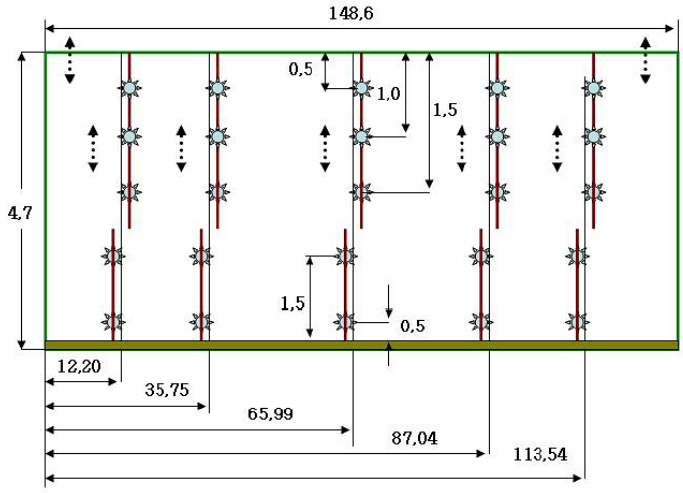

Figure 4.1: Places of 25 salinity sensors within the lock during the Stevin Locks experiments [6]. Lengths are shown in meters. It should be noted that this set-up is the exact same set-up as was used for generating Figure 2.11.

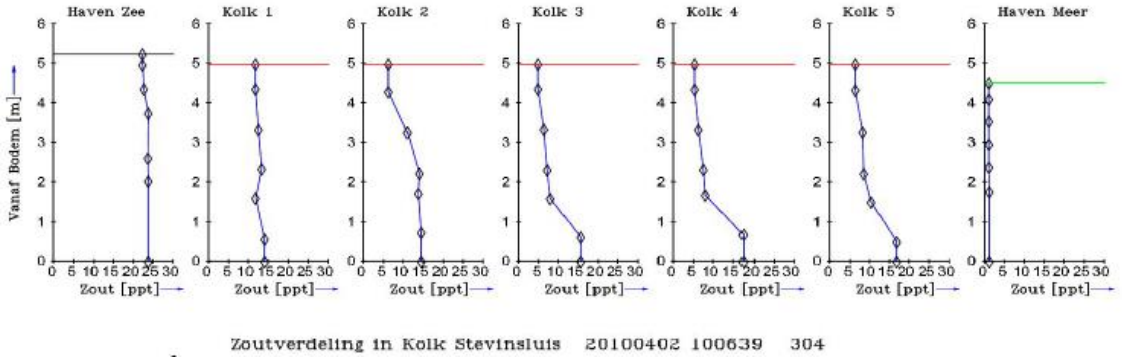

Figure 4.2: Salt concentration measurements at the Stevin Locks 3 minutes before opening of the lock gates. The salt concentrations at seaside and lakeside read respectively 25 ppt and 1 ppt.

4.2 Interpretation of the Measurements

Figure 4.3 shows the measurement data from the experiments on the 31st of March, which lasted between 17.30 and 20.00. They were carried out with five commercial vessels, of which their volumes and draught were known, listed here in Table 4.1 [6]. No exact values were given for the lengths and widths of the ships, but it was stated that they varied between 80 - 85 metres and 9,0 - 10,6 metres respectively.

The measurement data are a combination of three graphs, shown in Figure 4.3. By interpreting them separately, all data required for validation can be obtained. The function of each of the graphs and the data therein will now be explained.

Table 4.1: Properties and dimensions of sailing movements of graph 4.3 [6].

Ship Movement	***Direction***	***V_S [m^3]***	***d_s [m]***
'Uit 1'	From lock to seaside	*1920*	*2,8*
'Uit 2'	From lock to lakeside	*1000*	*1,5*
'Uit 3'	From lock to seaside	*1300*	*2,8*
'Uit 4'	From lock to lakeside	*2360*	*2,9*
'Uit 5'	From lock to lakeside	*1000*	*1,3*

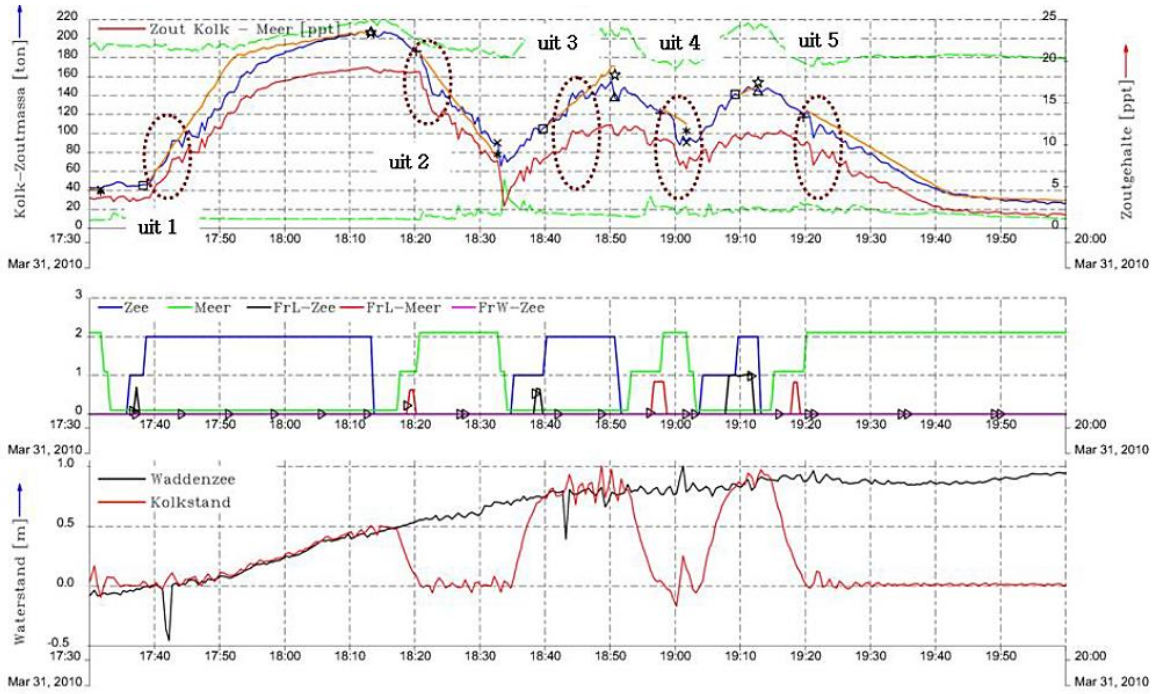

Figure 4.3: Measurements from shipping contributions to the amount of salt intrusion from the Stevin Locks experiments [6].

The *bottom* graph of Figure 4.3 shows the course of the water levels measured in meters above NAP in the lock in *red* and at seaside in *black*. The water level at lakeside is the IJsselmeer level and was constant at NAP+0,00m throughout the experiment [6]. This follows as well from the fluctuating red line around y = 0,0 m in the bottom graph of the measurements.

The *middle* graph of Figure 4.2 shows the possible lock gate stages on the y-axis of both lakeside and seaside. There are three stages for each lock gate. Stage *0* represents a door being closed, stage *1* represents the valves being open and stage *2* represents a lock gate being fully open. The *blue* plot in this graph is the lock gate stage at seaside and the *green* plot the lock gate stage at lakeside. The six smaller peaks below y = 1 in *black* and *red* show the application of bubble screens but will be disregarded for validation as they fall out of scope. However, as their presence is important, this will be discussed further in Chapter 6.

At last, the *top* graph in Figure 4.3 shows the estimates of suspended salt mass within the lock using the salinity sensors set-up as shown in Figure 4.1. This graph shows two y-axes. The y-axis on the right indicates the average salinity within the lock expressed in parts per thousand. This axis belongs to the *red* plot of the graph, which shows the course of the average of the salinities of the 25 sensors. The left y-axis indicates the salt mass within the lock in tonnes of suspended salt, which is obtained by multiplying the average salinity over the sensors (thus the *red* plot) with the volume of the lock (4.1). This is shown by the *blue* plot in the graph. It should be noted that this volume is calculated based on an empty lock, thus no volume reduction because of a present ship is accounted for in the *blue* plot. The *orange* plot is a so-called theoretical plotter which attempts to approach the salt mass in the lock throughout the experiments, of which the equation is given by (4.2) [6]. The speed of the present salt wedge for the theoretical plotter for opening the lock gates to seaside ($c_{th,z}$) is given by (4.3). For opening doors to lakeside, (4.4) is applied ($c_{th,0}$). Lastly, the *green* plots near the top and bottom are the bounds of the salt mass that can physically be present in the lock.

$$\Delta M_{th} = c_{th} * w * t * \Delta S \tag{4.2}$$

$$c_{th,z} = \frac{\rho_z - \rho_{mix}}{0.5(\rho_z + \rho_{mix})} \tag{4.3}$$

$$c_{th,0} = \frac{\rho_{mix} - \rho_0}{0.5(\rho_0 + \rho_{mix})} \tag{4.4}$$

The ship movements out of the lock are shown by the five dotted circles in the *top* graph, labelled 'uit' (translated: out). Five ship movements can thus be discerned. All these ship movements are ships exiting the lock, either to lakeside or seaside. The publication by Deltares did not mention ships entering the lock, nor are they visible from the measurements. At this time, this will not be addressed and will be further elaborated upon in the discussion in Chapter 6. Therefore, attention will only be paid to the exit of the ships in the five indicated areas.

4.3 Examination of the Measurements

Before the results of the experiments can be reproduced for both the ZSF - and the $2L\Delta t$ assumptions of this study, the measurements of Figure 4.3 must be examined for finding the required parameters to run the model. This procedure will be laid out now for ship displacement: 'uit 1'. The key parameters of the remainder of ship displacements will only be listed in a table.

The key parameters are the duration between the lock gates being open and the ship reaching either gate for exiting ($t_1 - t_0$), the duration between the ship reaching either gate and having sailed out completely ($t_2 - t_1$), the salt masses in the lock at these points in time (M_0, M_1, M_2), and the dimensions of the ships (l_s, w_s, d_s). General parameters (i.e. applicable to all simulations) include lock dimensions (l, w, d) and the water densities at both lock boundaries (ρ_0, ρ_z).

The points in time for the first sailing movement are indicated in Figure 4.4. This next section will elaborate on how this has been determined.

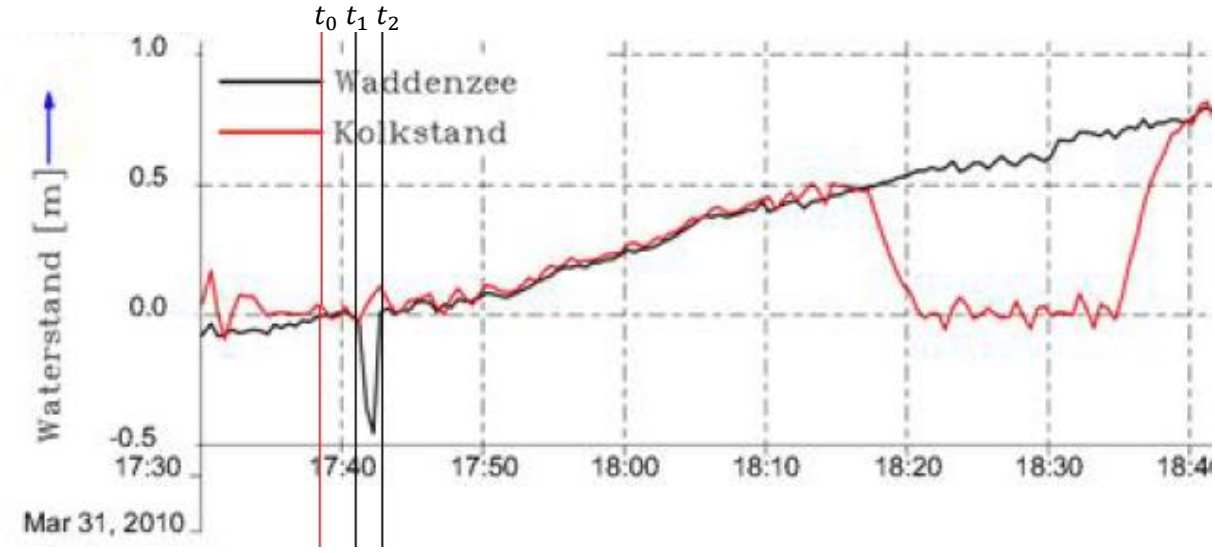

Figure 4.4: Estimate of sailing duration of ship 1. The horizontal difference in vertical black lines read a duration of approximately 1,9 minutes on the x-axis, which equals approximately 110 seconds. The water level at seaside for this duration is approximately constant at NAP+0,00m.

First, the length and width of the ship are estimated from dividing the given ship volume from Table 4.1 by its draught (4.5).

$$V_s/d_s = l_s w_s = 6{,}9 * 10^2\ m^2 \tag{4.5}$$

$$l_s = 80\ m, \qquad w_s = 8{,}6\ m$$

It should be noted that the length and width following from (4.5) are an estimate. This was made based on the result of the product of the length and width scales of the vessel, and the assumption that the vessel dimensions roughly correspond to the existing classifications of European inland navigation vessels (CEMT) [14].

Second, the duration of sailing through the lock gates ($t_2 - t_1$) can be determined from the bottom graph in Figure 4.3 and is shown in Figure 4.4. The depression due to sailing can clearly be seen from the water level measurements at seaside in this figure. From the length of the vessel and the duration of sailing, the sailing velocity can subsequently be determined. The velocity determined from this figure has been rounded to a single significant digit due to the rough time scales.

$$u_s \approx 80/100 = 7 * 10^{-1}\ m/s \tag{4.6}$$

The point in time when the doors can be considered fully open is given by the *red* line and time t_0. This is determined by placing the red line midway between lock gate phases 1 and 2, shown in Figure 4.5. The *black* lines that have been added (t_1, t_2) to the graph represent the sailing duration which followed from Figure 4.4. When extending these points in time to the top graph and reading off their respective crossing points with the measurement data of the *blue* plot (M_0, M_1, M_2), the amounts of intruded salt for the duration of sailing can be determined.

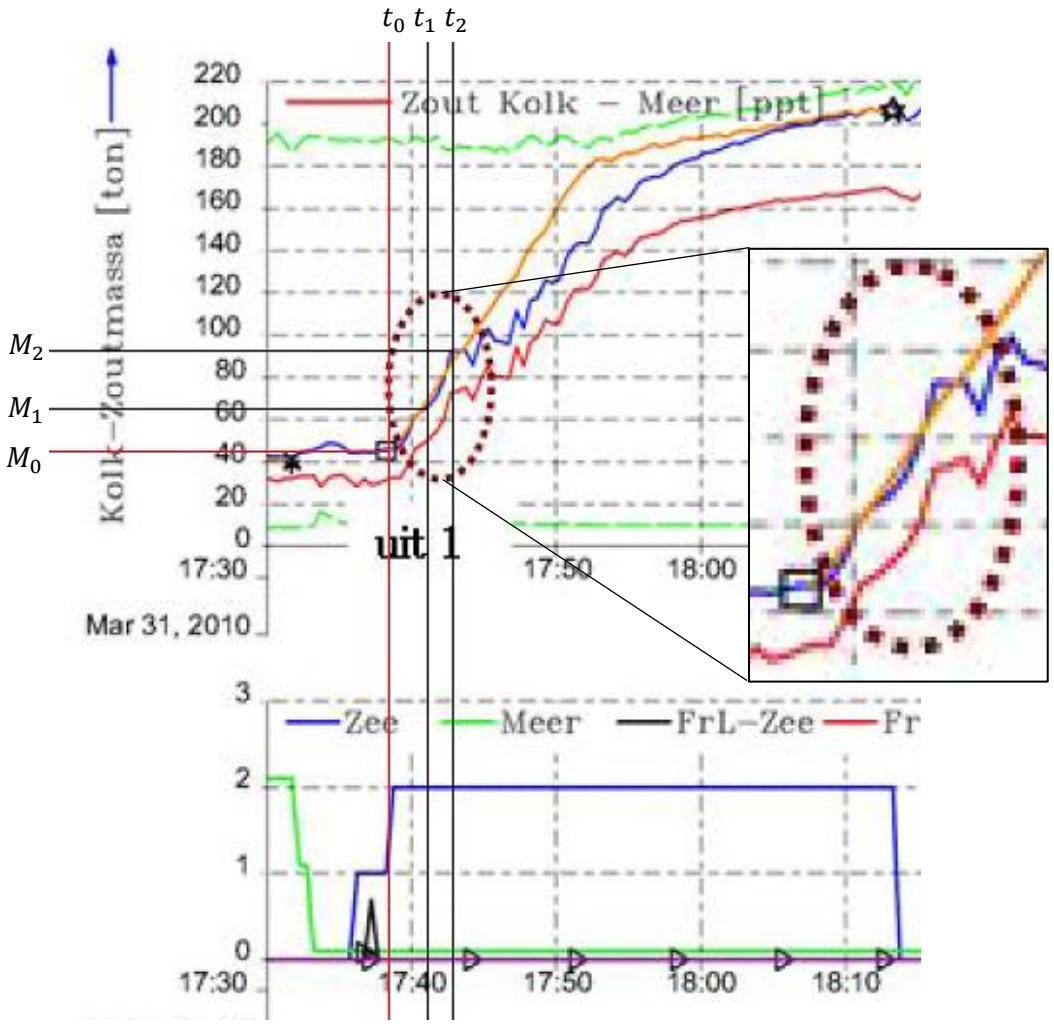

Figure 4.5: Estimate of amount of transported salt by shipping for ship 1. The red vertical and horizontal lines represent the point the doors are open, which is placed halfway the values of 1 and 2 of the gate phases in the bottom graph. The black lines represent the beginning and end of the sailing movement through the lock gates.

The resultant key parameters for ship movement 'uit 1' are listed in Table 4.2. The interface depth is calculated according to the salt mass present prior to shipping ($t = t_0$), (4.7). The homogeneous lock salinity for modelling with the ZSF assumptions is determined according (4.8).

$$d_{int} = d\left(1 - \frac{M_0}{V(\rho_z - \rho_0)}\right), \qquad S_{mix} = \frac{M_0}{V - V_s} \tag{4.7 \& 4.8}$$

$$d_{int}^{+} = \frac{10^3 * \Delta M_0}{\rho_z - \rho_0} * (lw - l_s w_s)^{-1} \tag{4.9}$$

When determining the depth of the interface according to (4.7) the presence of a ship is not considered in cases where its draught is greater than the depth of the interface. This is not correct. However, a simple closure could not be found here whereby the interface can be calculated directly for cases with a ship's draught deeper than the interface depth. Therefore, this is done indirectly by using an increment to the interface depth (d_{int}^{+}), given by (4.9). This is determined based on the deviations of initial salt masses (ΔM_0) in tonnes between the conceptual model and the results of the experiments. A similar approach to finding the key modelling parameters have been applied to the other four ship movements. Their values for all sailing movements are included in Table 4.2. The general parameters are included in Table 4.3.

Table 4.2: Key parameters of ship movements 'uit 1' to 'uit 5' from the Stevin Locks experiments.

Parameter	*Value for 'uit 1'*	*Value for 'uit 2'*	*Value for 'uit 3'*	*Value for 'uit 4'*	*Value for 'uit 5'*
Direction	From lock to sea	From lock to lake	From lock to sea	From lock to lake	From lock to lake
V_s [m³]	*1920*	*1000*	*1300*	*2360*	*1000*
d_s [m]	*2,8*	*1,5*	*2,8*	*2,9*	*1,3*
l_s [m]	*80*	*80*	*65*	*90*	*85*
w_s [m]	*8,6*	*8,3*	*7,0*	*9,4*	*9,0*
$t_1 - t_0$ [s]	*150*	*20*	*160*	*120*	*40*
$t_2 - t_1 = t_{pass}$ [s]	*110*	*110*	*60*	*100*	*80*
u_s [m/s]	*0,7*	*0,7*	*1,1*	*0,9*	*1,0*
h_z [m+NAP]	*0,00*	-	*0,75*	-	-
M_0 [tonnes]	*44*	*185*	*108*	*122*	*122*
M_1 [tonnes]	*64*	*180*	*118*	*110*	*118*
M_2 [tonnes]	*94*	*141*	*140*	*88*	*106*
d_{int} (t= t_0) [m]	*3,85*	*1,14 + d_{int}^{+}*	*2,62 + d_{int}^{+}*	*2,34 + d_{int}^{+}*	*2,35*
S_{mix} (t= t_0) [kg/m³]	*4,5*	*18,9*	*11,0*	*11,8*	*12,5*

Table 4.3: General parameters of Stevin Locks experiments for modelling with the conceptual model.

Parameter	*Value*
l [m]	*148,6*
w [m]	*14,0*
d [m]	*4,7*
V [m³]	*9778*
ρ_z [kg/m³]	*1025*
ρ_0 [kg/m³]	*1001*
h_0 [m+NAP]	*0,0*

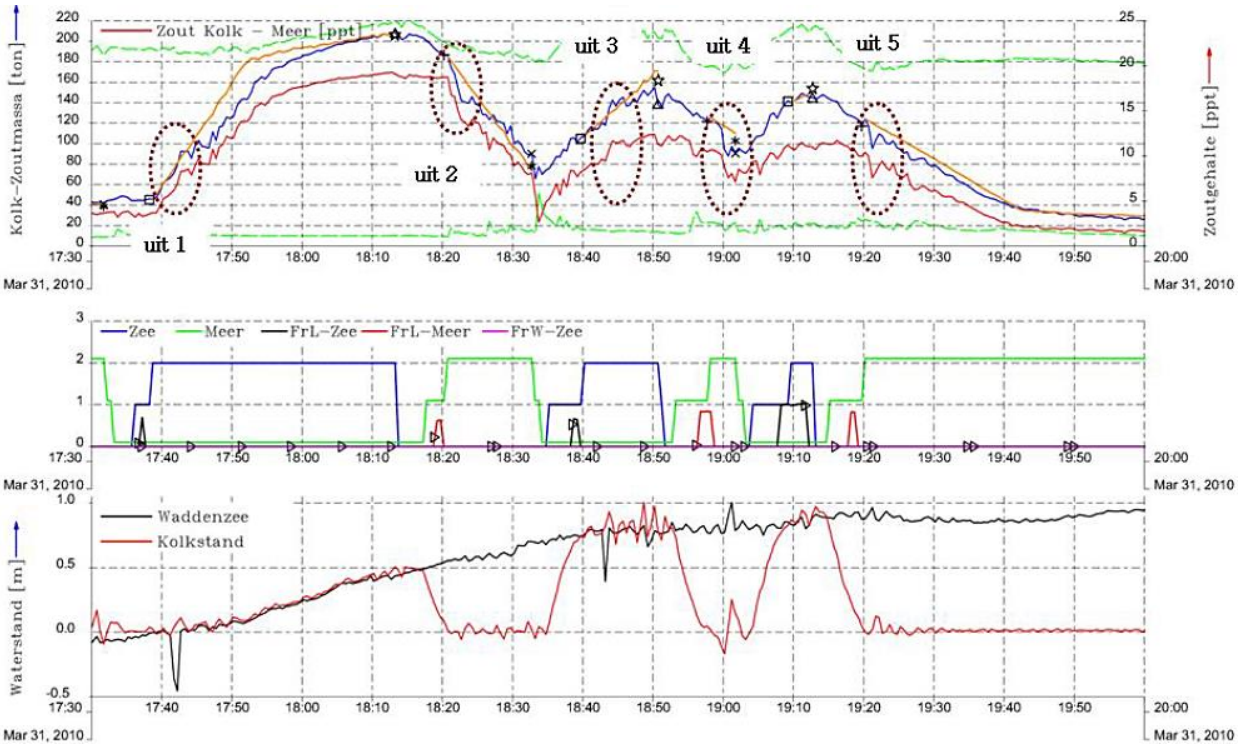

Figure 4.6: Measurements from shipping contributions to the amount of salt intrusion from the Stevin Locks experiments [6], reproduced for convenience of the reader.

4.4 Reproduction of the Measurements

Now all parameters for the computations are known, the sailing scenarios 'uit 1' to 'uit 5' can be recreated using the conceptual model for both sets of assumptions. The outputs of these computations are shown in Figures 4.7 to 4.11 of this paragraph. Each figure shows the courses of the salt mass in the lock using the approximation by the ZSF assumptions with a *dashed red* plot, the approximation by the $2L\Delta t$ assumptions with a *blue* plot, and the theoretical plotter of Figure 4.6 in *orange*. Additionally, each figure includes a corresponding segment of Figure 4.6, the original data, for comparison. The relevant durations of t_0, t_1, and t_2 are indicated here with vertical lines. In the figure segments of Figure 4.6, the red line corresponds to salinity measures. It is emphasized that the red line in these segments should not be compared with the *dashed red* plot of the outputs of the ZSF assumptions. In addition to the segments, the relevant salt mass values M_0, M_1, and M_2 for assessment of each modelling approach are included in a separate table beside each figure.

The salt mass M_0 is used as initial condition for the computations. For the duration given by $t_1 - t_0$ the lock will only be subjected to lock exchange, hence results using the conceptual model and the ZSF will be the same. As point in time t_1 approaches, the model will take account of shipping for the duration of $t_2 - t_1$ for both modelling approaches. Several minutes after point in time t_2 are included in the graphs, such that the comparison of the general trend of both modelling approaches to the Stevin Locks experiment segments is more convenient.

Ship displacement 'uit 1'

The simulation gives a reasonable approximation of the course of the salt mass. During the passage time between t_1 and t_2 the blue plot ($2L\Delta t$) approaches the experiments with more accuracy than the ZSF assumptions. What is remarkable is the underestimation of the amount of salt intrusion prior to shipping (duration between time points t_0 and t_1). This will be discussed further in the preliminary conclusion of this chapter.

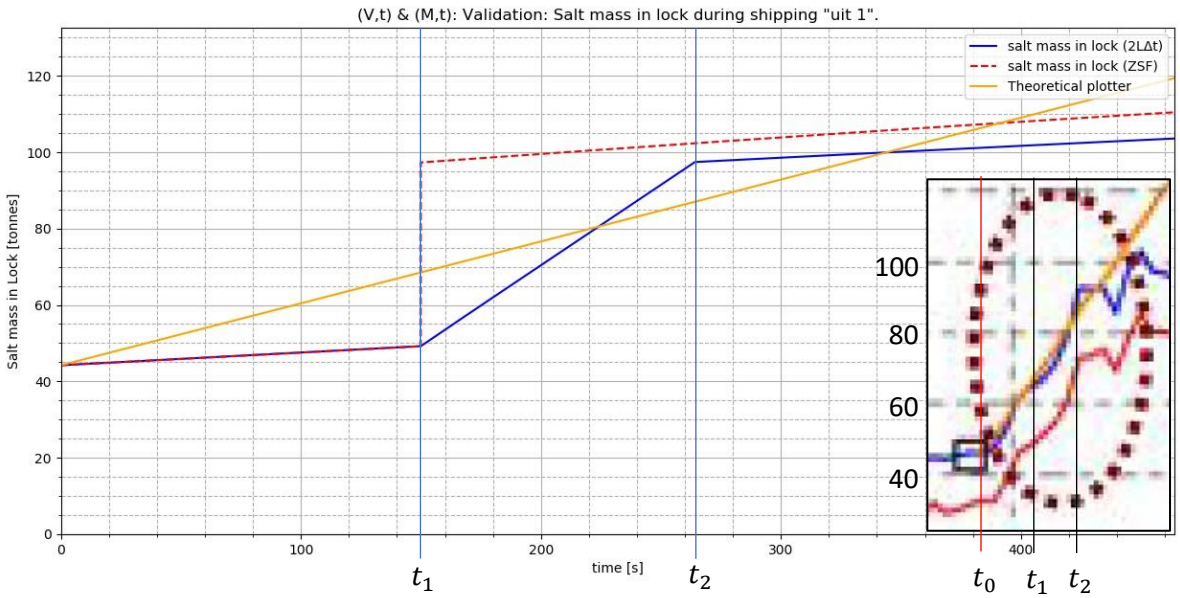

Figure 4.7: Modelling of validation case 1: 'uit 1' with the conceptual model in blue (2LΔt) and the ZSF in red. The theoretical plotter from Figures 4.3 and 4.5 is added in orange. The time stamps t_0, t_1 and t_2 correspond to respectively the points in time when the lock gates can be considered fully open, a present ship starts passing the lock gates and when a ship has completely left the lock.

Table 4.4: Relevant salt masses of the Stevin Locks experiments and computations with the conceptual model for validation.

'Uit 1'	*Experiment*	*Computation (ZSF)*	*Computation (2LΔt)*
M_0 [tonnes]	*44*	*44*	*44*
M_1 [tonnes]	*64*	*50*	*50*
M_2 [tonnes]	*94*	*102*	*98*

Ship displacement 'uit 2'

Because the present ship: 'uit 2' has a draught greater than the interface depth (listed in Table 4.3), using an interface depth based on an empty lock results in deviations to the initial salt mass M_0 of 185 tonnes from the Stevin Locks experiments. Therefore, an increment to the interface depth is required, given by d_{int}^{+}, determined according (4.9) as was mentioned in the previous paragraph.

$$d_{int}^{+} = -164\ mm \tag{4.9}$$

It is seen from Figure 4.8 that the conceptual model slightly underestimates the gradient of the course of salt mass here in comparison to the ZSF assumptions. From this it is cautiously stated that the exchange flow during sailing to lakeside is of a larger magnitude than assumed in the conceptual model. This means that the salt tongue may not be largely pushed back by the return current of an exiting ship, as assumed in the conceptual model. This will too be discussed further in the preliminary conclusion of this chapter.

Table 4.5: Relevant salt masses of the Stevin Locks experiments and computations with the conceptual model for validation.

'Uit 2'	*Experiment*	*Computation (ZSF)*	*Computation (2LΔt)*
M_0 [tonnes]	*185*	*185*	*185*
M_1 [tonnes]	*180*	*180*	*180*
M_2 [tonnes]	*141*	*145*	*155*

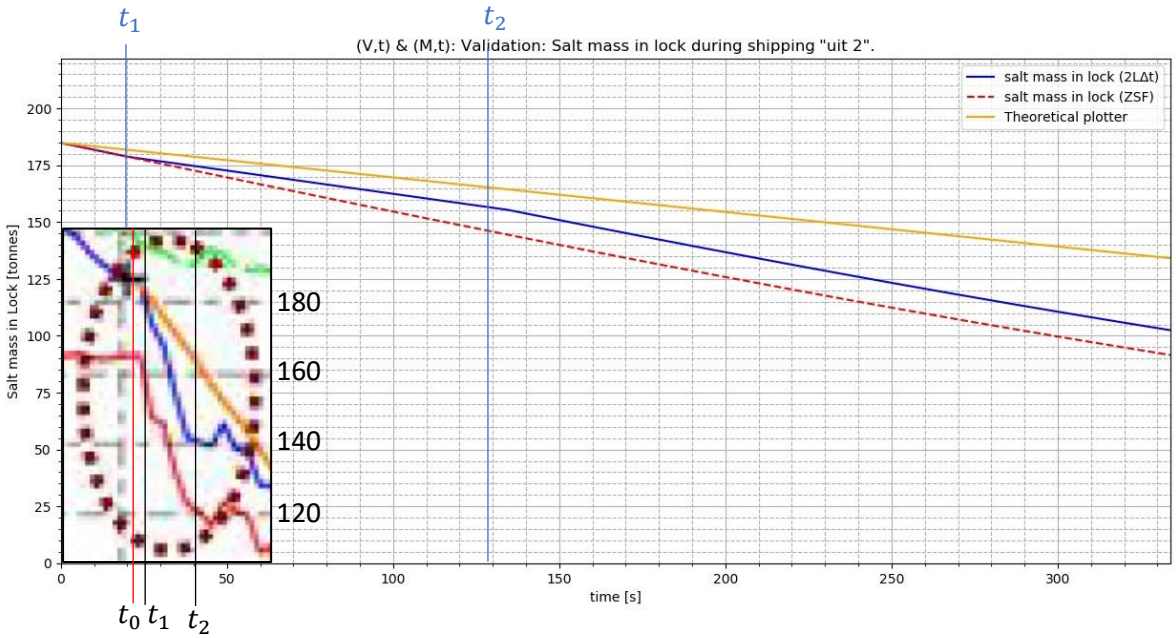

Figure 4.8: Modelling of validation case 2: 'uit 2'.

Ship displacement 'uit 3'

Ship displacement 'uit 3' and 'uit 1' have the same sailing directions. From the computation of ship movement 'uit 3' it can be concluded that the deviations between the experiments and the conceptual model ($2L\Delta t$) are larger than for ship movement 'uit 1'. As both ships have the same draught, it is expected that this deviation has to do with the differences in total ship volume (*1920 m^3* vs. *1300 m^3*). This could be explained by the presence of the propeller jet. After all, a larger ship needs a larger propeller thrust to accelerate and start, hence larger deviations between experiments and the conceptual model. This will be elaborated upon further in the preliminary conclusion of this chapter. Nevertheless, it is seen that the blue line approximates the experiments with more accuracy than the ZSF assumptions.

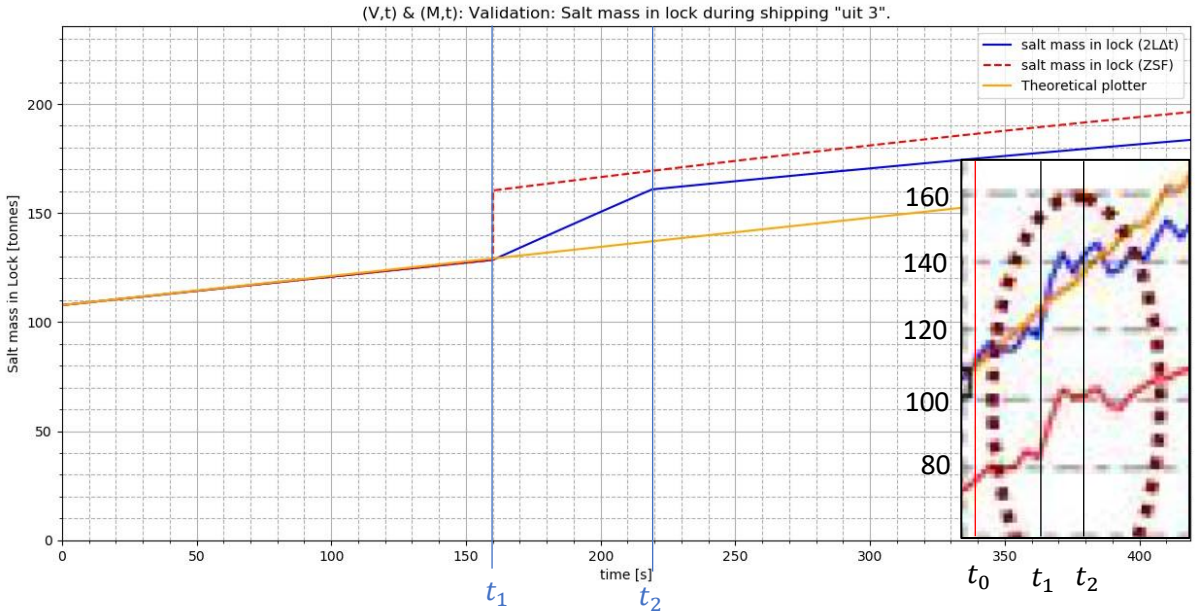

Figure 4.9: Modelling of validation case 3: 'uit 3'.

Table 4.6: Relevant salt masses of the Stevin Locks experiments and computations with the conceptual model for validation.

'Uit 3'	*Experiment*	*Computation (ZSF)*	*Computation (2LΔt)*
M_0 [tonnes]	*108*	*108*	*108*
M_1 [tonnes]	*118*	*116*	*116*
M_2 [tonnes]	*140*	*167*	*159*

Ship displacement 'uit 4'

The dimensions of ship 'uit 4' can be considered large, hence the larger required interface depth increment (d_{int}^{+}) to adjust the initial salt mass to M_0.

$$d_{int}^{+} = -366\ mm \tag{4.9}$$

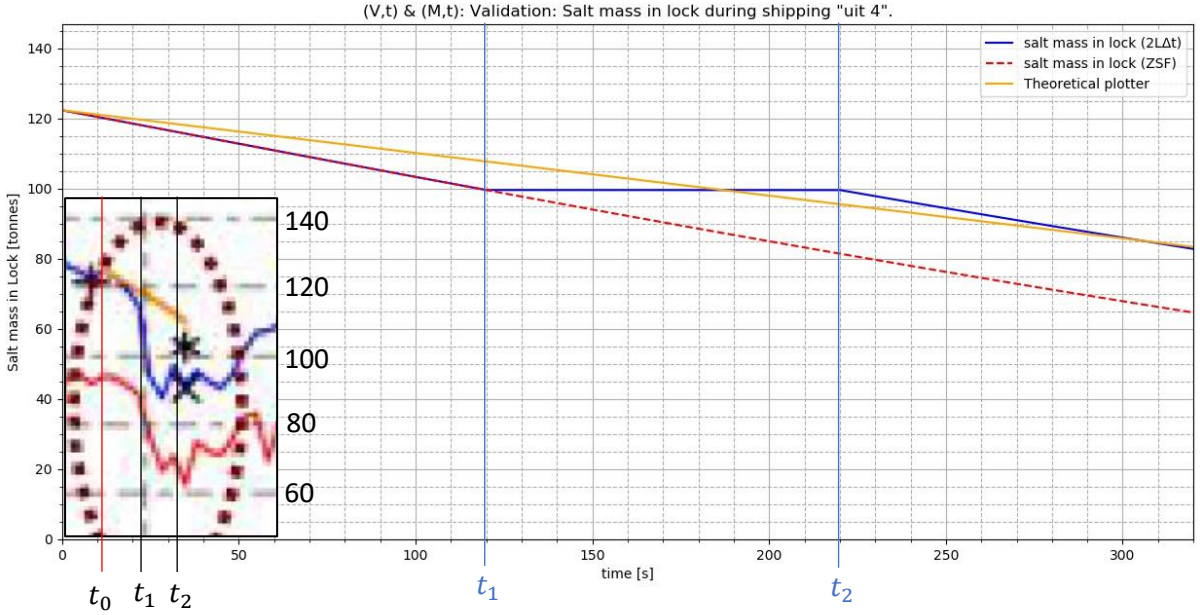

Figure 4.10: Modelling of validation case 4: 'uit 4'.

Table 4.7: Relevant salt masses of the Stevin Locks experiments and computations with the conceptual model for validation.

'Uit 4'	*Experiment*	*Computation (ZSF)*	*Computation (2LΔt)*
M_0 [tonnes]	*122*	*122*	*122*
M_1 [tonnes]	*110*	*100*	*100*
M_2 [tonnes]	*96*	*82*	*100*

Upon examination of the original experiment data of 'uit 4' it is seen that the salt mass in the lock greatly decreases because of a ship entering lakeside. This effect is not represented in both the ZSF and the two-layer assumptions (*red* and *blue* plot) from Figure 4.10. It is therefore expected that this is due to the propeller jet, which in practice must expel a large amount of water to accelerate. This would be in-line with previous observations, where the deviations between experiments and models are larger for increasing ship sizes. Furthermore, during passing of ship 'uit 4' the experiments show the salt mass within the lock appears to follow a horizontal trend. This trend can also be seen in the $2L\Delta t$ plot from Figure 4.10, whereas the ZSF assumptions estimate a linearly decreasing course of salt mass. It is therefore thought that apart from the initial drop in salt mass, the conceptual model approaches the general trend of the experiments with more accuracy than the ZSF assumptions.

Ship displacement 'Uit 5'

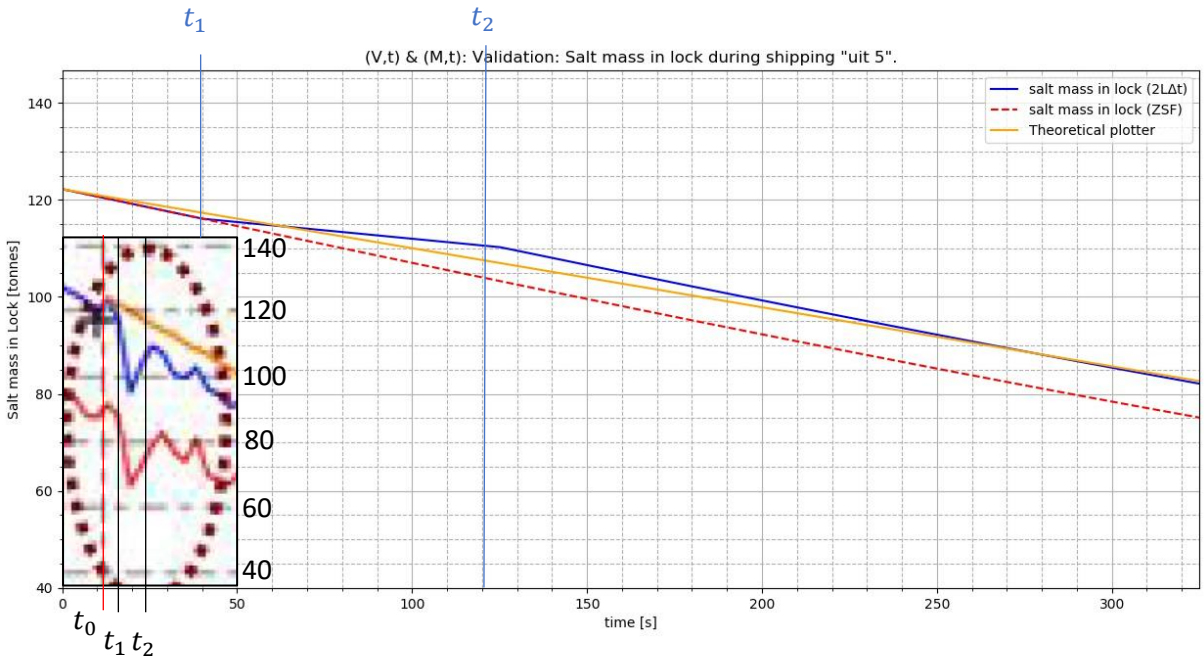

Figure 4.11: Modelling of validation case 5: 'uit 5'.

Table 4.8: Relevant salt masses of the Stevin Locks experiments and computations with the conceptual model for validation.

'Uit 5'	*Experiment*	*Computation (ZSF)*	*Computation (2LΔt)*
M_0 [tonnes]	*122*	*185*	*185*
M_1 [tonnes]	*118*	*117*	*117*
M_2 [tonnes]	*108*	*104*	*110*

From Figure 4.11 similar results as Figures 4.8 and 4.10 (same directions) are obtained: the conceptual model underestimates the salt flux from an exiting ship to lakeside. The results for this computation show that the ZSF assumptions tend to approach the quantification of salt mass at the Stevin Locks experiments with more accuracy than the $2L\Delta t$ assumptions, as the plots seem closer to the experiments. This is because the ZSF assumptions generally lead to larger salt fluxes, as could be seen from validation cases 1 to 4. However, the general trend of the course of the salt mass in the lock is approximated for the cases 'uit 1' to 'uit 5' by the refined assumptions ($2L\Delta t$). In the conclusion of this chapter, besides an assessment of the validation, the reason for this deviation will be discussed.

4.5 Preliminary Conclusion

In this chapter, measurements from salt intrusion experiments during sailing in the Stevin Locks were simulated with the conceptual model for both the assumptions of this study ($2L\Delta t$) and those of the ZSF. The aim was to show improvements in the sailing contributions of the ZSF resulting from the assumptions of this study. The most important computational parameters of these experiments are reproduced in Table 4.9. To compare the outcomes of both modelling approaches, the amounts of intruded salt mass for the sailing duration ($t_2 - t_1$) for the experiments and the computations are given in Table 4.10.

Table 4.9: Key parameters of the experiments for relating discrepancies of the computations.

	'Uit 1'	*'Uit 2'*	*'Uit 3'*	*'Uit 4'*	*'Uit 5'*
Direction	From lock to sea	From lock to lake	From lock to sea	From lock to lake	From lock to lake
V_s [m^3]	*1920*	*1000*	*1300*	*2360*	*1000*
d_s [m]	*2,8*	*1,5*	*2,8*	*2,9*	*1,3*
u_s [m/s]	*0,7*	*0,7*	*1,1*	*0,9*	*1,0*

Table 4.10: Values of amounts of intruded salt mass in tonnes of suspended salt per sailing movement for the experiments (exp.), computations with ZSF assumptions (ZSF), and two-layer assumptions with gradual sailing (2LΔt).

	'Uit 1'	*'Uit 2'*	*'Uit 3'*	*'Uit 4'*	*'Uit 5'*
M_2 - M_1 (exp.)	*30*	*39*	*22*	*-14*	*-10*
M_2 - M_1 (ZSF)	*52*	*45*	*51*	*-18*	*-13*
M_2 - M_1 (2LΔt)	*48*	*35*	*43*	*0*	*-7*

By comparing the quantifications of intruded salt mass for the ship movements ($M_2 - M_1$) in Table 4.10, two statements can be made. First, it is seen that the assumptions of this study ($2L\Delta t$) tend to approach the values of the experiments (labelled *exp.*) with slightly more accuracy for all ship movements, except 'uit 4'. Therefore, it is cautiously said that the assumptions of this study, albeit to a small extent, improve the formulation of salt intrusion at locks. In addition, Figures 4.7 to 4.11 show that the assumptions of this study lead to a greater similarity of the general course of the salt mass in the lock with the experiments at the Stevin Locks. This also follows, from the quantitative determination of the salt masses in Table 4.10.

Second, a distinguishing feature is the discrepancy between experiments and models for larger ships ('*uit 1'*, *'*uit *3'*) compared to smaller ships ('uit *2'*, 'uit *4'*, *'*uit *5'*). It is expected that this shows the absence of the propeller jet in the computations, as larger vessels need a larger propeller jet to accelerate. This characteristic has been observed several times in section 4.4 and it is now thought to be the reason for a too low salt flux when sailing to lakeside and a too high salt flux when sailing to seaside. This point of attention will be the basis of the following section.

Upon comparing the computations with the experiments more qualitatively, two things stand out for the conceptual model. These are the underestimation of the salt flux for ships exiting to lakeside, and the overestimation of the salt flux for ships exiting to seaside. In the modelling approach of this study, the salt wedge during exiting is largely pushed back as can be seen from the horizontal course of salt mass in the lock during t_1 and t_2 in for instance Figure 4.10. However, the experiments at the Stevin Locks show a relatively large drop in salt mass for all ships exiting towards lakeside. It is thought that this can be explained by having neglected the propeller jet. The observations of increased salt intrusion during exiting to lakeside and decreased salt transport during exiting to seaside has also been observed by Deltares [6]. This has been explained based on a theoretical schematization given in Figure 4.12. From this figure it is seen how the propeller jet of a starting ship generates a salt wedge when exiting towards lakeside and how it reduces the incoming salt wedge during exiting towards seaside. These emerging currents may cause the observed discrepancies. The publication from Deltares [6] adds that this is a possibility in relation to the flow regime. Simulations with the conceptual model in this chapter leave the possibility that this may indeed be at the root of the discrepancies.

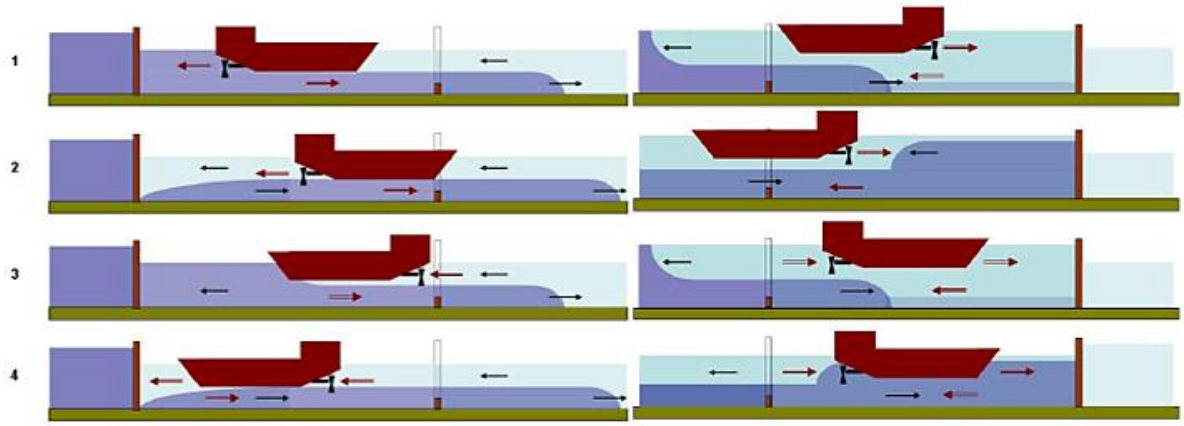

Figure 4.12: Possible flow patterns in the lock resulting from a propeller jet [6]. It is expected following from this chapter that these flow patterns are at the cause of the discrepancies between the conceptual model and the experiments. In pictures 3 and 4 the flow from the propellers is reversed for deceleration.

5 Sensitivity Analysis & Case Study

The previous chapter showed that the $2L\Delta t$ assumptions have a higher overall accuracy in terms of recreating the experiments at the Stevin Locks. The next step is to determine the conditions under which the differences between the model results arise and become significant. In the following chapter more attention will be paid to the range of modelling parameters that lead to discrepancies between the parametrized simulation approaches. This will be done in twofold. First, a sensitivity analysis on the navigation phase will be carried out. Initially, exchange flows will be neglected here. By means of an analytical comparison, it then attempts to find the range of modelling parameters and initial conditions that lead to discrepancies. An effort will then be made to nondimensionalize the results to find an independent factor between the results of the ZSF and the $2L\Delta t$ assumptions. Second, the sensitivity analysis will serve to find unfavourable (i.e. those that lead to great discrepancies) combinations of computational parameters and initial conditions. These will subsequently be used in a case study. The case study aims to show the effect of the most unfavourable parameters on the discrepancies in the modelling of the total amount of salt intrusion during a lockage. It will then be examined whether these discrepancies in their extreme state are significant over a tidal cycle, and if so, what discrepancies are to be expected during a practical example of lockages. Based on the sensitivity study carried out beforehand, a reasoned conclusion is then drawn on the benefit of improving the assumptions of the ZSF.

5.1 Sensitivity Analysis

This section will focus on the conditions under which differences in salt intrusion occur between the two sets of assumptions. The aim is to give an indication of the sensitivity of the differences for relevant parameters, but also to find the biggest discrepancies between modelling approaches. These parameters will then be applied to the case study.

5.1.1 Analytical Formulation: Excluding Exchange Flows

The first step in the analysis is to formulate an analytical formulation for the differences in salinity between the shipping contributions of the two modelling approaches. This will be done for a ship entering and exiting lakeside. Initially, the lock exchange is neglected. As a result, no salt intrusion is associated with an exiting vessel, and the focus lies with the return current. A start is therefore made at a ship entering the lock from lakeside. The amount of salt intrusion due to navigation in the ZSF (ΔM_{ZSF}) then depends solely on the differences in water density and the ship volume (5.1).

$$\Delta M_{ZSF} = V_s(\rho_{mix} - \rho_0) \tag{5.1}$$

To formulate the discrepancies, the salt mass flux of the $2L\Delta t$ assumptions must be summarized in a formulation as well. It was shown in $(3.22 - 3.31)$ that the displaced water volume of the return current during sailing ($V_{primary}$) of the continuity method equals the ship volume (5.2). Subsequently, the total amount of transported salt mass is obtained by multiplying the transported water volume with its average salinity for the duration of sailing (5.3).

$$V_{primary} = V_s \tag{5.2}$$

$$\Delta M_{2L\Delta t} = V_s \overline{S_x} \tag{5.3}$$

Here, a new variable ($\overline{S_x}$) is defined, which is the average salinity of the return current for the duration of sailing. Unfortunately, $\overline{S_x}$ is difficult to approach algebraically because the return current distribution over depth in the conceptual model is non-continuous. Before continuing with the analytical formulation, $\overline{S_x}$ will be addressed in more detail.

Average Return Current Salinity, $\overline{S_x}$

Upon neglecting the exchange flow during the simulation, the average salinity of the return current in the conceptual model, $\overline{S_x}$, depends on the location of the interface (in turn dependent on the initial conditions of the simulation) and the shape of the return current distribution. It is defined by the average ratio of the saline area ($\hat{A}_{primary,s}$) over the total area of the return current distribution for the sailing duration, given by (5.4). From (3.27) and (3.28) it is seen that the total area of the return current distribution equals $(A_c - A_s)$.

$$\overline{S_x} = \left(\sum_{t=0}^{\frac{t_{pass}}{\Delta t}} \frac{\hat{A}_{primary,s}}{(A_c - A_s)} \right) * (\rho_z - \rho_0) \tag{5.4}$$

The saline part of this return current distribution $\hat{A}_{primary,s}$ can rationally be formulated according (5.5), based on geometry of the left schematization from Figure 3.6, reproduced in Figure 5.1. The area $\hat{A}_{primary,s}$ is then calculated according to the depth of the interface relative to the ship draught. The interface depth in time ($d_{int}(t)$) depends on the amount of extruded saline volume during sailing ($V_z(t)$) according (5.6), earlier mentioned in (3.5), (3.8), and (3.31).

$$\hat{A}_{primary,s} = \begin{cases} \big(d - d_{int}(t)\big)w, & d_{int} \geq d_s \\ (d - d_s)w + \big(d_s - d_{int}(t)\big)(w - w_s), & d_{int} < d_s \end{cases} \tag{5.5}$$

$$d_{int}(t) = d_{int,0} + \frac{V_z(t)}{wl} \tag{5.6}$$

Unfortunately, no straightforward method of algebraically determining $V_z(t)$, the amount of extruded saline water during sailing, can be found because of its dependence to the initial conditions. Nonetheless, the algebraic formulation of (5.5) can still be used as the conceptual model can aid in providing values for $\overline{S_x}$.

Because the discrepancies between modelling approaches highly depend on the initial conditions, they will be included in the formulation. Both modelling approaches need similar quantities for the salt masses in the lock (as opposed to using ρ_{mix} for the ZSF, and h_0/d for the $2L\Delta t$ assumptions). Therefore, ρ_{mix} is expressed in (5.7 & 5.8) as a ratio of layer heights of fully saline and fresh water.

$$\rho_{mix} = \rho_0 + \frac{h_0(\rho_z - \rho_0)}{d}, \qquad h_0 = d - d_{int,0} \tag{5.7 \& 5.8}$$

(Please note that although ρ_{mix} is expressed as layer heights, the ZSF contribution ($M_{z,ZSF}$) is still based around a homogeneous lock computation. The expression is only converted for comparative purposes.)

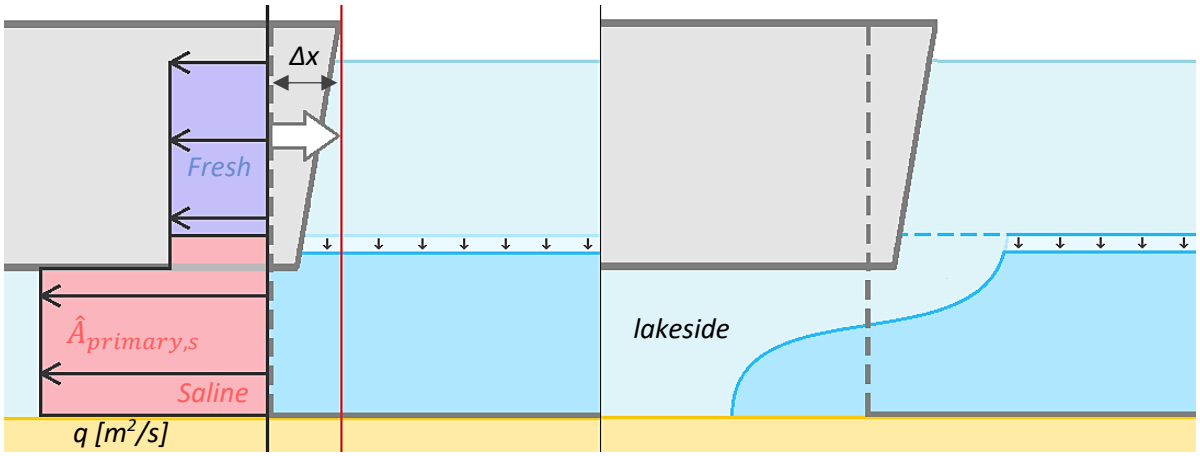

Figure 5.1: Schematization an entering ship from lakeside, with contributions to the salt intrusion by primary waves (left) and lock exchange (right), reproduced from Figure 3.5. The area of the saline part of the flux distribution is $\hat{A}_{primary,s}$.

The discrepancies between the outputs of the models are defined as Δ_{model} according (5.9). For positive values of Δ_{model}, the intruded salt mass for the two-layer computation, $M_{z,2L\Delta t}$, is of higher magnitude than that of the ZSF.

$$\Delta_{model} = \Delta M_{2L\Delta t} - \Delta M_{ZSF} \tag{5.9}$$

Δ_{model} can subsequently be rewritten using (5.1), (5.3), and (5.7) into (5.10). It is stressed that no exchange flow is included in this formulation and that this formulation deals with ships entering the lock.

$$\Delta_{model} = V_s \left(\overline{S_x} - \frac{h_0}{d} (\rho_z - \rho_0) \right) \tag{5.10}$$

The formulation of (5.10) cannot be created for exiting ships from the lock, while having neglected exchange flows. The return current in this case does not contribute to salt intrusion because it is not directed towards lakeside. Furthermore, by using $\overline{S_x}$ the formulation of (5.10) can no longer be further simplified. This therefore concludes on the formulation.

5.1.2 Computational Determination: Excluding Exchange Flows

In this section, the maxima of (5.10) for a range of initial conditions and ship sizes are attempted to be found to understand the conditions for discrepancies. This will be done by first computing the values of $\overline{S_x}$. The boundary conditions for these computations, such as lock size (adopted from the Krammer locks), water level at lakeside, and water densities are given in Table 5.1. The values of $\overline{S_x}$ are shown in Table 5.2 for shipping classes CEMT: VIa and IVa.

By comparing the ship volumes (V_s) to the computed salt intrusion in cubic meters for $h_0/d = 1$ (from Table 5.2) it is seen that a small deviation is present in the outputs, as these volumes are not equal (2700 m^3 vs. 2699,67 m^3; 9180 m^3 vs. 9179,15 m^3). This is thought to originate from rounding errors within the conceptual model. The amounts salt intrusion by shipping according to the ZSF can be calculated directly *f*ollowing from (5.1) and are shown in Table 5.3. The differences in the outputs of intruded salt mass between models (Δ_{model}) is obtained from subtracting the values of Table 5.3 to corresponding values of Table 5.2 according (5.9). The results are shown in Table 5.4. The same steps as were presented for the CEMT classes: VIa and IVa have been applied to computations with CEMT classes: IIIa and Va, and are included in Table 5.4 too. Moreover, the results of Δ_{model} are plotted in Figure 5.2. This figure will first be examined and discussed.

Table 5.1: General parameters of computations for the sensitivity analysis.

Parameter	Value
l [m]	*280,0*
w [m]	*24,0*
d [m]	*6,0*
V [m³]	*40320*
l_s [m]	*135,0*
w_s [m]	*17,0*
d_s [m]	*4,0*
V_s [m³]	*9180*
ρ_z [kg/m³]	*1035*
ρ_0 [kg/m³]	*1000*
h_0 [m+NAP]	*0,0*
u_s [m/s]	*0,6 * u_L (Appendix B)*

Table 5.2: Values of $\overline{S_x}$ and intruded saline volumes ($\rho = \rho_z$) for different shipping classes and initial conditions for the conceptual model.

$M_{z,2L\Delta t}$	CEMT: IVa (V_s= 2700 m³)		CEMT: VIa (V_s= 9180 m³)	
Initial Condition: (h/d)	$\overline{S_x}$	Computed salt intrusion [m³ saline water, ρ_z]	$\overline{S_x}$	[m³ saline water, ρ_z]
1 (fully saline)	34,996	2699,67	34,997	9179,15
5/6	30,509	2353,53	31,396	8234,83
2/3	26,025	2007,65	27,800	7291,76
1/2	21,189	1634,60	24,205	6348,70
1/3	14,125	1089,65	17,947	4707,23
1/6	7,061	544,69	8,917	2353,03
0 (fully fresh)	0,0	0,0	0,0	0,0

Table 5.3: Values of intruded saline volumes ($\rho = \rho_z$) for different shipping classes and initial conditions according the ZSF. The values for the initial condition ρ_{mix} correspond to the initial conditions (h/d) from Table 5.2 according (5.7).

$M_{z,ZSF}$	CEMT: IVa (V_s= 2700 m³)	CEMT: VIa (V_s= 9180 m³)
Initial Condition: (ρ_{mix})	[m³ saline water, ρ_z]	[m³ saline water, ρ_z]
1035,0 (fully saline)	2700,0	9180,0
1029,2	2250,0	7650,0
1023,3	1800,0	6120,0
1017,5	1350,0	4590,0
1011,7	900,0	3060,0
1005,8	450,0	1530,0
1000,0 (fully fresh)	0,0	0,0

Table 5.4: Differences in computed salt masses between the implementations of shipping of the conceptual model and the ZSF in tonnes of suspended salt.

Δ_{model}	**CEMT: IIIa**	**CEMT: IVa**	**CEMT: Va**	**CEMT: VIa**
Initial Condition: (h/d)	Δ_{model} *[tonnes]*	Δ_{model} *[tonnes]*	Δ_{model} *[tonnes]*	Δ_{model} *[tonnes]*
1 *(fully saline)*	*-0,006*	*-0,012*	*-0,019*	*-0,027*
5/6	*1,654*	*3,624*	*6,755*	*20,469*
2/3	*3,318*	*7,268*	*13,547*	*41,012*
1/2	*3,376*	*9,961*	*20,340*	*61,555*
1/3	*2,250*	*6,638*	*16,329*	*57,653*
1/6	*1,122*	*3,314*	*8,156*	*28,806*
0 *(fully fresh)*	*0,0*	*0,0*	*0,0*	*0,0*

What is evident from Figure 5.2, is that Δ_{model} is greatly affected by the initial conditions and the size of the ship. Furthermore, a shift towards the right (decreasing salt mass within the lock) in the horizontal coordinate of the peak intrusion is observed for increasing ship sizes. This can be explained based on the shape of the return current distribution. As a ship enters the lock from lakeside, the saline layer height decreases because of the return current. Consequently, the maximum discrepancy between the $2L\Delta t$-assumptions and the ZSF assumptions is obtained when the average interface depth during sailing corresponds to exactly the draught of the ship. In this way, the largest contribution due to a higher saline return current under the ship is considered compared to the ZSF. The x-coordinates of the peak intrusion therefore correspond to the initial conditions leading to an average interface depth during sailing which is equal to the draught of the respective ship.

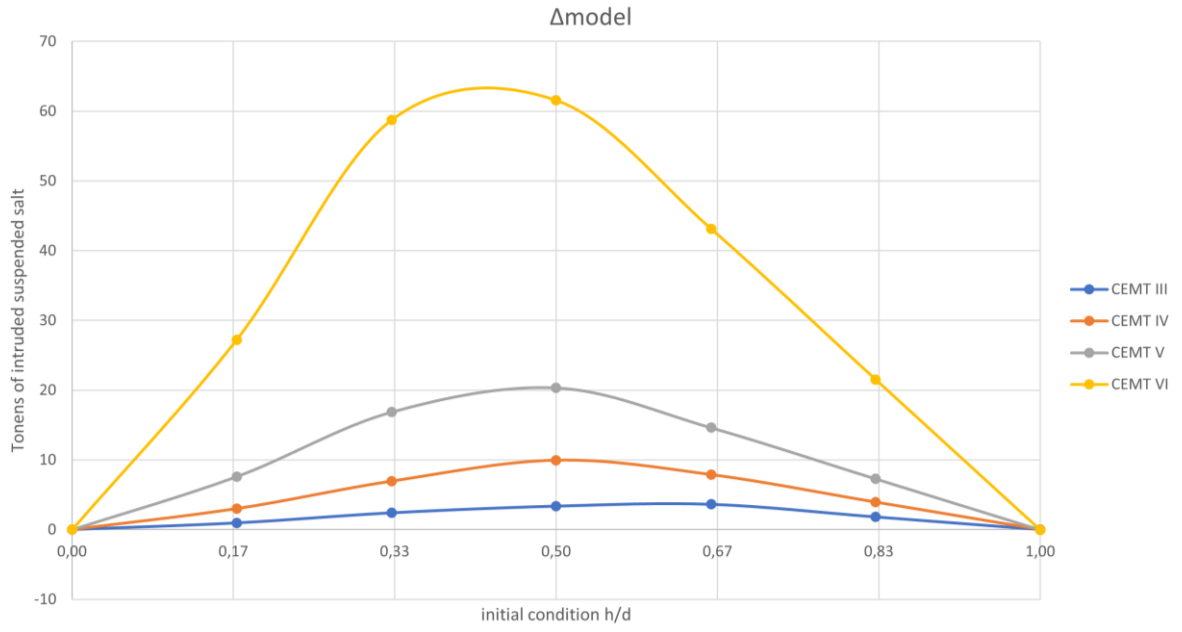

Figure 5.2: Results of calculated Δ_{model} for different shipping classes and initial conditions. The left of the x-axis shows a fully fresh lock and the right a fully saline lock. The results follow from Table 5.3. It is emphasised that the interpolated values between the dots are determined with excel and should therefore only guide as a means of showing the general trend.

The next step is to make the differences between the models independent of the applied model parameters, to arrive at a non-dimensional factor between both modelling approaches. Therefore, Δ_{model} will be nondimensionalised by dividing by a factor J. As Δ_M^* should become dimensionless, the unit of J is to be kilograms.

$$\Delta_M^* = \frac{\Delta_{model}}{J} \tag{5.11}$$

The route to arrive at a definition of J is a matter of educated guessing. Therefore, at this point, an appeal was made to the author's insight. By experimenting with the application of various characteristic parameters to the quantity J until all results of Figure 5.2 followed roughly the same course, the formulation given by (5.12) was found to do this with reasonable satisfaction. This is shown in Figure 5.3, which presents the final analysis of the discrepancies of a ship entering the lock without taking the lock exchange into account. Using algebra, (5.12) can be rewritten in (5.13). Consequently, by substituting (5.13) in (5.11), (5.14) is obtained.

$$J = V_s \Delta\rho \left(\frac{d_s}{d}\right) \frac{A_c}{A_c - A_s}, \qquad \Delta\rho = \rho_z - \rho_0 \tag{5.12}$$

$$J = V_s \Delta\rho \frac{d_s}{d - d_s} \tag{5.13}$$

$$\Delta_M^* = \left(\frac{\overline{S_x}}{\Delta\rho}\right) \frac{d - d_s}{d_s} + h_0 \left(\frac{1}{d} - \frac{1}{d_s}\right) \tag{5.14}$$

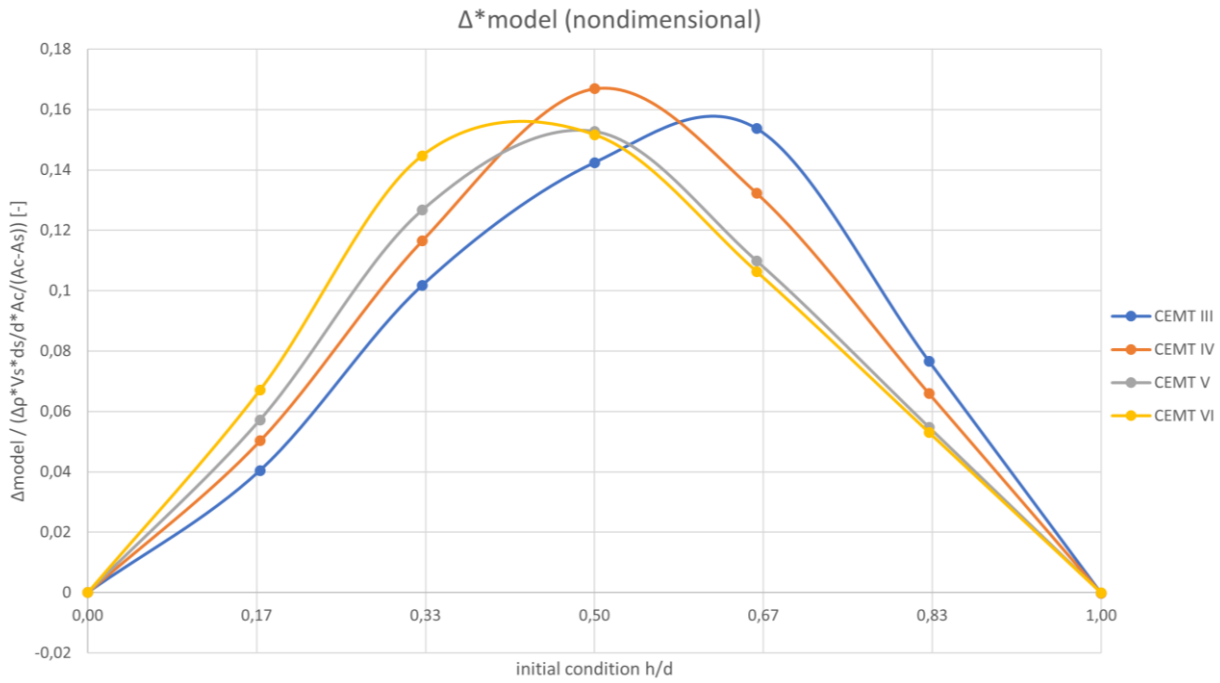

Figure 5.3: Results of calculated Δ_M^* for different shipping classes and initial conditions. This applies to an entering ship to the lock without taking account of the lock exchange. The y-axis represents the underestimation of shipping in the ZSF expressed as a salt mass over J, which can be interpreted as the overall underestimation of shipping in the ZSF in comparison to the conceptual model.

With the use of Δ_M^*, a statement can be made about the relative influence of the return current to the salt intrusion for the $2L\Delta t$ assumptions in comparison to the ZSF, without considering the change in volumes between the ship classes, density differences over the lock, differences in draught relative to the lock depth, and differences in cross-sectional area between locks and ships. Δ_M^* is plotted in Figure 5.3 for different initial conditions (h_0/d). Regardless of the used shipping class, roughly the same discrepancies are expected between both modelling approaches.

As it turns out, the discrepancies are, besides the volume of the ship and the density differences, dependent on a geometric factor $\left(\frac{d_s}{d-d_s}\right)$ to be interpreted as the relative ship's draught, i.e. the ratio of the draught over the depth underneath the ship. From a physical point of view, this makes sense. The effect through the geometric factor must be larger for larger discrepancies to normalize all outputs to the same nondimensionalized value. Since Δ_M^* is obtained by dividing Δ_{model} by the geometric factor (among V_s and $\Delta\rho$), this implies that the geometric factor thus needs to be larger for larger discrepancies. The geometric factor is larger for bigger ships, which holds that a larger discrepancy is obtained for larger ships. This physical representation is correct, as a larger ship will have a larger proportion of the return current distribution in the salt layer of the two-layer system. Thus, the total amount of salt intrusion that is additionally considered by the $2L\Delta t$ assumptions turns out to be proportional to the ratio between the draught of the ship and the depth below the ship. This is caused by the greater contribution of the return current below the ship than beside the ship at greater ship draughts. Additionally, the largest discrepancies between both approaches are obtained when the initial condition of the density in the lock is roughly halfway fully saline and fresh. These discrepancies amount to approximately 16 percent.

5.1.3 Computational Determination: Including Exchange Flows

The previous sections have shown that the contribution of shipping to salt intrusion depends on the volume of ships, the differences in density between seaside and lakeside, and the location of the interface according to (5.10). Moreover, it was seen that a nondimensional discrepancy is present, which describes the increased contribution of the return current using the $2L\Delta t$ assumptions, given by (5.14). During both analyses however, the lock exchange was neglected. In this section, the exchange flow will be reintroduced to the analysis to see if the discrepancies maintain their magnitude, and to see if the discrepancies still depend on (5.14). In addition, it will be examined whether the discrepancies, under forcing of the lock exchange, are significant enough to pose recommendations for refinements to the ZSF formulation.

Upon addition of the exchange flow, the discrepancies between the two modelling methods appear to depend on two other simulation parameters in addition to the initial condition h_0/d. These are the duration between opening of the lock gate and a ship exiting the lock (t_{door}), and the duration between a ship having left the lock and a ship entering (t_{wait}). Because in this analysis different initial conditions (h_0/d) will be used, each computation will make use of different time scales of the lock exchange, defined by t_{LE} given by (2.7) and repeated here in (5.15). As a result, the lock exchange has different degrees of significance when t_{door} and t_{wait} are varied, and different initial conditions (h_0/d) are used. Therefore, these durations are tested by their relative duration to the lock exchange time scales, given by t_{door}/t_{LE} and t_{wait}/t_{LE}.

$$t_{LE} = \frac{4l}{\sqrt{g\frac{\rho_z - \rho_0}{\rho_0}d}} \tag{5.15}$$

In this section, more insight in t_{door}/t_{LE} and t_{wait}/t_{LE} will be given. To give an insight into how these parameters affect discrepancies between modelling approaches, a series of simulations under different conditions will be presented. This will be done by carrying out simulations with both modelling approaches (ZSF and $2L\Delta t$) and determining the total amount of salt intrusion for different t_{door}/t_{LE} and t_{wait}/t_{LE}. The conditions of the simulations are supplied in Table 5.5. In order not to overload this section with graphs, all graphs will be included in a separate appendix (Appendix C).

Table 5.5: Values that the significant simulation parameters can take. Each combination of these modelling parameters will be tested.

Simulation Parameter	***Value***
h_0/d	*1/6; 2/6; 3/6; 4/6; 5/6; 6/6*
t_{door}/t_{LE}	*0; 1/3; 2/3*
t_{wait}/t_{LE}	*0; 1/3; 2/3; 3/3*
CEMT classes	*VIa; Va; IVa; IIIa*

From the dependence of the discrepancies to the duration of the lockage, it is highly unpractical to make a distinction between exiting of the lock and entering of the lock. This is because the individual sailing displacements between models cannot directly be compared with each other. This needs to be explained. The amount of salt intrusion accompanied by the navigation phase is highly dependent on the amount of salt in the lock (expressed as the initial interface height over the lock depth h_0/d). In the ZSF algorithm, the amount of salt intrusion during sailing to lakeside is determined by first adding a large volume of fresh water to the lock for ships exiting the lock, to then remove a portion of saline water for ships entering the lock at the end of the navigation phase. This causes the condition of salt mass in the lock (expressed as interface height over the lock depth h_0/d) just before entering to be different for the ZSF and $2L\Delta t$ per initial condition. This holds that a graph which shows the discrepancies between the modelling approaches cannot be depended on the condition h/d as this condition is not equal for different simulation approaches. The unpracticality of comparing individual sailing displacements also holds for comparing contributions of entering and exiting shipping within the same modelling approach, because of the nonlinear lock exchange in time.

To overcome this for lockage simulation including exchange flows, the contribution of shipping disturbances will be accounted for over the entire lockage phase (i.e. for exiting ships and consecutive entering ships). In this way, a simulation using one set of assumptions can be dependent on h_0/d, t_{door}/t_{LE}, and t_{wait}/t_{LE}, and can be compared with the other assumption set using the same parameters. The next section will therefore focus on t_{door}/t_{LE} and t_{wait}/t_{LE}, both to understand their respective influence on the salt intrusion discrepancies for both models and to choose values for these parameters that result in the largest discrepancies for the case study in the next section.

5.1.3.1 Door-open time (t_{door}/t_{LE})

First, the influence of the door-open time on the salt intrusion will be examined. The first comparison will be done using the first value for t_{door}/t_{LE} from Table 5.5. This will then be applied to simulations using an arbitrary CEMT shipping class. Then the results for different initial conditions and waiting times will be compared. The shipping class chosen for this section is CEMT: VIa.

The graphs in this section are created by summing the salt intrusion contributions from entering and exiting ships. Figure 5.6 shows the amount of salt intrusion by shipping according the $2L\Delta t$ assumptions for different initial density conditions (h_0/d) and waiting times (t_{wait}/t_{LE}), using no door-open time (t_{door}/t_{LE} = 0). It is created from the summation of the values from Figure 5.4 and Figure 5.5, which respectively show the amount of salt intrusion for exiting and entering ships in the lock per initial conditions h_0/d.

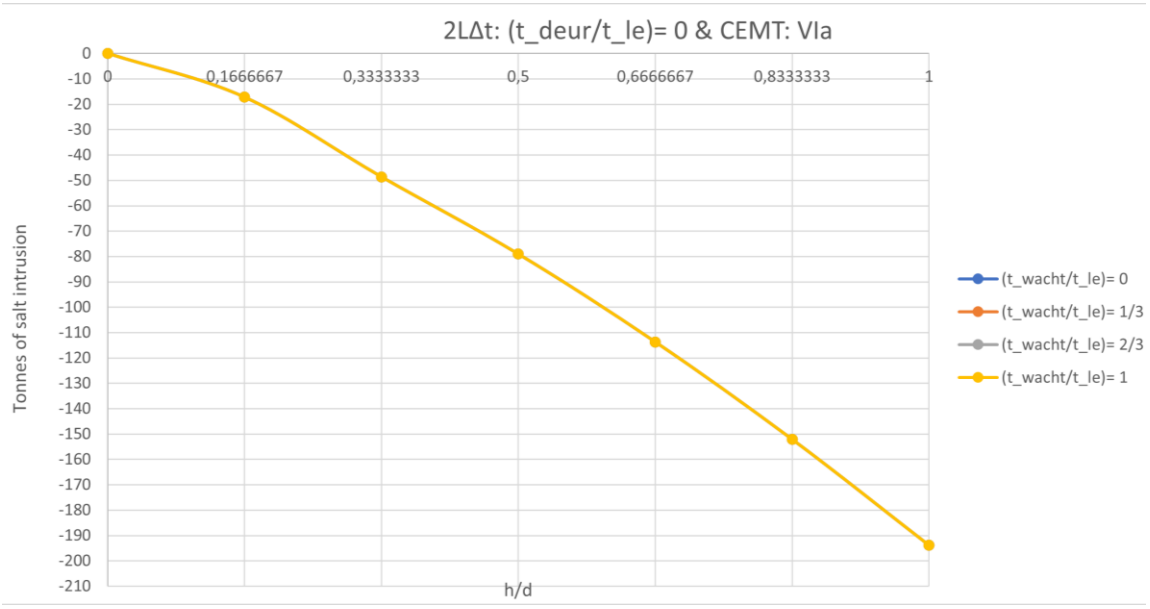

Figure 5.4: Simulations with $2L\Delta t$ assumptions, t_{door}/t_{le}= 0, and different t_{wait}/t_{le} for ships exiting the lock to lakeside.

Figure 5.4 shows that the influence of ships leaving the lock on salt intrusion can only be seen in the pushing back of the salt wedge towards the lock. This represents a negative value in the total amount of salt intrusion caused by shipping. As the salt intrusion by exiting ships is not dependent on the waiting time (i.e. the time between ships leaving and entering the lock), the plots overlap in such a way that no differences can be seen for different t_{wait}/t_{LE}. However, Figure 5.5 shows that for ships entering the lock, the amount of salt intrusion due to shipping depends on the waiting time. By increasing this waiting time less salt water is available in the lock to be included in the salt intrusion by shipping into the lock. This is in line with Figure 5.5, which shows a decreasing contribution from shipping as waiting times increase.

By adding Figures 5.4 and 5.5, Figure 5.6 is obtained. This figure shows the total amount of salt intrusion by shipping in the navigation phase at lakeside (*lockage phase 2*), for the $2L\Delta t$ assumptions, using no door-open time, shipping class CEMT: VIa, and various waiting times.

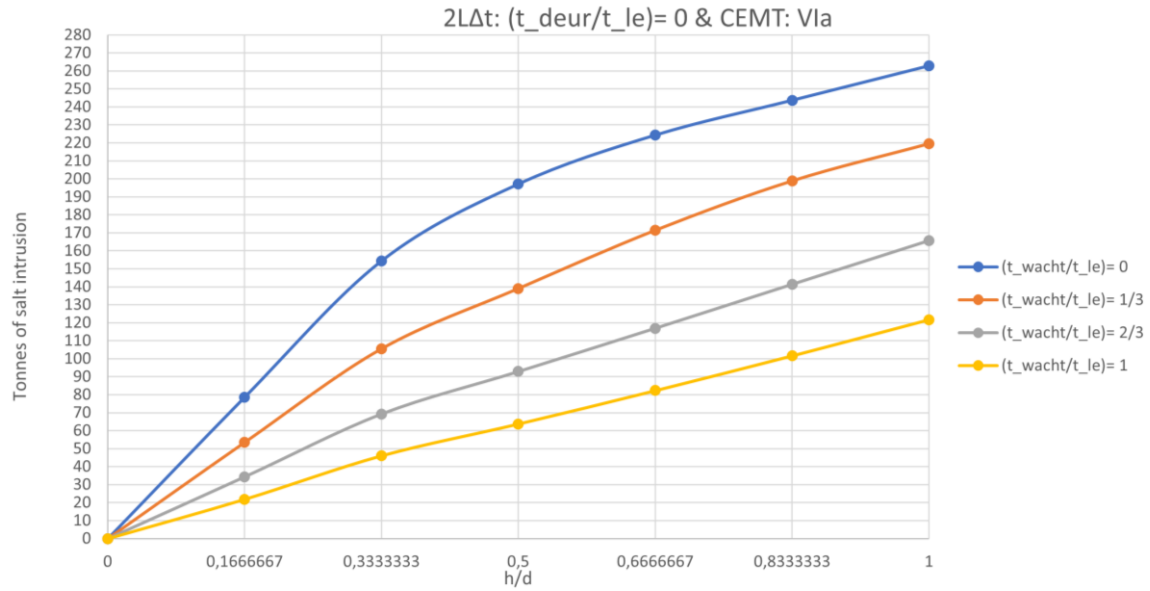

Figure 5.5: Simulations with $2L\Delta t$ assumptions, t_{door}/t_{le}= 0, and different t_{wait}/t_{le} for ships entering the lock from lakeside.

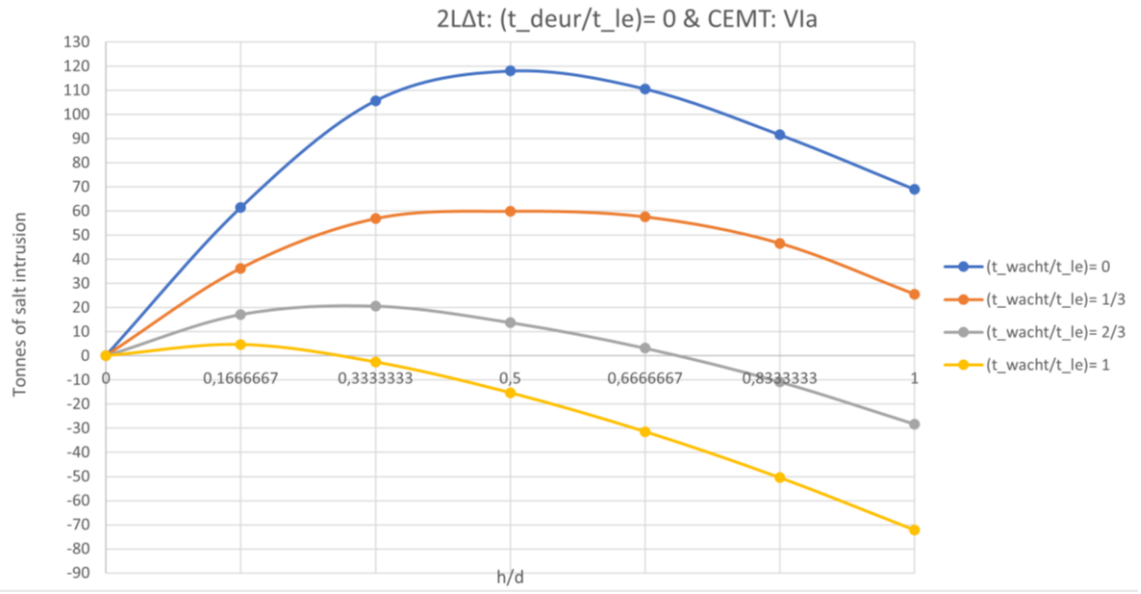

Figure 5.6: Simulations of the entire navigation phase at lakeside with $2L\Delta t$ assumptions, t_{door}/t_{le}= 0, and different t_{wait}/t_{le} between ship movements.

What is seen in Figure 5.6, is that according the $2L\Delta t$ assumptions the contribution of shipping to the salt intrusion is positive (meaning an increment to the total amount of salt intrusion) for small waiting times and ship sizes. As t_{wait}/t_{LE} and V_s increases, the contribution of shipping becomes negative, meaning shipping reduces the total amount of salt intrusion with respect to lockages without shipping.

The aim of the next simulations is to expand on this analysis and show the behaviour of the differences in computed amounts of salt intrusion using different waiting times (t_{wait}/t_{LE}) and door-open times (t_{door}/t_{LE}).

Table 5.6: Overview of Figure numbers for computations with different t_{door}/t_{LE} values.

Parameter	$2L\Delta t$	ZSF	$2L\Delta t$ - ZSF
$t_{door}/t_{LE} = 0$	Figure 5.6	Figure C.3	Figure 5.8
$t_{door}/t_{LE} = \frac{1}{3}$	Figure C.1	Figure C.4	Figure 5.9
$t_{door}/t_{LE} = \frac{2}{3}$	Figure C.2	Figure C.5	Figure 5.10

Figures 5.6, and C.1 and C.2 in Appendix C, show how increasing the door-opening time reduces the absolute contributions from shipping to the salt intrusion. Another observation from the figures is the creation of an inflection point (as seen in Figure C.2) for increasing door-open times. This feature arises from the graph of exiting ships once t_{door}/t_{LE} increases to 2/3, which is shown in Figure 5.7. For more saline initial conditions (h_0/d > 2/3) the interface has not reached the draught of the ship yet for t_{door}/t_{LE} = 2/3, thus the influence of the interface depth on the amount of transported salt by the return current here is limited. For decreasing initial density conditions (h_0/d < 2/3), the influence of the interface depth seems to be of higher magnitude as seen from the higher gradient shown in Figure 5.7 for more saline locks. Physically, this can be explained by the interface depth increasing to below the ship's draught, which explains the inflection point.

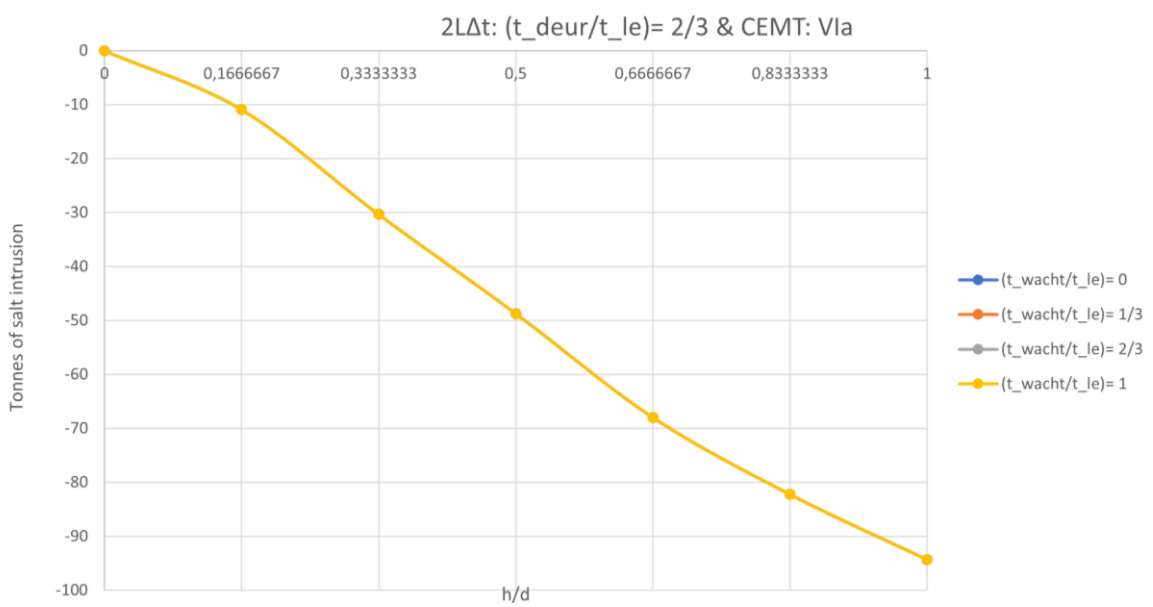

Figure 5.7: Simulations with $2L\Delta t$ assumptions, t_{door}/t_{le}= 2/3, and different t_{wait}/t_{le} for ships exiting the lock to lakeside. For increasing t_{door}/t_{le} an inflection point is formed.

The same parameters will be tested but now for the ZSF assumptions. The figures start with t_{door}/t_{LE}= 0, shown in Appendix C as Figure C.3.

Figures C.3 to C.5 show the total contribution of shipping to the salt intrusion, using the same modelling parameters as Figures 5.6, C.1, and C.2 (t_{door}/t_{LE} = 0, 1/3, and 2/3). C.3 to C.5 show that the shape of the plots remains unvaried for different durations. Furthermore, the courses of salt intrusion for the ZSF assumptions show the same character as the course of salt intrusion for entering ships using the $2L\Delta t$ assumptions (Figure 5.5). Carefully, it is stated that the similarity between the ZSF computations and Figure 5.5 already show that the greatest changes between the modelling approaches appear to be the influence of the return current on the exchange flow, and thus not so much the salt intrusion by return currents itself.

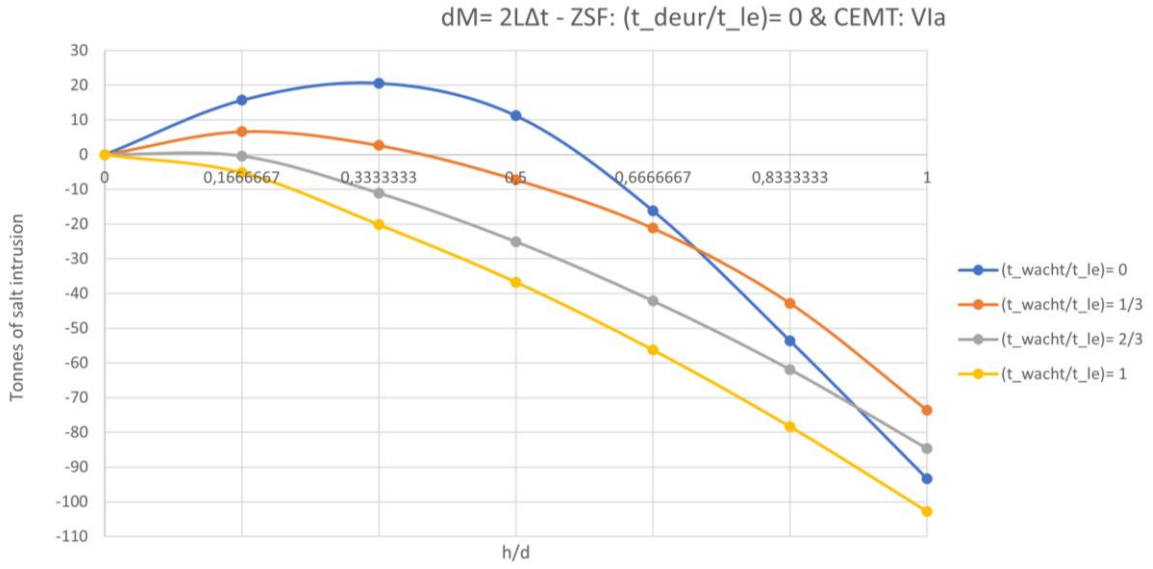

Figure 5.8: Differences in $2L\Delta t$ and ZSF assumptions with t_{door}/t_{le}= 0, and different t_{wait}/t_{le}.

The next set of figures (figures 5.8, 5.9, and 5.10) show the discrepancies between both modelling approaches ($2L\Delta t$ and ZSF). These figures are obtained by subtracting the results of the ZSF simulations from the $2L\Delta t$ simulations according (5.9). These graphs are created based on the same principle as the sensitivity analyses from section 5.1.2 (Figure 5.2), where the exchange flow was neglected.

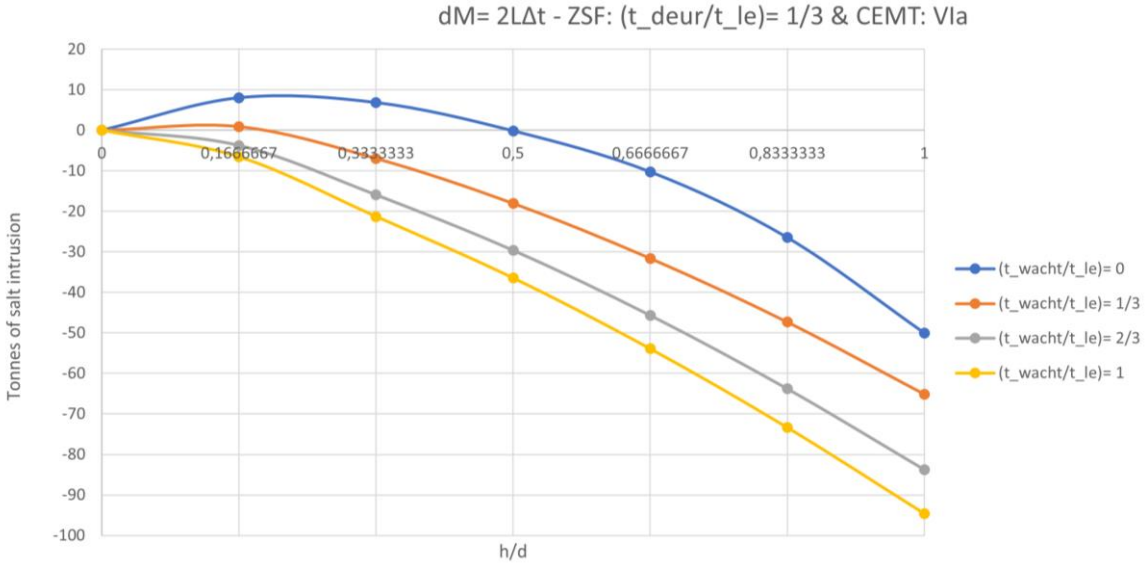

Figure 5.9: Differences in $2L\Delta t$ and ZSF assumptions with t_{door}/t_{le}= 1/3, and different t_{wait}/t_{le}.

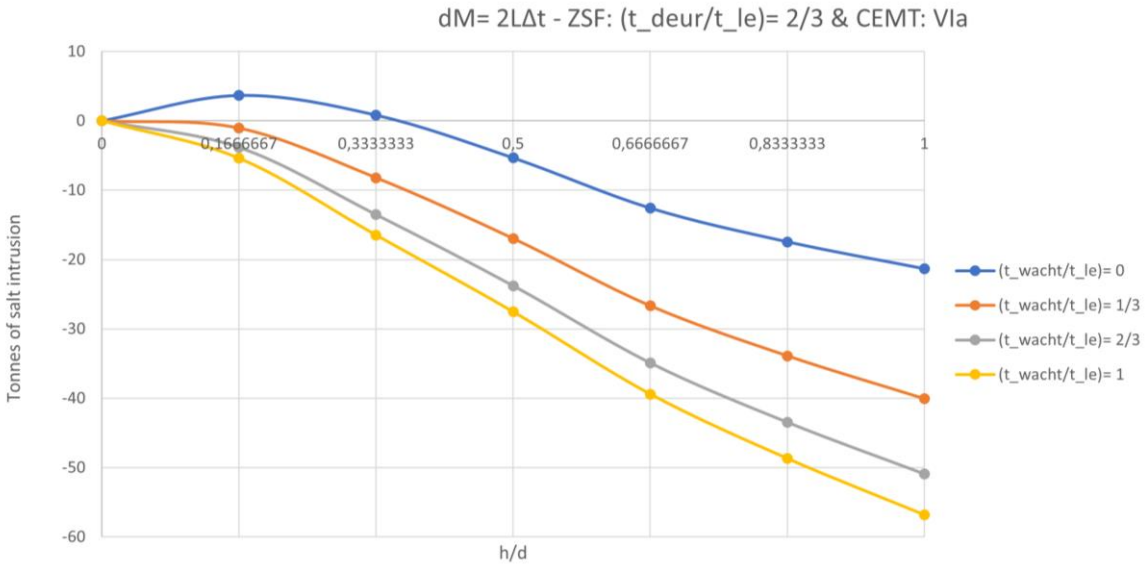

Figure 5.10: Differences in $2L\Delta t$ and ZSF assumptions with t_{door}/t_{le}= 2/3, and different t_{wait}/t_{le}. The plots show similar inflection points as Figure 5.8 from using the results of t_{door}/t_{le}= 2/3.

Upon examination of Figures 5.8 to 5.10 the following conclusions can be drawn:

For the most part, a larger contribution of shipping to the salt intrusion is determined for the ZSF assumptions in comparison to the $2L\Delta t$ assumptions. It is expected that this is mainly due to the influence of the return current on the lock exchange during the exiting of ships. The amount of salt present in the lock is higher during the exit of a ship than during the entry of a ship. Therefore, the amount of salt that is pushed back to the lock is higher than the extra contribution from the return current to the salt intrusion during entry of the lock. For increasing waiting times between consecutive

exit and entry of the lock, this effect increases hence the larger negative values of salt intrusion for larger t_{wait}/t_{LE}.

The largest discrepancies are obtained for the smallest door-open time (t_{door}/t_{LE}). Therefore, the door-open time that will be applied for the case study and the upcoming analysis will be t_{door}/t_{LE} = 0. By doing so, a situation is created which poses the biggest differences between simulation approaches. It will then be assessed whether the discrepancies in this state are significant within the entire lockage cycle.

5.1.3.2 Waiting time (t_{wait}/t_{LE})

For the last set of simulations of this section, the door-open time is set at t_{door}/t_{le}= 0 and ship size and waiting times are varied. The figure numbers for this section are provided in Table 5.7.

For the $2L\Delta t$ assumptions and increasing waiting times (t_{wait}/t_{LE}) and ship volumes (V_s), the results in Appendix C (Figures C.9 to C.12) show the influence of the return current on the lock exchange during exiting increases with respect to entering. This means that for increasing waiting times, the total amount of salt intrusion by shipping is to a greater degree dependent on the exiting than on the entry of ships. This is expected, as increasing the waiting times results in more salt to be transported by lock exchange prior to the entry of ships.

Table 5.7: Overview of Figure numbers for computations with different t_{door}/t_{LE} values.

Parameter	$2L\Delta t$	ZSF	$2L\Delta t$ - ZSF
$t_{wait}/t_{LE} = 0$	Figure C.6	Figure C.10	Figure 5.11
$t_{wait}/t_{LE} = \frac{1}{3}$	Figure C.7	Figure C.11	Figure 5.12
$t_{wait}/t_{LE} = \frac{2}{3}$	Figure C.8	Figure C.12	Figure 5.13
$t_{wait}/t_{LE} = 1$	Figure C.9	Figure C.13	Figure 5.14

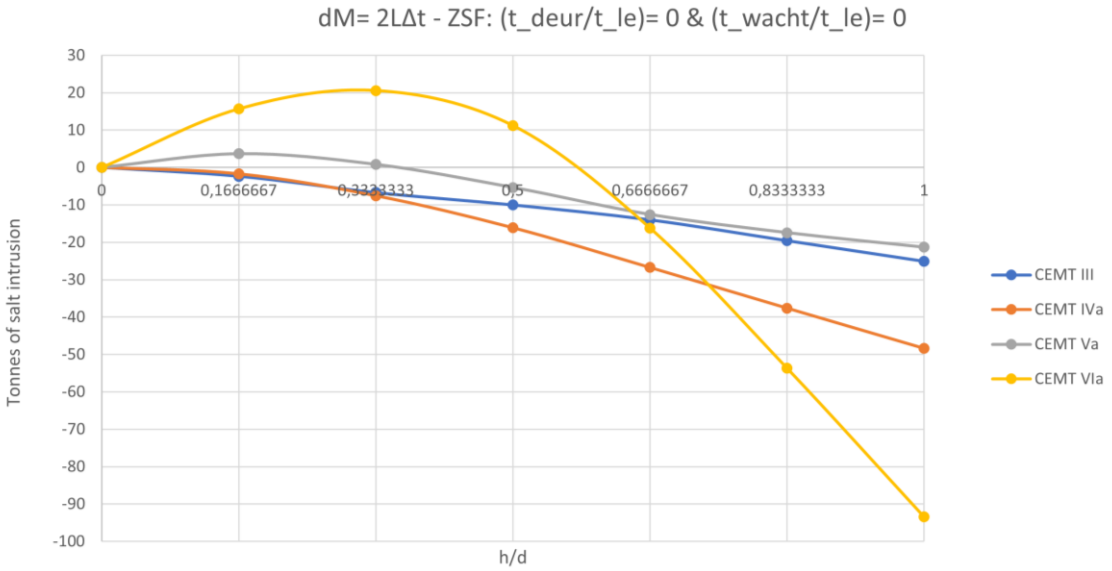

Figure 5.11: Differences in $2L\Delta t$ and ZSF assumptions with t_{door}/t_{le}= 0, t_{wait}/t_{le}= 0, and different shipping classes.

For the ZSF assumptions, the results in Appendix C (Figures C.13 to C.16) show the same course as the simulations using CEMT: class VIa and varying the waiting time and door-open time (Figures C.3 to C.5). Finally, the discrepancies between shipping contributions are shown for different waiting times and shipping classes in Figures 5.11 to 5.14.

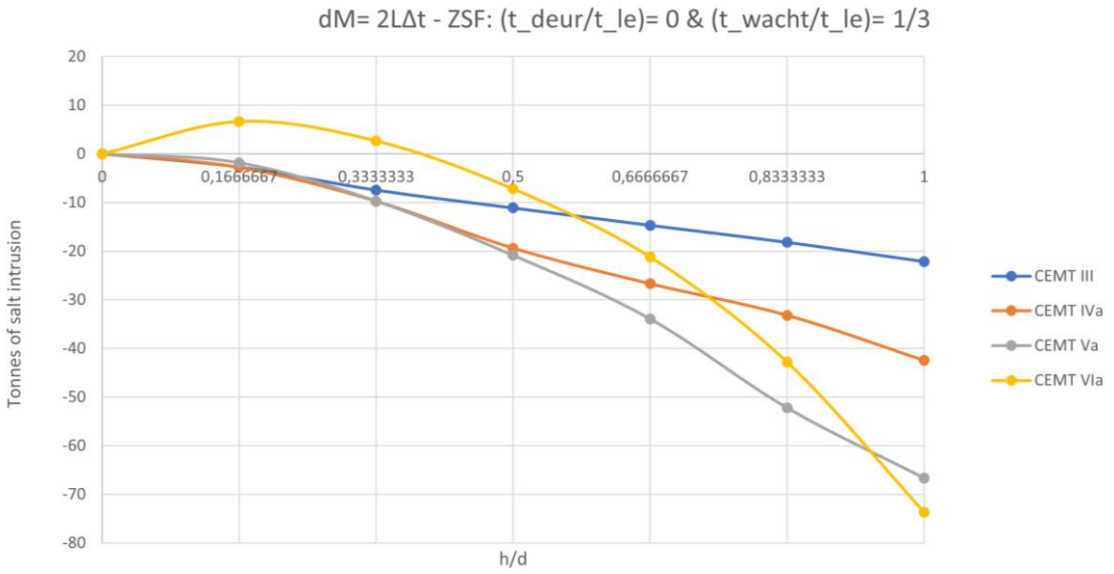

Figure 5.12: Differences in $2L\Delta t$ and ZSF assumptions with t_{door}/t_{le}= 0, t_{wait}/t_{le}= 1/3, and different shipping classes.

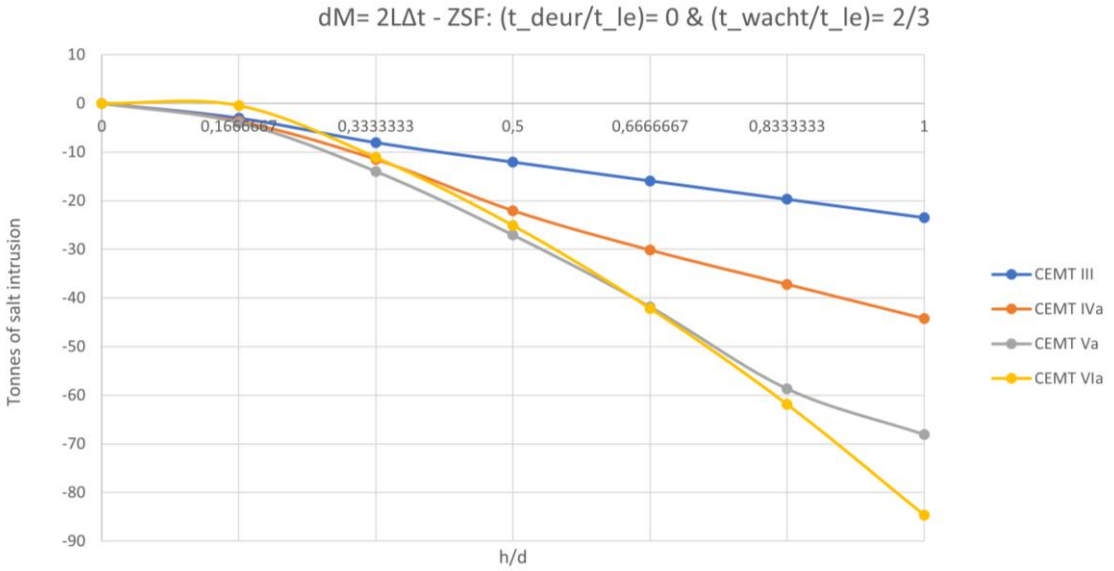

Figure 5.13: Differences in $2L\Delta t$ and ZSF assumptions with t_{door}/t_{le}= 0, t_{wait}/t_{le}= 2/3, and different shipping classes.

The differences between the calculated quantities of salt intrusion in Figures 5.11 to 5.14 clearly show the extent of the effect of the return current on the lock exchange. Upon considering a full navigation phase, like in this paragraph, taking account of pushing back the exchange flow by the return current to the lock can result in discrepancies of up to 100 tonnes of salt intrusion with the ZSF. This thus turns out to be the main reason for discrepancies between both modelling approaches.

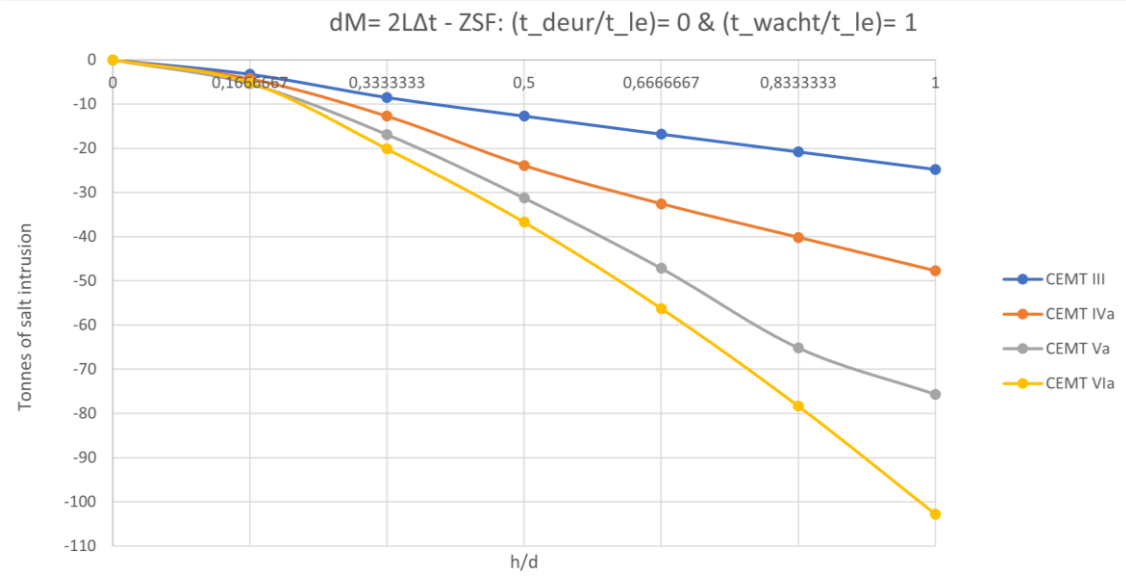

Figure 5.14: Differences in $2L\Delta t$ and ZSF assumptions with t_{door}/t_{le}= 0, t_{wait}/t_{le}= 1, and different shipping classes.

5.1.4 Preliminary Conclusion

This paragraph has broadened on the range for which discrepancies are to be expected between lockage simulations with the ZSF assumptions and the $2L\Delta t$ assumptions. This final section presents the examination of the results and aims to form a preliminary conclusion on the sensitivity of discrepancies regarding salt intrusion by shipping.

From section 5.1.1 it followed that by neglecting exchange flows from the consideration, discrepancies of shipping contributions between both modelling approaches are dependent on the differences in return current density, shipping volumes, and initial conditions according to (5.10).

From section 5.1.2 it followed that the $2L\Delta t$ assumptions generally lead to larger amounts of salt intrusion because of the refined return current distribution, as compared to instantaneous shipping in the ZSF. This discrepancy turns out to be the biggest for all shipping classes once the stratification has roughly equal layer heights (h_0/d = 1/2). Furthermore, upon neglecting the exchange flow from the simulation, the discrepancies appear to be dependent on a dimensionless factor according to Figure 5.3, given by (5.14). This was obtained with the use of a geometric factor $\left(\frac{d_s}{d-d_s}\right)$, which should be interpreted as the relative draught of the ship to the depth of the lock. Moreover, the maximum discrepancy follows from Figure 5.3 and is approximately 16% higher than the contribution from shipping in the ZSF.

From section 5.1.3 it was found that discrepancies between approaches are increasing when introducing the lock exchange. From this finding it is stated that the discrepancies are dependent on lockage duration (t_{door}/t_{LE}, and t_{wait}/t_{LE}). This makes it considerably more difficult to make the discrepancies non-dimensional. Given this dependence, no unanimous result was found on the sensitivity of discrepancies in this case, and therefore no statement could be made for which range of parameters refinements can be recommended for the ZSF. However, the difference between the two model assumptions has shown that the greatest discrepancy between the calculated quantities of salt intrusion depends on the pushing back of the salt tongue when leaving the lock. This finding will be at the base of the case study in the next paragraph.

From this paragraph, the following modelling parameters are chosen for the case study:

$$h_0/d = 1 \qquad t_{door}/t_{LE} = 0 \qquad t_{wait}/t_{LE} = 1$$

These values represent a fully saline lock ($h_0 = d$), and no door-open - and waiting time ($t_{door} = 0$ & $t_{wait} = 0$). It was found that these parameters result in the greatest discrepancies between modelling approaches. In the next paragraph, these parameters will be applied to a case study to examine if the differences between modelling approaches are significant in such an extreme case.

5.2 Case Study Based on Krammer Locks

This paragraph presents the case study, comparing the ZSF and $2L\Delta t$ assumptions in different scenarios. This will be done based on the Krammer Locks. First, a full lockage phase of navigation to lakeside is shown using the parameters that lead to the largest discrepancies. It is then checked if the discrepancies are significant. Next, half tide cycles for high and low tide will be considered, using simulation parameters that correspond to lockages in practice. This will give insight in the overall significance of the discrepancies for realistic cases.

The modelling results depend on usage assumptions (such as the lock size or number of lockages per tidal cycle):

- Lock size is 280 meters in length, 24 meters in width, and 6 meters in depth at NAP+0,00m (taken from the dimension of the Krammer locks).
- The flow area of the lock valves, including μ, has been set to 12,0 m^2 based on the design of the Krammer locks. The top of the lock valves is positioned at NAP-3,50m and the bottom at NAP-5,00m from the design of the Krammer locks [17].
- Regarding modelling of full lockages during high tide, the lockage cycle starts with levelling to lakeside. To do so, the water level in the lock must equal the water level at seaside of the prior phase, which equals NAP-0,46m (Figure 5.15). Consequently, the initial interface level has been set to NAP-3,23m, such that the simulation starts with equal fresh and saline water volumes.
- The initial conditions of lock - and interface level for the low tide situation are NAP+0,46m and NAP-2,77m respectively.
- The used ship size is vessel class CEMT: VIa of 135 meters in length, 17 meters in width, and 4 meters in draught [14].
- Sailing speeds are constants and set to 0,6 times the limiting speed corresponding to the CEMT class and lock size, resulting in a velocity of 0,96 m/s. (see Appendix B).
- The tidal amplitude is 1,5 meters.
- The distribution of lockages over a tidal cycle is constant. 10 lockages will be applied per tidal cycle, resulting in 5 lockages during high tide and low tide (Figure 5.8).
- Water densities of both lakeside and seaside will be assumed constants of respectively 1000,0 and 1035,0 kg/m^3.
- The step size Δt used for iteration in the conceptual model has been set to 0,1 seconds.

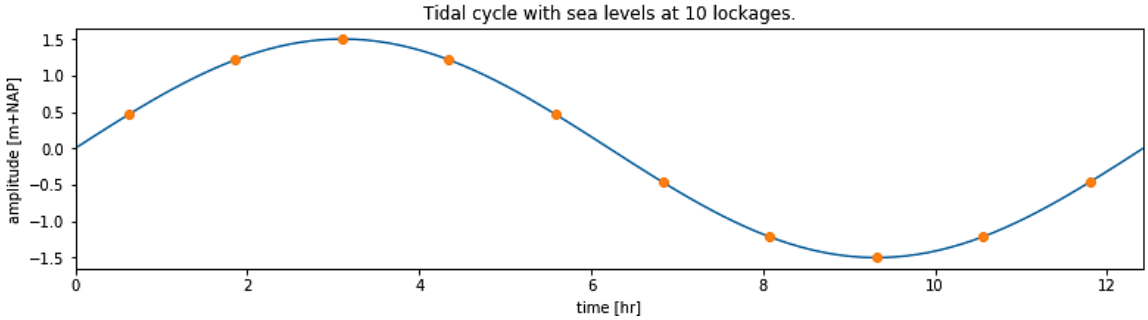

Figure 5.15: Tidal cycle discretized in several lockages equally far apart. The orange dots represent the water levels for consecutive lockages. Reproduced from Figure 3.2.

5.2.1 Significance of Discrepancies over Navigation Phase

Figure 5.16 shows the outputs of a single lockage phase during high tide using the parameters of maximum discrepancies. The final amount of salt intrusion using the $2L\Delta t$ assumptions is **883** tonnes. The *green* plot in these plots shows the amount of transported salt mass by return currents. During the exiting of the lock, it is seen that the contribution of the return current is negative (i.e. negative amount of salt intrusion). After a full lockage phase of navigation at lakeside, the total contribution of the return current equals **-72 tonnes**, shown by the *green* plot.

Figure 5.16: Output of computation of a lockage phase using the conceptual model and the 2LΔt assumptions. The black, blue, and purple lines correspond to volumes shown on the left y-axis. The red line corresponds to amounts of salt intrusion at lakeside, measured in tonnes on the right y-axis. Please note the right y-axis starts at -200 tonnes.

Next, the parameters are applied to a computation using the ZSF assumptions. The outputs are shown in Figure 5.17. A total salt intrusion of ***985*** tonnes is calculated. The contribution by the return current, implemented by exchanging a ship's volume of water, is carried out at the last timestep according to the ZSF assumptions and is therefore hardly visible. Therefore, an additional 50 seconds is added to the end of the plot. From the simulation it follows that the contribution of the return current amounts to **30** tonnes.

According to the algorithm of the ZSF, the amount of suspended salt in the lock is tracked in terms of present salt mass, in contrast to the $2L\Delta t$ assumptions where it is tracked in terms of the saline volume in the lock. Since both approaches produce outputs in different quantities, it is difficult to compare them. Therefore, the outputs of the ZSF will be converted to volumes of fresh and saline

water. By dividing the salt mass in the lock over the density differences, the saline volume is obtained. The fresh volume is obtained from the difference between the total volume and the saline volume in the lock. This translation is shown in Figures 5.17 and 5.18.

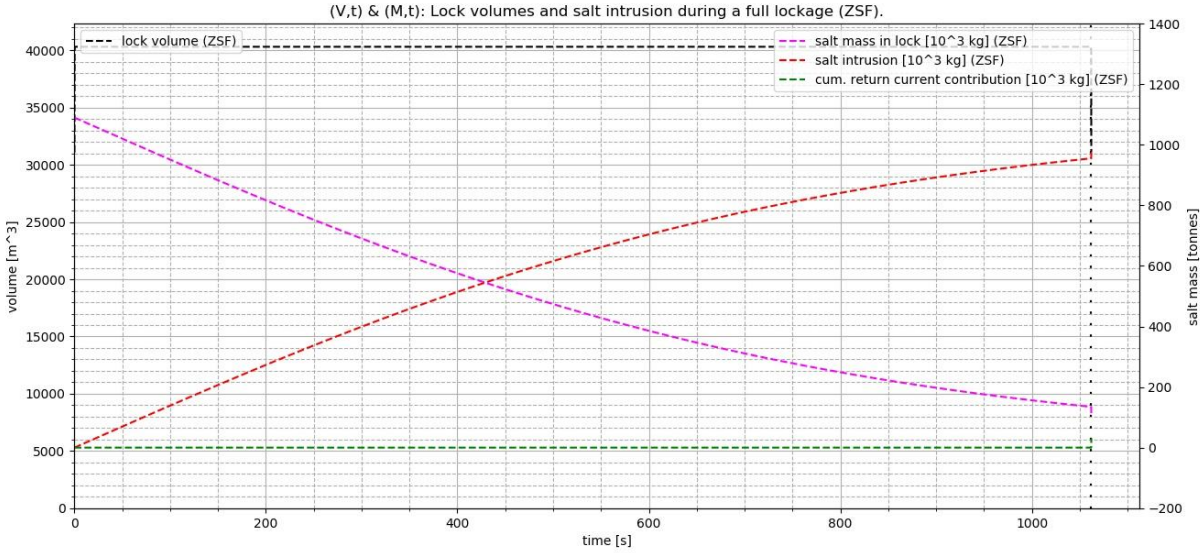

Figure 5.17: Output of computation of lockage phase navigation at lakeside using the conceptual model and the ZSF assumptions. An additional 50 seconds has been added to the x-axis range to promote readability of the final timesteps.

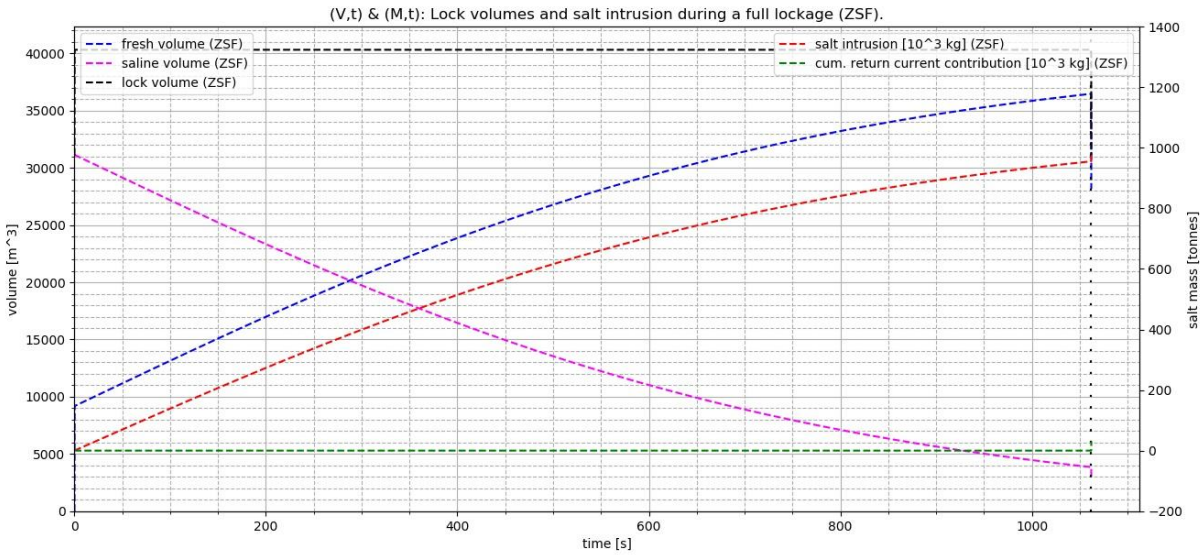

Figure 5.18: Output of computation of a full lockage using the conceptual model and the ZSF assumptions. It should be noted that according the ZSF assumptions, no separate fresh and saline volumes are obtained as the lock is homogeneously mixed.

Subsequently, Figures 5.16 and 5.18 are overlaid in Figure 5.19. This figure clearly illustrates the differences between outputs of both modelling approaches for a full lockage phase. From Figure 5.19 it is seen that the total discrepancy between modelling approaches indeed equals **102** tonnes as was roughly estimated from section 5.1.3 (Figure 5.14). The total salt intrusion for the $2L\Delta t$ assumptions and ZSF assumptions equal **883** tonnes and **985** tonnes respectively. Therefore, it can be stated that in the most extreme case the discrepancy that occurs between both modelling approaches equals about 11% of the total amount of salt intrusion. This is mainly caused by the influence of the return current on the salt tongue during the exiting of a ship.

Furthermore, the attention is drawn to the difference in gradient between the *red dotted* and *blue continuous* plots. It is seen the *blue* plot falls less quickly than the *red* plot. This is explained by the extra saline water in the lock in the simulation with the $2L\Delta t$ assumptions. This is due to the pushing back of the salt tongue into the lock during the exiting of a ship ($0\ s < t < 140\ s$). The lock exchange according to the relative lock exchange formula is of slightly different magnitude, as the time scale and the salt volume are shifted relative to each other.

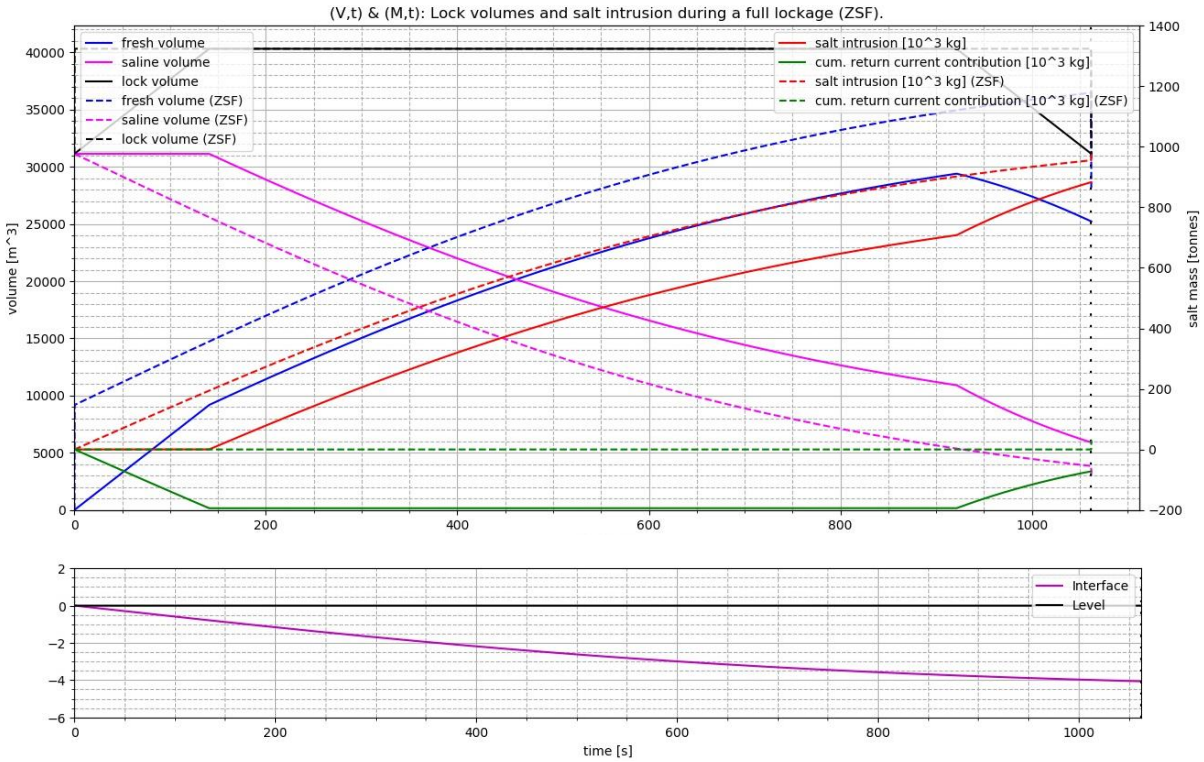

Figure 5.19: Outputs of both modelling approaches for a single lockage phase of navigation at lakeside, using the parameters that lead to the biggest discrepancy. The results shown are an overlay of the 2LΔt assumptions computation of Figure 5.5 and ZSF assumption computation of Figure 5.7. The interface of the bottom figure (purple plot) represents the 2LΔt interface.

5.2.2 Significance of Discrepancies over Tidal Cycle

Next to the examination of the discrepancies during the most extreme state, it is of value to examine the expected discrepancies for a realistic case. This will be carried out for half tide cycles. For these simulations, the total duration of the navigation phase will be chosen from a realistic point of view. Therefore, a t_{door} of 5 minutes, and a t_{wait} of 10 minutes will be applied such that the total duration of a navigation phase equals 20 minutes.

$$h_0/d = 0{,}5 \qquad t_{door}/t_{LE} = 0{,}27 \qquad t_{wait}/t_{LE} = 0{,}55$$

Because the entire lockage cycle is considered here, the results also reveal the discrepancies of the levelling phases. In the previous paragraph, no comprehensive analysis of discrepancies during the levelling phase has been carried out. Nevertheless, it is expected that in this case study, general discrepancies of the levelling phases can be assessed. A similar 'salt intrusion contribution' plot is added to the upcoming figures as the *green* lines in the previous figures. The contribution of levelling to the salt intrusion is shown in the *blue* horizontal plot.

5.2.2.1 High Tide

Figure 5.20 shows the outputs of consecutive lockages during high tide for the $2L\Delta t$ assumptions. After the first lockage the results appear to show an equilibrium character as seen from the pattern of fresh and saline courses. After consecutive lockages, the total contribution from the return current to the salt intrusion (*green* plot) is merely **-58** tonnes which is around 1% of the total amount of salt intrusion (**4114** tonnes). From the *blue* horizontal line, a relatively large contribution from levelling can be seen as compared to the shipping disturbances. The total amount of salt intrusion from levelling amounts to **1032** tonnes.

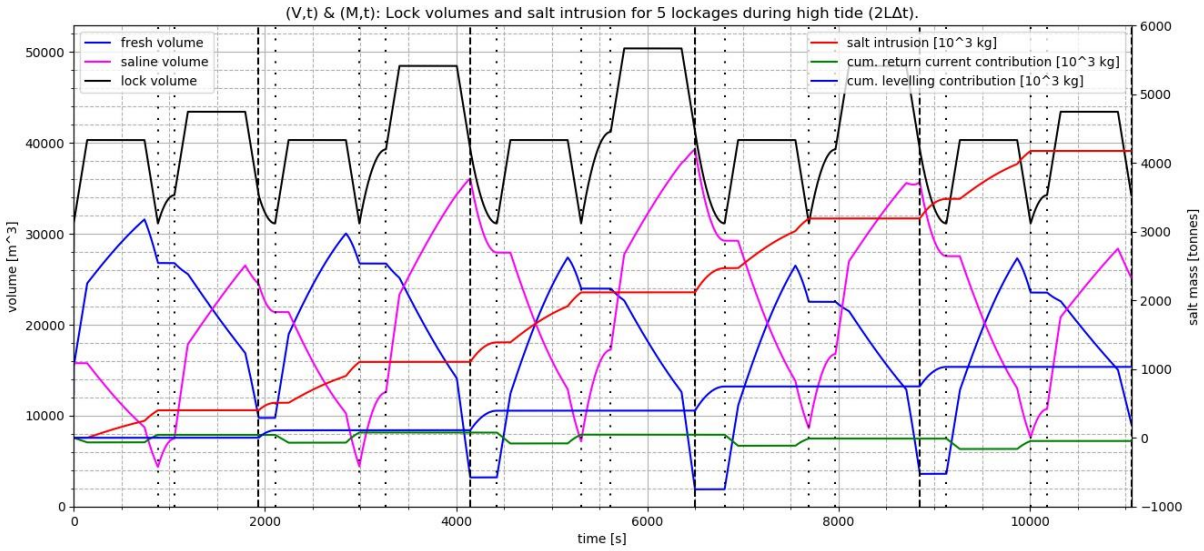

Figure 5.20: Simulation of 5 consecutive lockages during high tide for the $2L\Delta t$ assumptions.

Figure 5.21 shows the outputs of the same case but now for the ZSF assumptions. After five consecutive lockages during high tide, the contribution from return currents to the salt intrusion is **290** tonnes of the total amount of salt intrusion of **3718** tonnes. The total amount of salt intrusion from levelling amounts to **817** tonnes. It is thus seen that the ZSF results in less salt intrusion from levelling and more salt intrusion from return currents with respect to the $2L\Delta t$ assumptions. A statement on this will be made in the preliminary conclusion at the end of this paragraph.

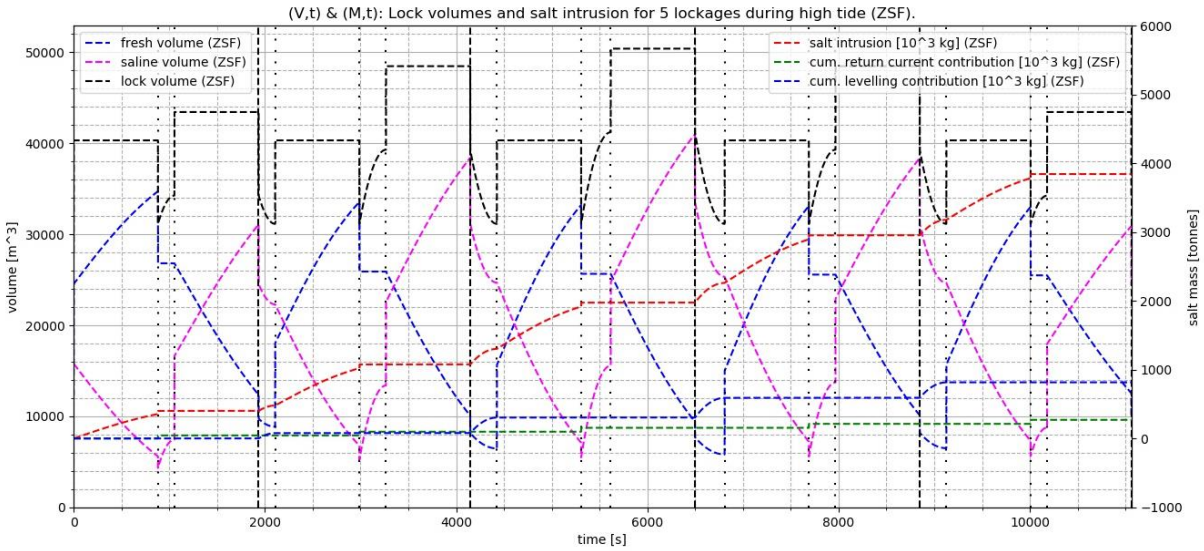

Figure 5.21: Simulation of 5 consecutive lockages during high tide for the ZSF assumptions.

5.2.2.2 Low Tide

Figures 5.22 and 5.23 show the outputs of computations of five lockages during low tide for the $2L\Delta t$ assumptions and ZSF assumptions respectively. The blue horizontal plots show that correctly no levelling contribution is calculated, except for the first lockage phase when the transition from high tide to low tide occurs. This is in-line with the expected results. According the $2L\Delta t$ assumptions a total amount of salt intrusion of **1833** tonnes is calculated. For the low tide situation, the total amount of transported salt by return currents amounts to **304** tonnes. This means that the net salt intrusion from shipping during low tide is higher than during high tide.

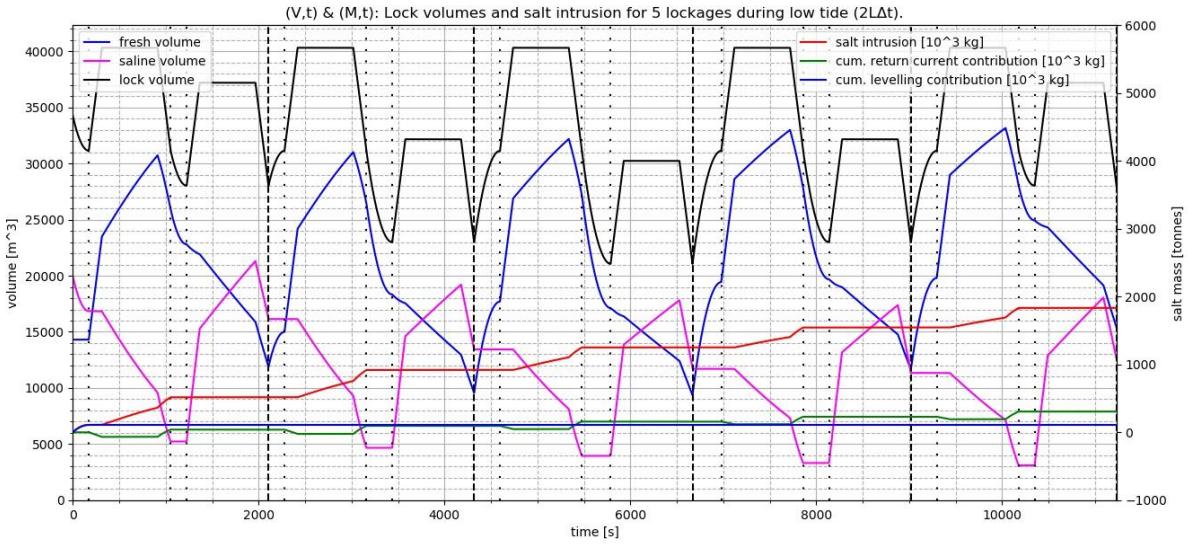

Figure 5.22: Simulation of 5 consecutive lockages during low tide for the $2L\Delta t$ assumptions.

For the ZSF assumptions in Figure 5.23, roughly similar answers are obtained. The total salt intrusion using these assumptions is equal to **1845** tonnes, where a contribution of **238** tonnes is found for return currents. It is seen that roughly the same amounts of salt intrusion are calculated as for the $2L\Delta t$ assumptions.

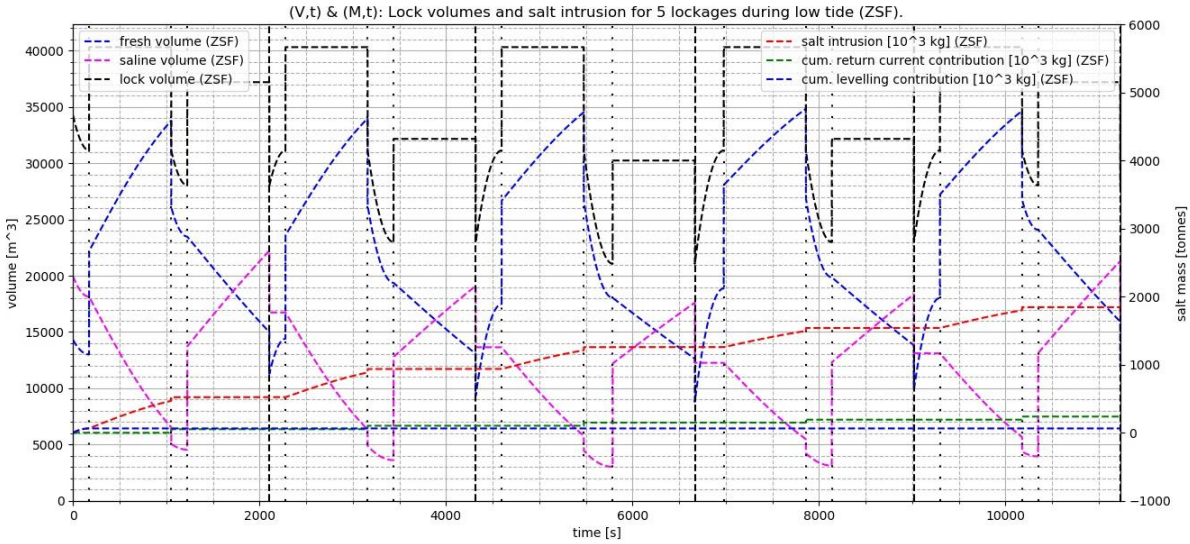

Figure 5.23: Simulation of 5 consecutive lockages during low tide for the ZSF assumptions.

5.2.3 Preliminary Conclusion

In this paragraph, case studies have been carried out with the most unfavourable (i.e. leading to largest discrepancies) modelling parameters and with realistic modelling parameters. These studies were conducted to expand on the range for which improvements can be expected between the $2L\Delta t$ - and ZSF assumptions. The upcoming figures 5.24, 5.26, and 5.27 show the amounts of salt intrusion according both modelling approaches for the extreme case, high tide, and low tide respectively for summarization of the findings of this paragraph. The outcomes for these simulations are included in Table 5.8. The following notable findings have emerged.

In the most extreme case, a discrepancy of approximately **100** tonnes of suspended salt is found during one lockage for a lock with dimensions of the Krammer locks and ships with dimensions of CEMT class: VIa (**883** tonnes for $2L\Delta t$ vs **985** tonnes for ZSF; negative discrepancy). This amounts to approximately 11% of the total salt intrusion. However, this case is obtained by using a fully saline lock. From Figures 5.20 to 5.23 it is seen that this level of salinity is hardly reached using realistic simulation parameters.

Table 5.8 shows the amounts of salt intrusion for the case study of consecutive lockages using realistic model parameters.

Figure 5.24: Simulation of lockage phase that led to the biggest discrepancies between modelling approaches (Figure 5.19).

Table 5.8: Parametrized salt intrusion estimates in tonnes for five consecutive lockages for high - and low tide.

Five lockages w/ realistic parameters	***High tide: $2L\Delta t$***	***High tide: ZSF***	***Low tide: $2L\Delta t$***	***Low tide: ZSF***
Total Salt intrusion	*4114*	*3718*	*1833*	*1845*
Salt intrusion by return currents	*-58*	*290*	*304*	*238*
Salt intrusion by levelling	*1032*	*817*	-	-

It can be seen from Table 5.8 that in both simulations different amounts of salt intrusion have occurred due to exchange flows. This follows from the fact that the discrepancies of salt intrusion between model approaches are not entirely due to the differences due to return currents and levelling.

This can be explained by the changes in the initial conditions between the ZSF and the $2L\Delta t$ assumption, as both sets of assumptions use the same code to account for the lock exchange. Furthermore, the following recommendations result from the preliminary validation, the case study, and the sensitivity analyses, and form the basis of the recommendations section.

The validation showed that the $2L\Delta t$ assumptions can lead to improvements compared to the ZSF by using refined descriptions for the shipping contributions to salt intrusion. Differences occur in these shipping contributions for different model parameters. These differences in the results can be translated into an applicable model factor for the ZSF, such that the results are in-line with the $2L\Delta t$ outcomes. The sensitivity analyses have shown that the largest discrepancy arises because of pushing back the exchange flow into the lock. This generally results in a reduced amount of salt intrusion in the $2L\Delta t$ model compared to the ZSF. The effects of pushing back the salt wedge during exiting can be captured using a model factor, referred in this study as f_{exit}. This factor is inversely proportional to the amount of salt mass in the lock. Thus, the amount of salt intrusion decreases for saltier lock chambers. In addition, this factor is to be proportional to the ship volume V_s and density differences $\Delta\rho$, and relevant lockage duration parameters t_{door}/t_{LE} and t_{wait}/t_{LE}. It will now be attempted to make an estimate of the bounds of the model factor f_{exit}.

The factor is to be applied to the amount of salt intrusion over the entire navigation phase, thus including the contribution by lock exchange. This is considered more convenient than applying a factor to the contribution of shipping, as the latter will lead to a sign change in most cases. It was seen that by using the parameters that lead to the biggest discrepancies, a total f_{exit} of $883/985 \approx 0{,}89$ was required. Since the validation chapter has shown that the contribution of pushing back the salt tongue in the $2L\Delta t$ model is overestimated compared to practice, the $2L\Delta t$ assumptions underestimate the total salt intrusion during exiting of the lock. What can be said further is that this is the only process that can generate a negative amount of salt intrusion. Therefore, the value of f_{exit} of 0,89 can be interpreted as the lower bound of the factor.

The upper bound of f_{exit} follows from the maximum positive discrepancy between the ZSF and $2L\Delta t$ assumptions over a navigation phase. These turn out to be obtained for initial condition (h_0/d) equal to 0,333, and t_{door}/t_{LE} and t_{wait}/t_{LE} equal to 0 (observed from Figure 5.11). For these values a discrepancy of approximately **20** tonnes is obtained between the ZSF and the $2L\Delta t$ assumptions. The

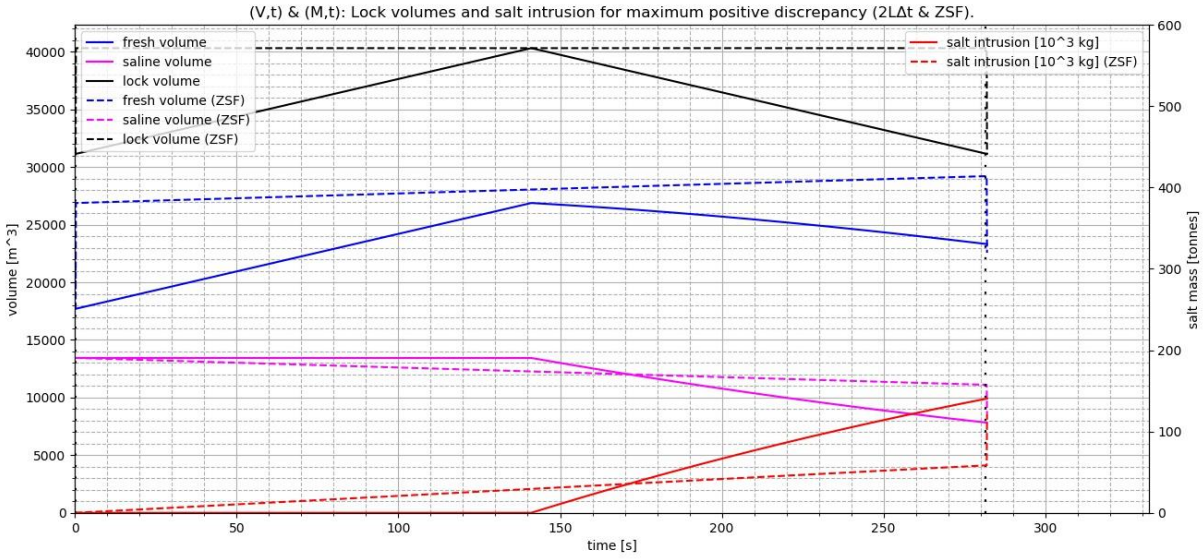

Figure 5.26: Maximum positive discrepancy case for the $2L\Delta t$ and the ZSF assumptions. The final amounts of salt intrusion for the $2L\Delta t$ and the ZSF assumptions are 141 and 122 tonnes, respectively.

full navigation phase for this case is simulated and shown in Figure 5.26. The final amounts of salt intrusion for the $2L\Delta t$ and ZSF assumptions equal **141** and **122** tonnes respectively. The upper limit for f_{exit} thus becomes equal to $141/122 \approx 1{,}16$. The factor's bounds are given by (5.16). It should be stressed that these bounds are an indication of the expected discrepancies and are therefore not strict bounds.

Since the $2L\Delta t$ assumptions overestimate the pushing back of the salt tongue towards the lock, it is possible that the actual amount of salt intrusion by shipping is higher than calculated with the $2L\Delta t$ assumptions. Therefore, it is added that the lower limit of f_{exit} is considered more reliable than the upper limit. Nevertheless, the sensitivity analysis showed that for the most part a lower amount of salt intrusion is obtained with the $2L\Delta t$ assumptions. The upper bound is therefore only applicable in specific situations, for example when the lock passages can be considered as relatively short. Therefore, it is estimated that mainly an f_{exit} of approximately between 0,9 and 1,0 is applicable.

$$0{,}89 < f_{exit} < 1{,}16 \tag{5.16}$$

In addition, from this study it follows that a similar model factor is required for the levelling phase. Therefore, the author would propose to include a factor in the ZSF to the transported salt mass by levelling for the levelling phases (f_{level}). However, not much attention has been paid to this in this study. Nevertheless, it will be attempted to provide insight in its magnitude. It was seen that more salt intrusion is obtained from the use of a two-layer system and lock valves, which for the greater part convey saline water. Therefore, the levelling factor (f_{level}) is to be proportional to the amount of salt mass in the lock. It is estimated from Table 5.8 and the preliminary analyses that this factor should be on average **1,25**, based on the differences in levelling contributions for averaged, realistic lockage parameters. Nevertheless, because this has not been investigated in depth, no further conclusion on its magnitude will be given.

What can be said however, is that this factor is never to be below 1,0. This specific case where the ZSF assumptions consider more salt intrusion during levelling than the $2L\Delta t$ assumptions only occurs if the amount of salt in the lock is very low (i.e. interface level below the bottom level of the lock valve), and the tidal situation is high tide. In this case, for the $2L\Delta t$ assumptions mainly fresh water is transported to the lakeside by levelling, where for the ZSF assumptions, suspended salt is conveyed because of the homogeneous lock density assumption. Regarding this specific case, it should be said that prior to the levelling phase, a levelling phase to seaside should be employed, as well as a navigation phase to seaside. Having a nearly fully fresh lock after having levelled to seaside (thus using saline water for levelling upwards) and having opened the lock gates at seaside is impossible. Therefore, the lower bound of f_{level} is 1,0.

As previously stated, no statement on the upper bound of f_{level} is made because this has not been investigated.

$$1{,}0 < f_{level} \tag{5.17}$$

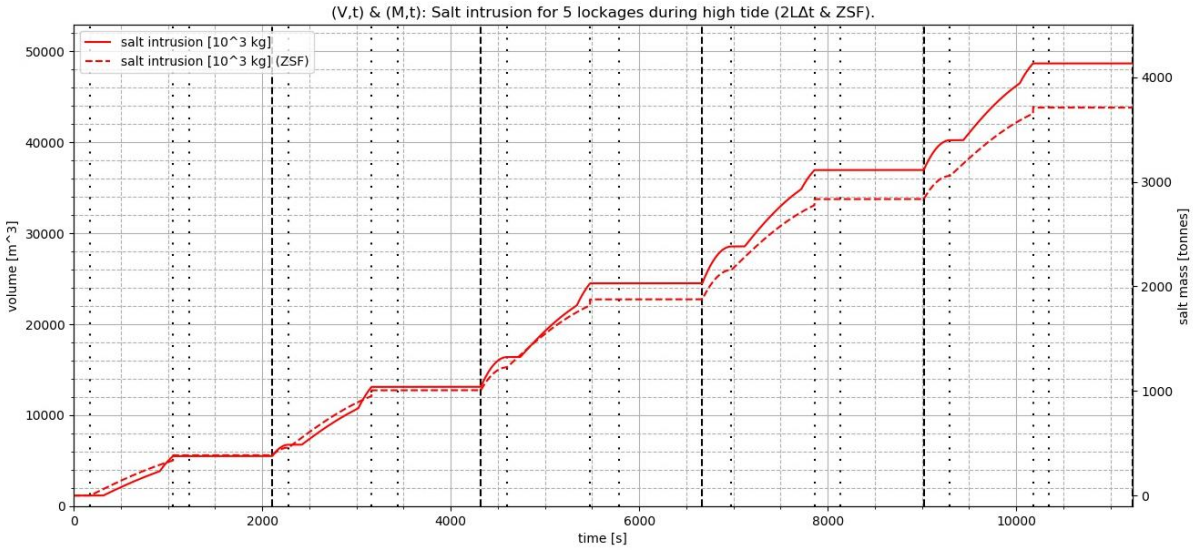

Figure 5.26: Salt intrusion during simulation of 5 consecutive lockages in practice during high tide for the $2L\Delta t$ - and ZSF assumptions.

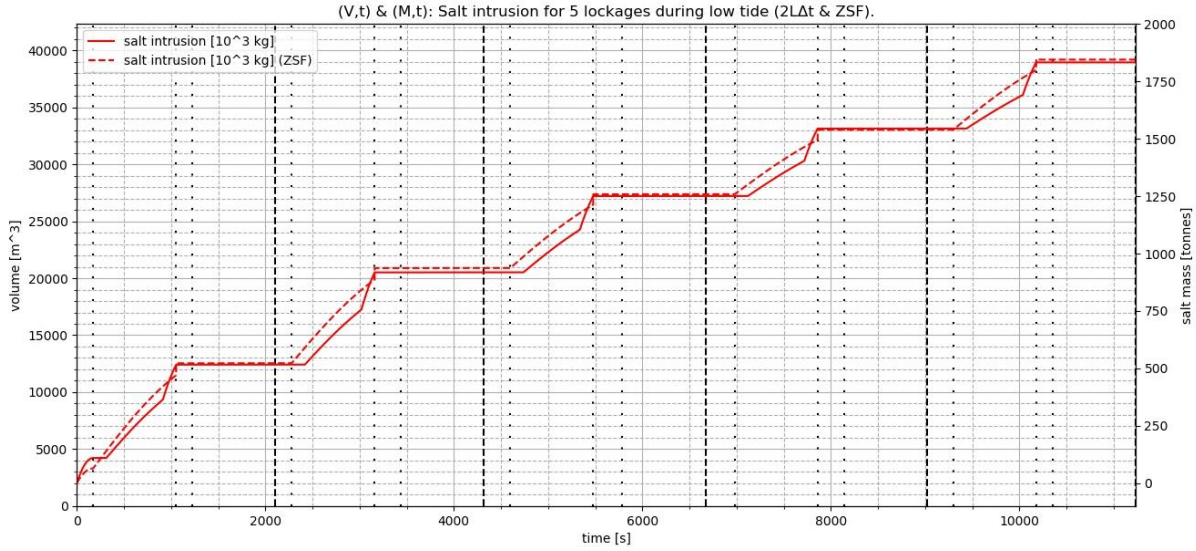

Figure 5.27: Salt intrusion during simulation of 5 consecutive lockages in practice during low tide for the $2L\Delta t$ - and ZSF assumptions.

6 Discussion

This chapter discusses the areas of uncertainty, before providing the conclusion in the next chapter. It deals with three distinct topics: internal consistency of the conceptual model, the presence of mixing during a lockage, and uncertainties in the validation part.

Internal Consistency of the Conceptual Model

The conceptual model considers changes in the interface depth due to the presence of the ship. It is possible the interface depth changes from the influence of a ship while the saltwater volume in the lock remains the same, as was seen in section 3.2.2 on the static water displacement of gradual shipping. Therefore, the interface depth (d_{int}) and the saline volume (V_{saline}) must be calculated independently. It was found that after one lockage there is a small deviation between the calculated value of d_{int} and its theoretical value, obtained from manually converting V_{saline} to an interface depth including the present ship. To demonstrate, this the author would like to point the attention to Figures 6.1 and 6.2, and $(6.1 - 6.3)$ on the next page. It is seen that after a single lockage, the interface depth deviates with 5 millimetres from the theoretical, geometrically obtained value of the saline volume. Many attempts have been made to improve this deficiency, without result. To not allow this effect to build up for several lockages, it was decided that after a full lockage and at a point in time when the lock contains no ship, the interface depth will be adjusted according to the volume of suspended salt that is present in the lock (V_{saline}). It is presumed with certainty that the discrepancies are due to the formulations for adjustments to the interface depth resulting from the activity of the ship in the interface layer (additional static water displacements, section 3.2.2). Therefore, it is believed the calculated volumes (V_{saline} and V_{fresh}) are of greater reliability, hence the adjustment of d_{int} to the geometrical value of the interface depth of V_{saline}.

Mixing, Propeller Jets, and Bubble Screens

For the determination of the salt intrusion, this study uses a two-layer system for the density distribution within the lock. Using such a distribution implies that no mixing takes place. In contrast, propeller jets of ships and bubble screens both contribute to the total mixing in the lock. This assumption is therefore unjustified from a practical point of view. Nevertheless, this fact does not hinder the results of this study. It is of value to have investigated the salt intrusion using assumptions of the opposite end of the spectrum regarding mixing. That having said, it is expected that the discrepancies between the ZSF and reality are therefore more optimistic as was brought forward by the discrepancies between the ZSF and the $2L\Delta t$ assumptions.

Validation

As was mentioned in Chapter 4, the amount of validation data to test the assumptions of this study is sparse: the graph from Chapter 4 (Figure 4.3) was the only available piece of validation data that was found. As mentioned in Chapter 4, there is also uncertainty in the data on ships entering the lock. The entry of ships cannot be seen in the validation data. Moreover, from studying the graph bubble screens were applied for some duration during the experiments. No regard was taken with the

application of bubble screens in this study. These points together have an unfavourable effect on the reliability of the validation.

```
~~~~~~~~~~~~~~~~~~~~~~~~~~~~~~~~~~~~~~~~~~~~~~~~~~~~~~~~~~~~~~~~~~~~~~~~
        initiële condities
        peil kolk -0.46 +mNAP
        interface -3.23 +mNAP
        zoetvolume 12249.45 m3
        zoutvolume 15775.66 m3
        kolkvolume water 28025.11 m3
        kolkvolume incl schip 37205.11 m3
        scheepsklasse 1x Rijnmax schip
        10 passages per getijdecyclus van 12.42 uur
~~~~~~~~~~~~~~~~~~~~~~~~~~~~~~~~~~~~~~~~~~~~~~~~~~~~~~~~~~~~~~~~~~~~~~~~

-2LΔt assumptions-

*begin simulatie*
---------------------
---------------------
passage 1  stap 1 : nivelleren naar meerzijde
---------------------
passage 1  stap 2 : deur open meerzijde
---------------------
passage 1  stap 3 : nivelleren naar zeezijde
---------------------
passage 1  stap 4 : deuren open zeezijde

cumulatief zoutlek 13591.61 m3; 475.71 tonnes
---------------------
---------------------
    *einde simulatie*

~~~~~~~~~~~~~~~~~~~~~~~~~~~~~~~~~~~~~~~~~~~~~~~~~~~~~~~~~~~~~~~~~~~~~~~~
eind condities
        peil kolk 0.46 +mNAP
        interface -1.46 +mNAP
        zoetvolume 8751.64 m3
        zoutvolume 25503.25 m3
        kolkvolume water 34254.89 m3
    *check kolk volume incl schip 43434.89 m3

        cumulatief zoutlek 13591.61 m3
~~~~~~~~~~~~~~~~~~~~~~~~~~~~~~~~~~~~~~~~~~~~~~~~~~~~~~~~~~~~~~~~~~~~~~~~
--- 63.2 seconds ---
done
```

Figure 6.1: Image of numerical output from the conceptual model. These outputs helped in checking on internal consistency at the development, after which it was found a small discrepancy is formed between the interface depth and the saline volume.

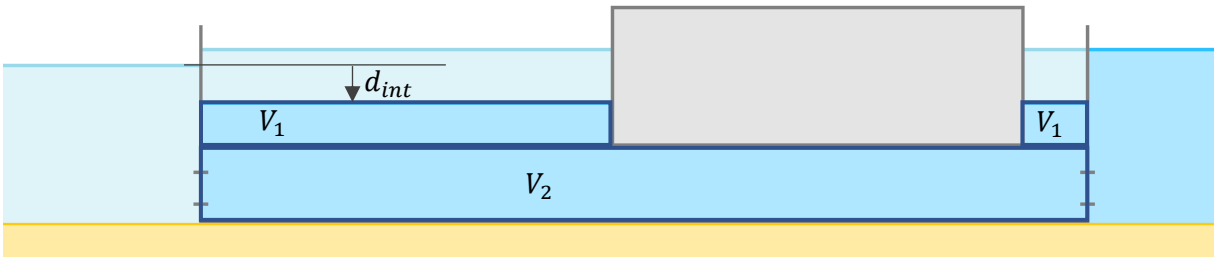

Figure 6.2: Schematization of the final conditions from Figure 6.1. From recalculating the interface depth, it is seen a small deviation with the conceptual model outputs from Figure 6.1 is present.

$$V_2 = (d + h_{lock} - d_s) * lw = (6{,}46 - 4) * 280 * 24 = 16531{,}2\ m^3 \quad (6.1)$$

$$V_1 = V_{saline} - V_2 = 25503{,}25 - 16531{,}2 = 8972{,}05\ m^3 \quad (6.2)$$

$$d_{int} = \left(d - \frac{V_2}{lw} - \frac{V_1}{lw - l_s w_s}\right) = 6 - 2{,}46 - \frac{8972{,}05}{280 * 24 - 135 * 17} = 1{,}51\ m \quad (6.3)$$

7 Conclusion

In this master thesis an attempt has been made to answer the following question:

To what extent can the accuracy of the salt intrusion estimate of the ZSF be improved by replacing the assumptions of homogeneous lock density and instantaneous shipping with assumptions of greater physical representativeness?

To answer this research question, a causal-comparative method is chosen where the influences of spatial lock density and - shipping contributions on the salt intrusion are investigated. A combination of a literature review, a sensitivity analysis and a case study is pursued. The research is subsequently formulated in threefold:

- What is a more realistic description of the return current and density distribution in the lock based on literature?
- What is the impact of the new implementations of shipping and density distribution in the lock on the computed salt intrusion as compared to the ZSF?
- For what range of applicability do the new assumptions provide an improvement to the parametrized salt intrusion estimate?

This has been investigated by modelling a lock passage according to the algorithm of the ZSF in which refined descriptions for return currents and the density distribution are implemented, after which it is tested against the ZSF. This chapter presents the answers to these questions and thereby aims at answering the main question of this study.

Research Question 1

What is a more realistic description of the return current and density distribution in the lock based on literature?

The ZSF is a parametrized salt intrusion model that contains assumptions of which the physical representation can be optimized. These assumptions are application of instantaneous shipping and the use of a homogeneous lock density. The assumptions entail respectively that sailing is modelled by exchanging a ship volume with a similar water volume from its sailing destination, and that all water, and therefore all suspended salt, which enters the lock is instantly mixed and evenly distributed.

The literature study of Chapter 2 has presented the author and the reader with two alternative assumptions. These are application of a return current volume flux distribution according to continuity in combination with gradual shipping, and the use of a stratified lock density. The motivations for these choices will now be supported.

There are several reasons to test if parametrized salt intrusion estimates in locks can be improved using a stratified system as opposed to a homogeneous system. First, the free-flowing processes that influence the density within the lock (i.e. levelling, exchange flows to lakeside) all occur

over the bottom of the lock which promote stratification. Second, salt water has a higher density than fresh water, which makes it sink in comparison to fresh water. And last of all, it is of value to test parametrized salt intrusion from shipping in a stratified lock as it assumes the other extreme of density distribution with respect to a homogeneous lock, which has not been done so far in literature.

For the return current concerned, the implementation of instantaneous shipping in the ZSF neglects all dynamic effects that are present during the sailing process. Instead, this study will investigate a gradual shipping implementation where the ship is displaced from the lock in small time steps. By using gradual shipping, aim is set at adding a degree of this dynamicity to the salt intrusion formulation. This is achieved with the help of an extra assumption, namely the alternating displacements assumption. This assumption holds that a ship is displaced from the lock or in the lock alternately with the exchange flow. By doing so, the return current can affect the present exchange flow as well. Moreover, during gradual sailing the return current will be able to affect a changing lock density, subsequently contributing to the dynamicity. An improved description for the return current, in comparison to instantaneous shipping, is then the use of the return current volume flux distribution of Schijf [12]. In this study, this is simplified to the continuity method. By using this return current distribution, a larger contribution of flow is taken underneath the ship than next to the ship. This is more realistic than instantaneous shipping because of the larger flow area under the ship in practice, compared to instantaneous shipping with a homogeneous lock which can be considered as having a uniform return current distribution in depth.

It is believed that the assumptions of gradual shipping with a return current distribution according Schijf, and a stratified lock density represent the physics in a more accurate way and therefore provide refinements to the parametrized salt intrusion estimate of the ZSF.

Research Question 2

What is the impact of the new implementations of shipping and lock density on the computed salt intrusion as compared to the ZSF?

Chapter 4 showed that the accuracy of the salt intrusion estimate using the $2L\Delta t$ assumptions is increased compared to the ZSF. However, no conclusion can be drawn on the extent to which the $2L\Delta t$ assumptions imply refinements in Chapter 4 alone.

Therefore, this issue is investigated in Chapter 5. It has first been examined for cases without exchange flows. Following from Figure 5.3, the joint contribution from a return current distribution according to the continuity method and a two-layer system ensures that, in extreme cases, 16% more salt intrusion is obtained with respect to the ZSF. This case is obtained when the average interface depth during the sailing process is equal to the draught of the ship. This follows from the nondimensionalization, which showed that discrepancies between modelling approaches form a parabolic relationship when the amount of salt intrusion is divided by the factor J, defined by (5.13).

When the alternating current is added to the equation, the discrepancies turn out to be more sensitive to the influence of the return current on the alternating current when leaving the lock. For the most part, the differences between the shipping implementations tend towards an increased amount of salt intrusion for the ZSF assumptions. This is due to pushing back the exchange flow to the lock during exiting of a ship, which has the greatest impact on discrepancies between the two modelling approaches. This arises because during exiting of the ship the effect of the return current on a lock with more saline water is larger than the effect of an incoming vessel on a less saline lock. This is due to the exchange flow between exit and entry of ships. The impact from the $2L\Delta t$ assumptions thus entail generally less salt intrusion for navigation phases.

Although the discrepancies on the levelling phases were not investigated in depth, the preliminary conclusion of section 5.2.3 substantiated that for all lockage scenarios more salt intrusion is obtained from levelling when using the two-layer assumption in combination with lock gate valves. The maximum impact of this difference has not been investigated, however.

Research Question 3

For what range of applicability do the new assumptions provide an improvement to the parametrized salt intrusion estimate?

What was shown in Paragraph 5.2, is that when considering the entire navigation phase in a case study, and using the most unfavourable parameters (i.e. the parameters that lead to the biggest discrepancies), the discrepancies between modelling approaches reduces to 11%. The maximum discrepancy is negative, meaning the ZSF assumptions take account of more salt intrusion. This discrepancy is obtained under the following conditions:

$$h_0/d = 1 \qquad t_{door}/t_{LE} = 0 \qquad t_{wait}/t_{LE} = 1$$

Similarly, the maximum positive discrepancy was isolated from the sensitivity analyses over the navigation phase and tested in a case study. It was seen that over the entire navigation phase, the amount of salt intrusion is increased by 16% regarding the ZSF assumptions. This discrepancy is obtained under the following conditions:

$$h_0/d = 0{,}333 \qquad t_{door}/t_{LE} = 0 \qquad t_{wait}/t_{LE} = 0$$

Subsequently, simulations were performed to find the discrepancies for realistic model parameters such that conclusions can be given for typical lockages. These were obtained by running the simulations for successive lockages, such that roughly equilibrium states of salt concentration in the lock were achieved. The following results were obtained and are reproduced in Table 7.1.

Table 7.1: Reproduction of parametrized salt intrusion calculations from Paragraph 5.2 for high - and low tide.

Parameter	*High tide: $2L\Delta t$*	*High tide: ZSF*	*Low tide: $2L\Delta t$*	*Low tide: ZSF*
Total Salt intrusion [tonnes]	*4114*	*3718*	*1833*	*1845*
Salt intrusion by return currents [tonnes]	*-58*	*290*	*304*	*238*
Salt intrusion by levelling [tonnes]	*1032*	*817*	-	-

It follows from Table 7.1 that approximately the same results are obtained for low tide and that for high tide a larger contribution of the return flows is calculated for the ZSF. Furthermore, both simulations have amounted for different amounts of salt intrusion by exchange flows, as the discrepancies between the total amount of salt intrusion is not entirely due to the discrepancies by return currents and levelling. This must be explained from the changes in initial conditions between the ZSF and $2L\Delta t$ assumptions, as both formulations use the same code for accounting for the lock exchange within the conceptual model.

For five consecutive lockages during high tide, the differences between the modelling approaches amount to approximately 9% of the total salt intrusion. At low tide this decreases to 4%. It is thus observed that the discrepancies are smaller for fresher locks. It can therefore be concluded that the discrepancy between the return current contributions is proportional to the amount of salt in the lock. This finding, together with the sensitivity analyses of section 5.1 including exchange flows, conclude that the most significant difference between the models is the effect of the return current on the lock exchange during exiting of the ship. This largely causes less salt intrusion than estimated by the ZSF. Therefore, by using a stratified lock in combination with a more realistic return current distribution, refinements to the ZSF are to be expected for more saline locks as the return current will have a greater influence on the lock exchange.

It also follows that the discrepancies are proportional to the duration of the simulation. For the $2L\Delta t$ assumptions and increasing waiting times (t_{wait}/t_{LE}) and ship volumes (V_s), the results in Appendix C (Figures C.9 to C.12) show that the influence of the return current on the lock exchange increases during exiting the lock compared to entering the lock. This further substantiates that for increasing waiting times, the total amount of salt intrusion by shipping is to a greater degree dependent on the exiting than on the entry of ships.

Main Question

To what extent can the accuracy of the salt intrusion estimate of the ZSF be improved by replacing the assumptions of homogeneous lock density and instantaneous shipping with assumptions of greater physical representativeness?

The amount of salt intrusion that occurs during consecutive lockages in practice depends on a complex mix of processes. This thesis states that the description of shipping currents according to continuity and the salt distribution in the lock is a step forward compared to current implementations. By applying the aforementioned assumptions, it was found that, in general, less salt intrusion is obtained during the navigation phases than assumed in the ZSF. Specifically, a reduction of five to ten percent is expected. Moreover, it was found that in the levelling phase more salt intrusion is obtained because of using lock valves and stratification. Also, the validation chapter shows that the $2L\Delta t$ assumptions approach the experiments with more accuracy. It is thus argued that by using the $2L\Delta t$ assumptions, a reasonable improvement in the accuracy of salt intrusion can be obtained.

8 Recommendations

What follows from the case studies, the validation step and the sensitivity analyses is that it is recommended to further investigate the following points of attention.

The author would propose to include a model factor (f_{exit}) in the ZSF which is inversely proportional to the salt mass in the lock and the lockage duration. Thus, decreasing the amount of salt intrusion by shipping for saltier locks. This follows from the finding that generally less salt intrusion is obtained for more saline lock volumes because of pushing back the exchange flow to the lock during exiting. The validation step showed, however, that the salt tongue should not be pushed back completely during the exit, as this is responsible for discrepancies between the Stevin lock experiments and the $2L\Delta t$ assumptions. Since the ZSF assumptions do not involve salt intrusion when ships sail out, applying a factor to this sailing movement would not make any difference to the computed amount of salt intrusion. Therefore, the factor (f_{exit}) should be applied to the total amount of salt intrusion over the entire navigation phase. Regarding its magnitude, it was seen that by using the parameters that lead to the biggest discrepancies, a total f_{exit} of $883/985 \approx 0{,}89$ was required. As the validation chapter has shown that the contribution of pushing back the salt tongue is overestimated in the $2L\Delta t$ model in comparison to practice, the value of f_{exit} of $0{,}89$ can be interpreted as the lower bound of the factor. This is further substantiated from the fact that this is the only process that can generate a negative amount of salt intrusion. The upper bound of f_{exit} follows from the maximum positive discrepancy between the ZSF and $2L\Delta t$ assumptions, which is found to be $141/122 \approx 1{,}16$. Since the $2L\Delta t$ assumptions overestimate the pushing back of the salt tongue towards the lock, it is possible that the actual amount of salt intrusion by shipping is higher than calculated with the $2L\Delta t$ assumptions. Therefore, more certainty is added to the lower bound of f_{exit} than to the upper bound. The sensitivity analysis showed that for the most part a lower amount of salt intrusion is obtained with the $2L\Delta t$ assumptions. It is estimated that mainly an f_{exit} of around 0,9 is applicable, and the upper bound is of considerably less importance.

In addition, the author would propose to include a factor in the ZSF to the contribution of transported salt mass during levelling (f_{level}). It was seen that more salt intrusion is obtained from the use of lock valves, which for the greater part convey salt water, in combination with a two-layer system. This levelling factor is therefore to be proportional to the amount of salt mass in the lock. It is estimated based on Table 7.1, that this factor should be on average 1,25. Nevertheless, because this has not been investigated in depth, no further conclusion on its magnitude will be given. Also, no statement on the upper bound of f_{level} is made because this has not been investigated. What can be said however, is that this factor is never to be below 1,0. This specific case where the modelling approach of the ZSF takes into account more salt intrusion during levelling compared to the $2L\Delta t$ assumptions only occurs if the amount of salt in the lock is very low (i.e. interface level is below the bottom level of the lock valve), and the tidal situation is high tide, such that with the $2L\Delta t$ assumptions mainly fresh water is transported to the lakeside by levelling. Regarding this specific case, prior to be able to level to lakeside during high tide, a levelling phase to seaside should be employed. Having a

fully fresh lock after having levelled to seaside (thus using saline water for levelling upwards) is therefore impossible, hence the lower bound of f_{level} being $1{,}0 < f_{level}$.

Follow-Up Studies

With a view to improving the estimates of the parametrized salt intrusion, the biggest discrepancy at present has been found to be the neglecting of the propeller jet. This can be expressed by two missing processes: additional salt flux due to the propeller jet, and in particular the presence of circulating currents in the lock chamber during acceleration and deceleration of ships. The validation study showed that the presence of the propeller jet plays an important role in the amount of salt intrusion. First, the discrepancies between the experiments and the $2L\Delta t$ assumptions increase for larger ships during sailing. Second, an initial decrease in salt mass was observed for ships sailing towards lakeside. It is estimated that the latter can be attributed to the influence of an accelerating ship, as previously mentioned by Deltares where it was stated to be a possibility. No studies can be found in literature that address this twofold phenomenon. It is therefore recommended to further investigate and parametrize the currents that arise throughout the lock chamber resulting from an accelerating or decelerating ship, as well as the additional salt flux from the propeller jet during sailing.

As already mentioned, no further research was carried out into the magnitude of the required levelling factor (f_{level}). Therefore, it is recommended that more research is conducted on its size and expected overall value. This includes a similar analysis of the influences that determine its size to add an additional parametrized contribution to the ZSF.

References

[1] O.M. Weiler, "*Zoutindringing door schutsluizen, overzicht projecten en aanzet formulering t.b.v. netwerkmodellen.*", Kennisprogramma Natte Kunstwerken, Deltares 2017.

[2] O.M. Weiler, "*Zoutindringing schut- en spuisluizen Opzet en verkenning Zeesluisformulering*", Kennisprogramma Natte Kunstwerken, Deltares 2018.

[3] D. Vreeken, Memo: "Implementatie waterverplaatsing schepen.", 2016.

[4] O.M. Weiler, "*Evaluatie bellenschermen Noordersluis IJmuiden – Noodmaatregel tijdens de droogte van 2018.*", Deltares 2019.

[5] O.M. Weiler, "*Verkenning noodmaatregelen verzilting IJsselmeer – schutoperatie en bellenschermen.*", Deltares 2019.

[6] R.E. Uittenbogaard, J.M. Cornelisse, *"Ontwerpstudie en praktijkproef zoutlekbeperking Volkerak sluizen – beschrijvingen resultaten praktijkproef Stevin sluis en evaluatie maatregelen Stevin sluis."*, Deltares 2011.

[7] P.P.D. van der Ven, T.S.D. O'Mahoney, O.M. Weiler, "*Methods to assess bubble screens applied to mitigate salt intrusion through locks",* 2018.

[8] R. Rotunno, J.B. Klemp1, G.H. Bryan, D.J. Muraki, "*Models of non-Boussinesq lock-exchange flow.*", 2010.

[9] G. Abraham, P. van den Burgh, P. de Vos, "*Pneumatic barriers to reduce salt intrusion through locks.*", Rijkswaterstaat 1973.

[10] P. Van der Burg, P. De Vos, "*Luchtbellenschermen in schutsluizen.",* Rijkswaterstaat 1962.

[11] A. Vrijburcht, Doctoral Thesis, "*Forces on ships in a navigation lock induced by stratified flows.",* T.U. Delft 1991

[12] J.B. Schijf, from: *PIANC's 17th International Navigation Congress.*, 1949.

[13] T. Robijns, "*Flow beneath inland navigation vessels.*", T.U. Delft 2014.

[14] CEMT-classes from: https://www.itf-oecd.org/sites/default/files/docs/wat19922e.pdf

[15] P. Groenenboom, "*Numerical simulation of intrusion of salt water during gate opening of the Stevin lock gates."*, Deltares 2010.

[16] A. De Loor, A. Heinsbroek, "Vormgeving nivelleeropeningen roldeuren Krammersluizen.", Rijkswaterstaat 2020.

[17] Van Hattum & Blankenvoort, "Memo: Info m.b.t. horizontale belastingen op de TE-en.", 1998.

Appendices

A Outputs of the Conceptual Model

In this appendix, outputs are presented from the conceptual model that was developed according to Chapter 3. The following computations will be presented:

- Lock exchange towards lakeside and seaside for a duration of 4 t_{LE}.
- Levelling phases (lockage phases *1* and *3*, respectively levelling to lakeside and seaside) during high tide and low tide.
- Navigation phases (lockage phases *2* and *4*, respectively navigation at lakeside and seaside).
- A full lockage, five lockages during high tide, and five lockages during low tide.

The computation parameters that have been used for the outputs are listed in Table A.1. The initial interface depth is set to half the water depth in the lock for all computations.

Table A.1: General usage parameters for all computation of this paragraph.

Parameter	***Value***
V [m³]	*40320*
l [m]	*280,0*
w [m]	*24,0*
d [m]	*6,0*
d_{int} [m]	*3,0*
ρ_0 [kg/m³]	*1005*
ρ_z [kg/m³]	*1030*
h_0 [m+NAP]	*0,0*

A.1 Lock Exchange

The theoretical lockage duration, t_{LE}, is defined according (2.7) and (2.8), and follows for the $2L\Delta t$-assumptions according $(A.1)$ upon applying the corresponding density differences and saline layer thickness.

$$t_{LE} = \frac{4l}{\sqrt{g\frac{\rho_z - \rho_0}{\rho_0}(d - d_{int})}} \approx 1300\ s \qquad (A.1)$$

Figures A.1 and A.2 show computations of only lock exchanges towards lakeside and seaside. For lock exchange to lakeside in Figure A.1, the salt mass in the lock is transported out of the lock by exchange flows. This is seen by the decline of the *purple* plot which represents the saline lock volume in cubic meters. The *blue* plot is the amount of freshwater volume, whereas the *black* plot represents the total lock volume of water, both in cubic meters. These volumes are to be read on the left y-axis.

As the exchange flow propagates, any salt water that has entered lakeside will be regarded as salt intrusion, which is calculated in tonnes of suspended salt. This is shown by the *red* plot and measured on the right y-axis. From the initial conditions, a total amount of $M = lw(d - d_{int})(\rho_z - \rho_0) = \mathbf{504}$ tonnes of suspended salt mass are present. From Figure A.1 it is seen that the lock exchange is in-line with the times scales from literature (Figure 2.7).

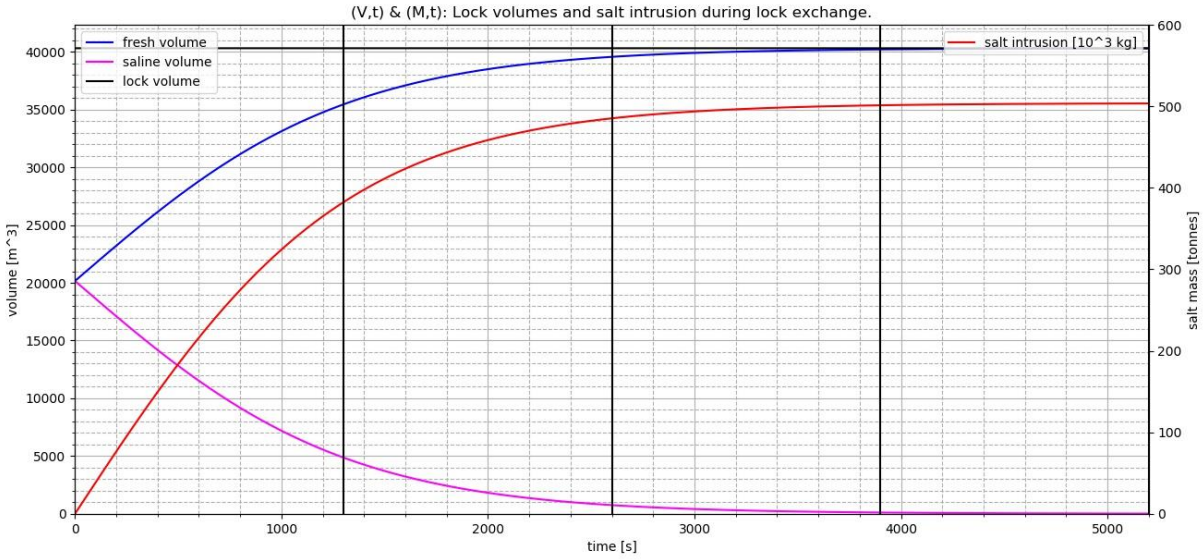

Figure A.1: Lock exchange towards lakeside for a duration of $4t_{LE}$ (5200 seconds) with the conceptual model according to the relative lock exchange formulation. The t_{LE} time scales are shown in the figure by the black vertical lines. The saline water volume from the lock is exchanged with fresh water which results in a fully fresh lock after $4t_{LE}$.

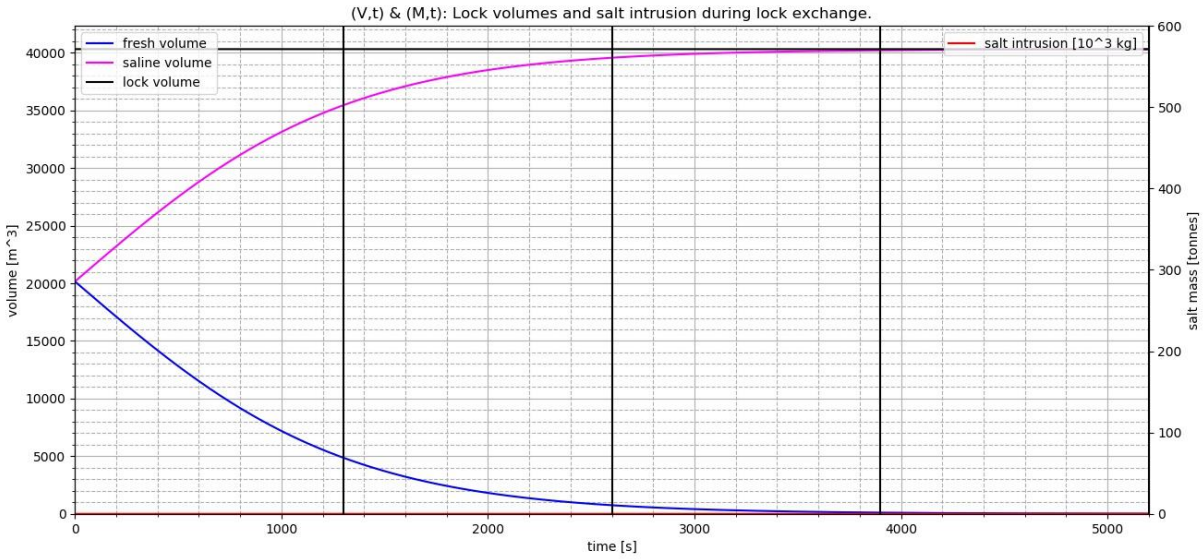

Figure A.2: Lock exchange towards seaside for a duration of $4t_{LE}$ (5200 seconds) with the conceptual model according to the relative lock exchange formulation. The t_{LE} time scales are shown in the figure by the black vertical lines. The freshwater volume from the lock is exchanged with saline water which results in a fully saline lock after $4t_{LE}$.

A.2 Levelling Phases

Next, the levelling phases (lockage phases *1* and *3*) will be addressed. The water level at seaside (h_z) used for levelling is given by the first value from the sinusoidal course of tidal forcing, shown in Figure 3.2, reproduced in Figure A.14. Both high - and low tide cases are included in this section to show their effect on the outputs. First, levelling to lakeside (lockage phase *1*) will be laid out for both tidal situations, before going to levelling to seaside (phase *3*).

The first value of h_z which follows from the sinusoidal tidal forcing amounts to 0,46 meters. To magnify the effects of levelling and to improve readability of the upcoming graphs, the levelling height is set manually to 1,50 meters.

A.2.1 Levelling towards lakeside during high tide

First, the high tide situation of lockage phase *1* is covered. The situation schematized in Figure 3.14 for convenience. The water level in the lock equals $d + h_z$, which amounts to 7,5 meters. The initial interface depth is set to half the water level, thus $d_{int} = 3{,}75$ meters (measured from the water level downwards). For the duration of levelling, a total amount of 10080 cubic meters is transported for a head difference of 1,5 meters. If the falling interface during levelling does not reach the top of the gate valves, all this water volume is saline and therefore $M = V_z(\rho_z - \rho_0) = \mathbf{252}$ tonnes of salt intrusion is expected.

The top of the lock valve is set at NAP-3,5m and the bottom of the lock valve to NAP-5,0m [17], following the original design of lock gates at the Krammer locks.

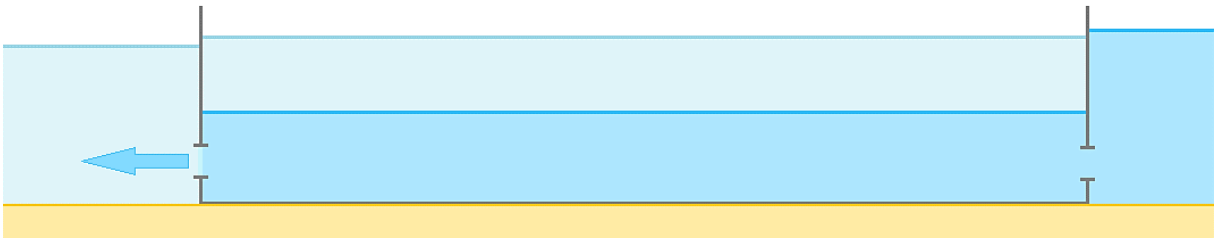

Figure A.3: Schematization of levelling to lakeside during high tide.

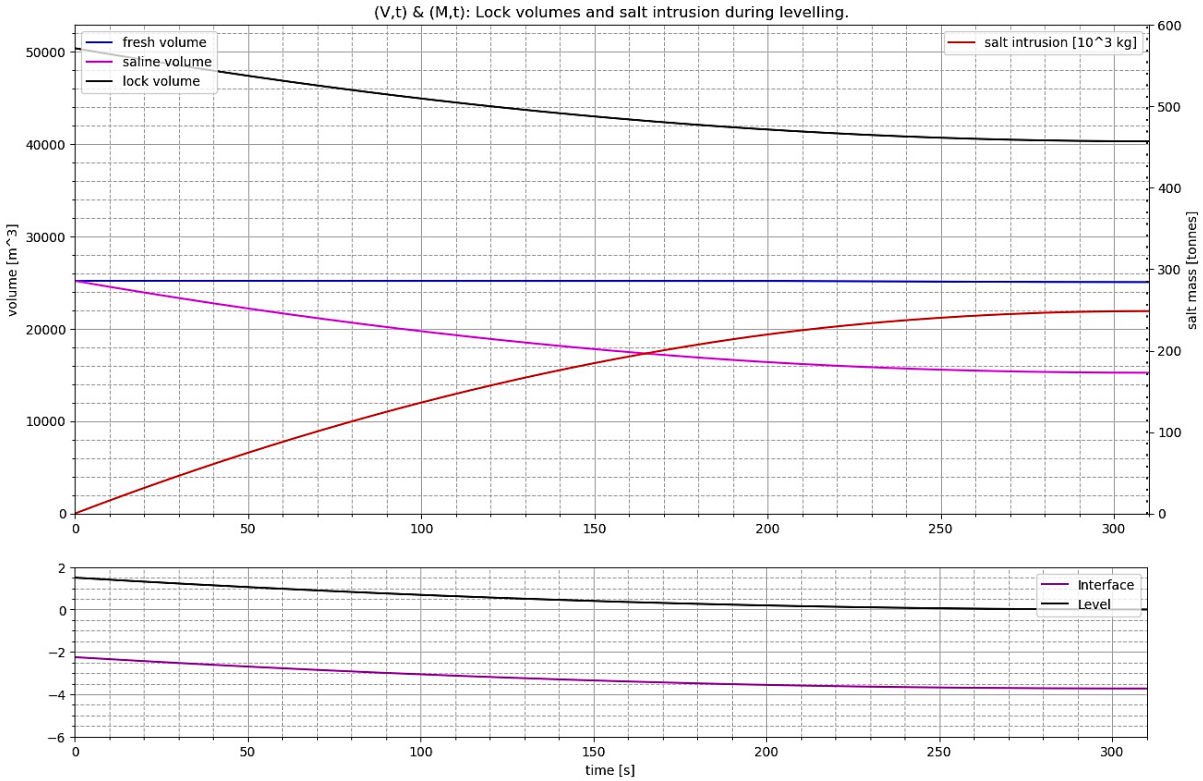

Figure A.4: Levelling towards lakeside in the conceptual model during high tide. The bottom graph shows the interface level declination over the duration of levelling.

The initial interface depth relative to NAP prior to levelling can be calculated according $(A.2)$.

$$d_{int,0} = \frac{h_z - d}{2} = -2{,}25\ m \qquad (A.2)$$

Now, it will be checked if the $2L\Delta t$ output is in-line with expectations. If all the water taken out of the lock during levelling in Figure 3.15 had been saline, the interface depth should result in -3.75 meters at the end of the levelling process. This results in an interface depth that is deeper than the top of the lock valves and therefore fresh water should be transported along with the levelling discharge. Upon examining Figure A.4 more closely, a vague decrease of the freshwater volume is indeed seen near the end of the levelling process (*blue* plot). This effect cannot be seen clearly from the graph, however. To make the shift of levelling discharge from saline to fresh through the lock valves stand out better, the computation is carried out again. This time, the interface depth is set just above the lock valves, given by $d_{int,0}$. The results are shown in Figure A.5 As the interface depth reaches NAP-3,5m the freshwater volume in the lock starts to decrease, verifying the expected behaviour.

$$d_{int,0} = -3{,}25\ m$$

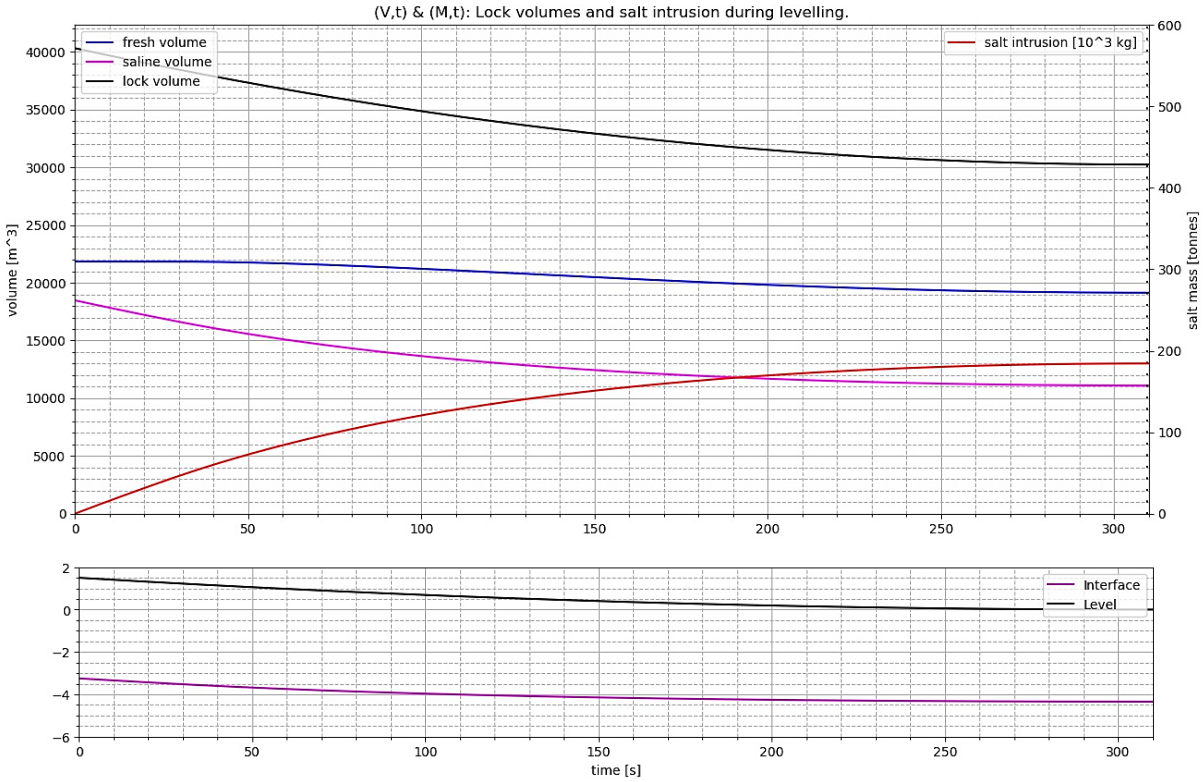

Figure A.5: Levelling towards lakeside in the conceptual model during high tide with a higher initial interface depth. It is seen when the interface level reaches NAP-3,5m the amount of transported fresh water by levelling increases significantly.

A.2.2 Levelling towards lakeside during low tide

Second, the same lockage phase is repeated for low tide. The water level at seaside is set to NAP-1,5m. From the schematization of Figure A.6, it is evident that this situation has no salt intrusion. The results of the computation are shown in Figure A.7.

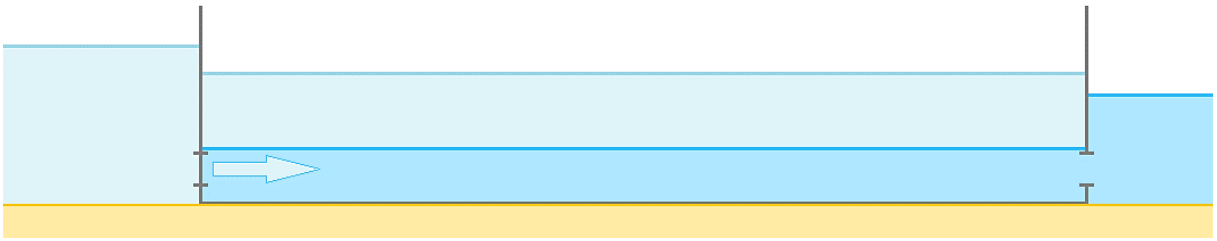

Figure A.6: Schematization of levelling to lakeside during low tide.

The graph shows an expected behaviour of levelling to sea level during low tide will therefore not be discussed further.

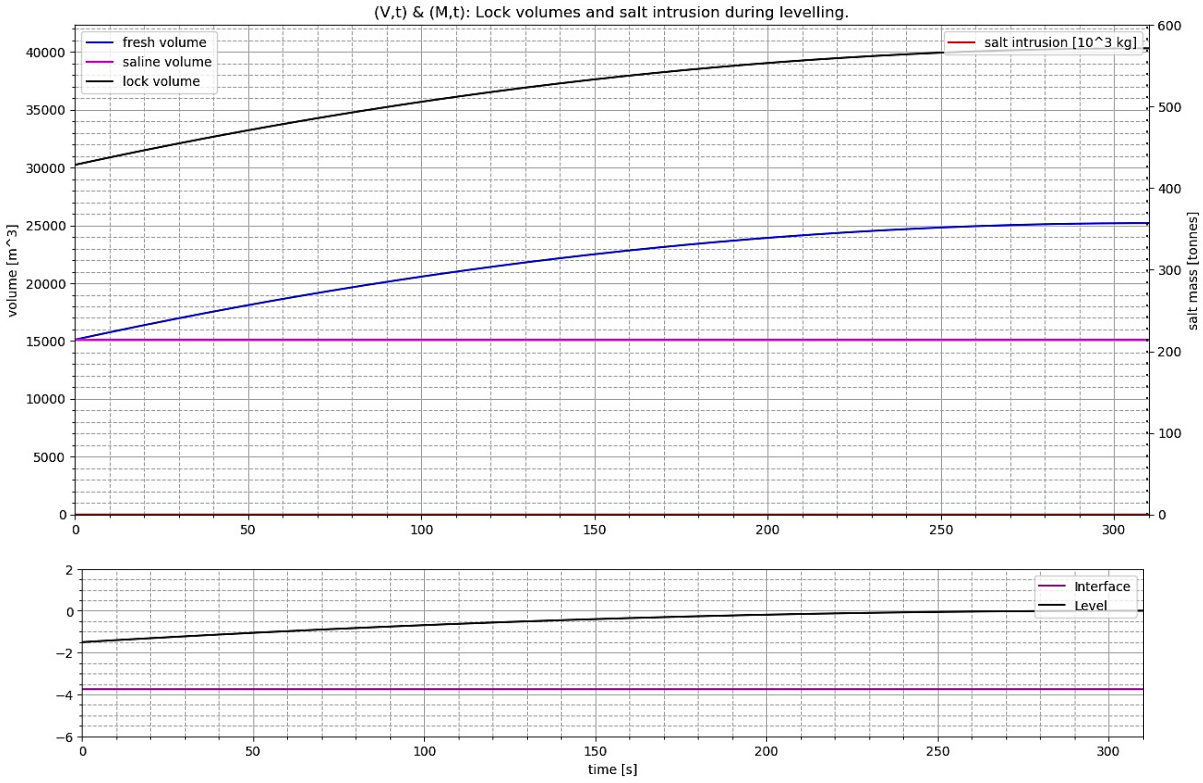

Figure A.7: Levelling towards lakeside in the conceptual model during low tide. The bottom graph shows no interface level change as levelling is now done with fresh water. This follows from the changes to the freshwater volume in the lock too, as is seen in the top graph.

A.2.3 Levelling towards seaside during high tide

Third, lockage phase *3* is laid out during high tide. As can be seen from Figure A.8, this is done by increasing the saline volume within the lock which results in a rise in lock level. The computation is shown in Figure A.9.

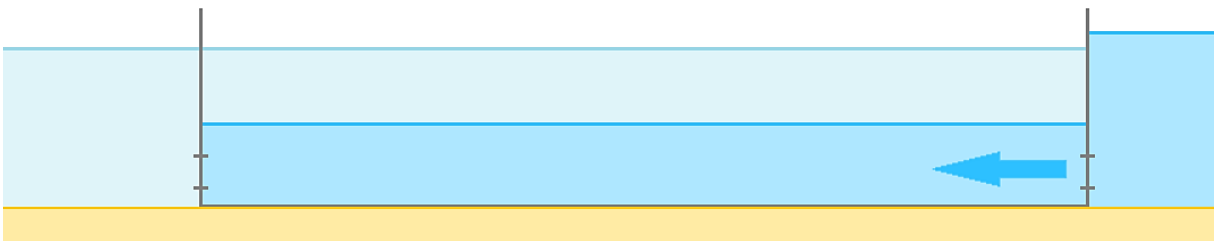

Figure A.8: Schematization of levelling to seaside during high tide.

In terms of results, these look almost the same as the computation of levelling towards lakeside during low tide and do therefore follow the expected results of lockage phase *3*.

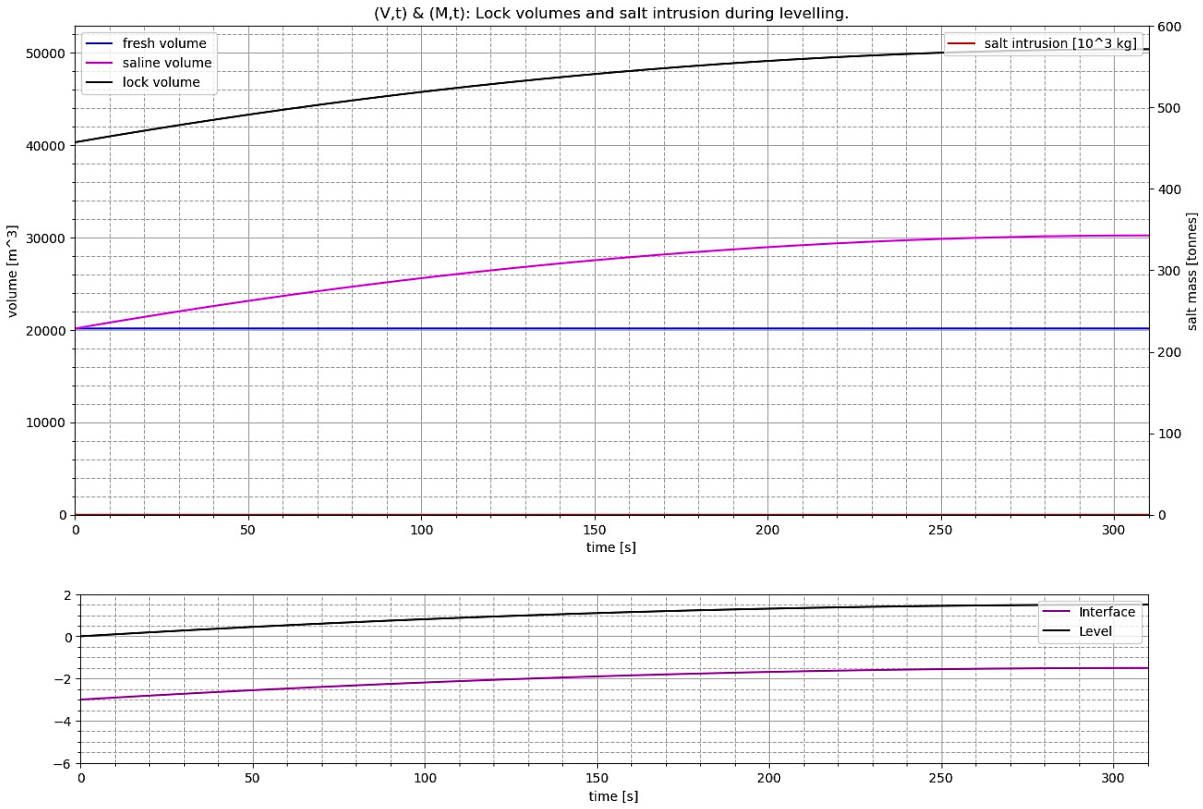

Figure A.9: Levelling towards seaside in the conceptual model during high tide.

A.2.4 Levelling towards seaside during low tide

Last of the levelling phases, lockage phase *3* is reconsidered during low tide. Like levelling to lakeside during high tide, the discharged water density from the lock is dependent on the initial interface level and the levels of the gate valves.

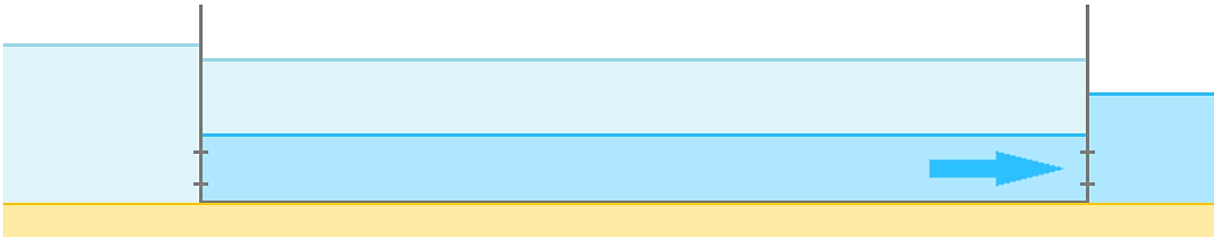

Figure A.10: Schematization of levelling to seaside during low tide.

The water level at the lock before levelling equals NAP+0,0m. Consequently, the interface depth before levelling is set to NAP-3,0m. Because the levelling height is 1,5 meters, this results in an interface depth which will fall below the top level of the lock gate valve. The results are therefore expected to contain a similar inflection point as the fresh volume plot of Figure A.7. From Figure A.11, it is seen that this case indeed results in the same shape in courses of lock volumes.

This part concludes on the outputs of lockage phases *1* and *3*. In the next section, lockage phases *2* and *4* will be covered, representing the navigation phase at lakeside and seaside respectively.

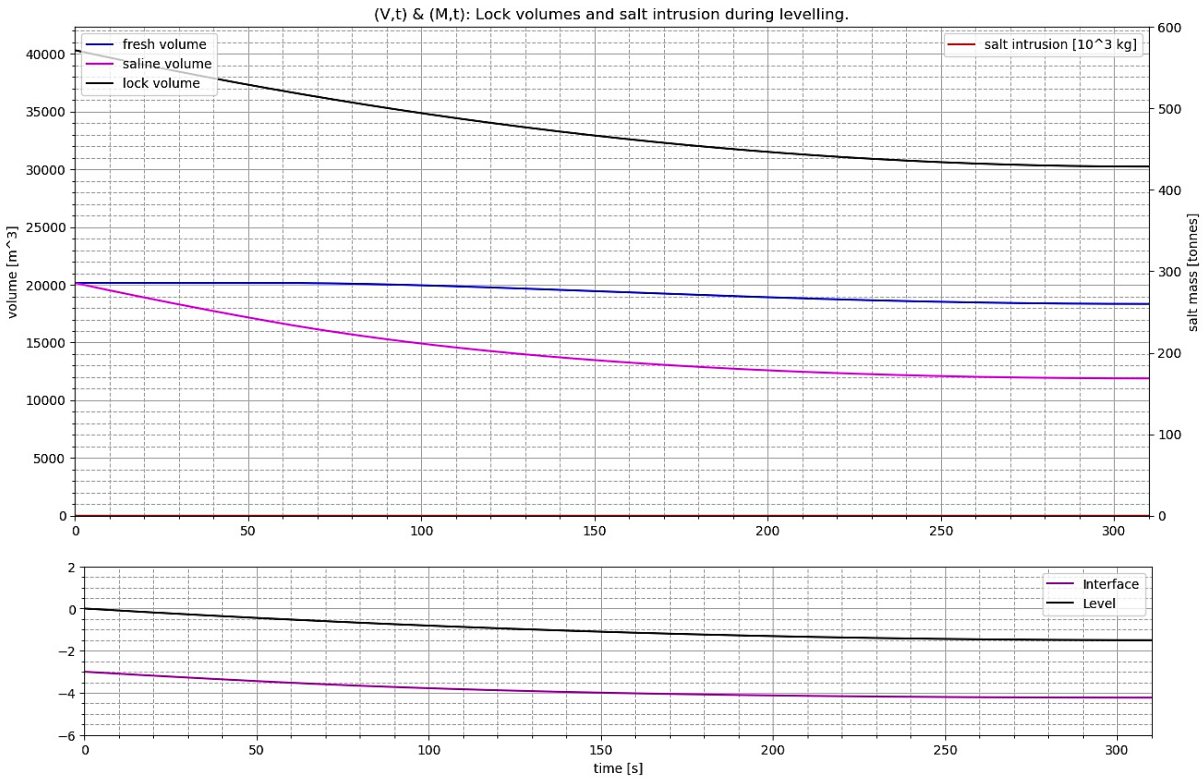

Figure A.10: Levelling towards seaside in the conceptual model during low tide.

A.3 Navigation Phases

In this section, two computations will be shown of lockage phases *2* and *4* where navigation of ships and lock exchange are both included. The first computation shows the lock volumes and the amounts of salt intrusion for sailing to lakeside from the lock, and vice versa (phase *2*). The second computation focuses on the same processes but to seaside (phase *4)*.

The dimensions of ships will be from the CEMT: VIa class, of which the dimensions are included in Table A.2. The velocity of the ship is taken 60% of the limiting speed (Appendix B). All parameters have been explained, except for t_{door} and t_{wait}. t_{door} represents the waiting time between the doors being open or closed and a ship departing from or entering the lock, and t_{wait} represents the waiting time between a ship entering the lock after an exiting ship has left the lock. These will arbitrarily be assumed 4 minutes and 10 minutes respectively, such that the entire lockage takes 18 minutes, apart from the sailing duration.

Table A.2: Additional usage parameters for shipping for lockage phases 2 and 4.

Parameter	***Value***
V_s [m^3]	*1920*
l_s [m]	*135,0 (CEMT: VIa)*
w_s [m]	*17,0 (CEMT: VIa)*
d_s [m]	*4,0 (CEMT: VIa)*
u_s [m/s]	*0,96 (0,6*u_L)*
t_{door} [min]	*4*
t_{wait} [min]	*10*
h_z [m+NAP]	*0,0*

The amount of water in the lock is calculated according (2.9).

$$V - V_s = 31140\, m^3$$

A.3.1 Navigation at lakeside

The results of the computation at lakeside are shown in Figure A.12. The figure is divided in separate parts (*A* to *E*). Regions *A* and *E* represent the waiting time between opening of the doors and a ship exiting the lock to lakeside. After duration t_{door}, the ship leaves the lock towards lakeside in region *B*. This duration is equal to l_s/u_s which is approximately 140 seconds. During this sailing duration, it is seen the amount of salt intrusion remains unchanged. This shows the salt tongue is largely pushed back to the lock by the return current, as was explained in subsection 3.2.3.4. After this duration, the waiting time begins for a duration of t_{wait} which is shown in region *C*. During this time, the water volume in the lock remains equal to the lock volume (V) and only the lock exchange affects it. This is seen by a falling *purple* plot and rising *blue* and *red* plots. After the waiting time, a ship of similar dimensions as in region *B* enters the lock in region *D*. Opposed to a ship leaving the lock, the magnitude of the salt tongue directed towards lakeside is now enlarged. This is seen by the increment in the gradient over the course of the *red* plot for region *D*.

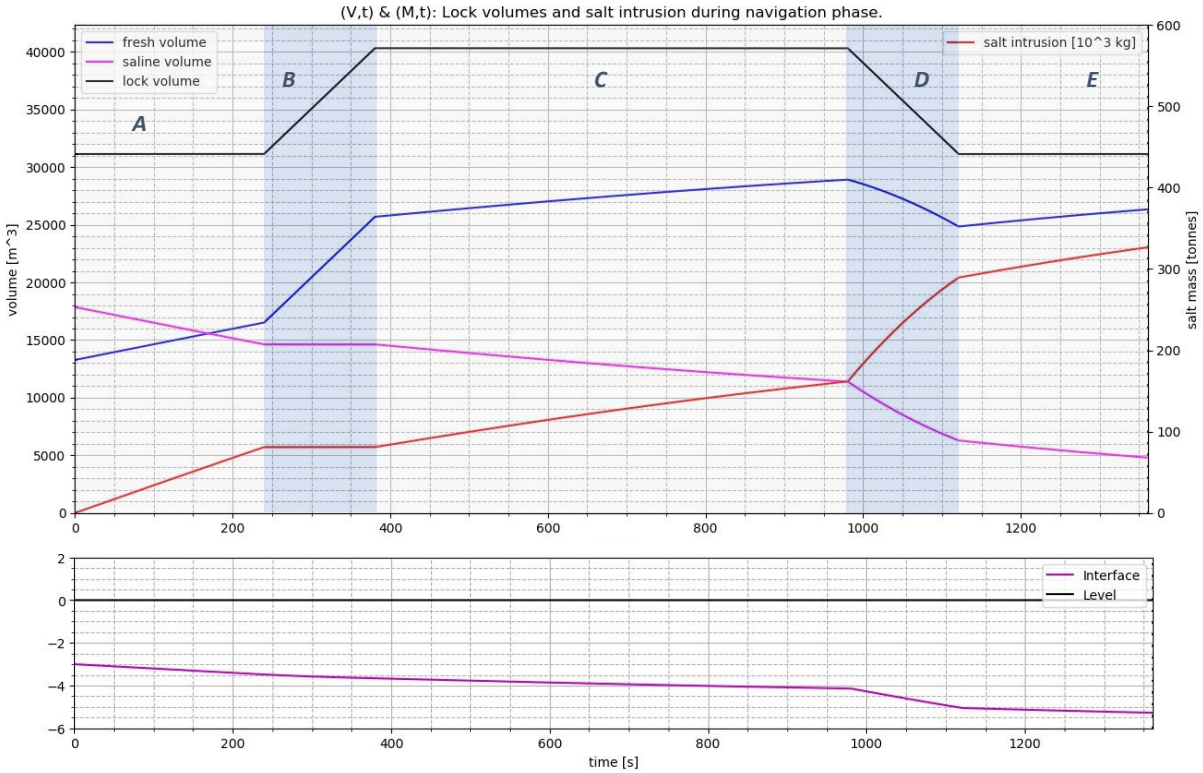

Figure A.12: Computation of the navigation phase to lakeside for shipping class CEMT: VIa with water volumes in m³ in the lock and salt intrusion in tonnes given in the top graph, and the course of the interface in the bottom graph.

A.3.2 Navigation at seaside

To conclude the navigation phase, lockage phase *4* is shown which represents navigation at seaside. The results are shown in Figure A.13. It is seen that the freshwater volume completely drains from the lock over the course of the simulation. This is the result of a smaller ratio of fresh water to saline water in the lock in comparison to Figure A.12. Nevertheless, the conceptual model can take this effect into account by limiting the amount of fresh volume transported out of the lock. It was decided not to compensate for the smaller amount of fresh water in Figure A.13, but to rather show this effect.

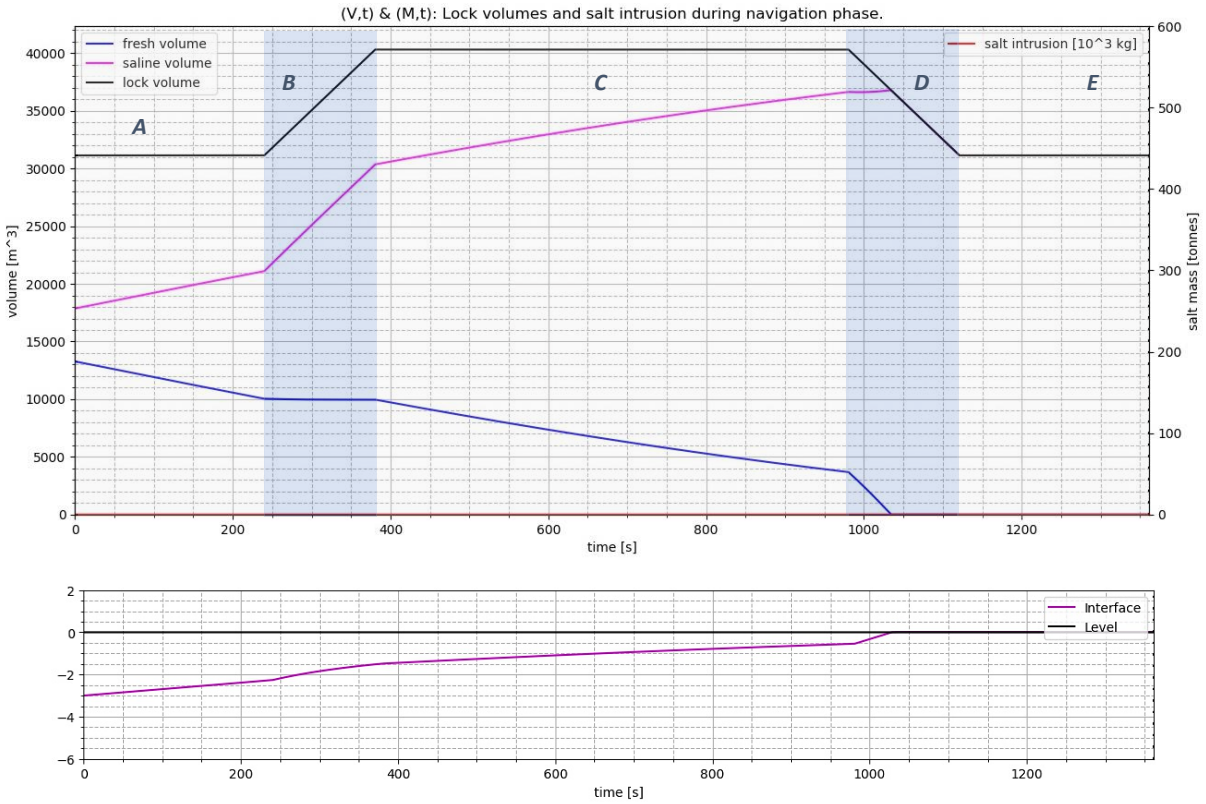

Figure A.13: Computation of the navigation phase to seaside for shipping class CEMT: VIa with water volumes in cubic meters in the lock and salt intrusion in tonnes given in the top graph, and the course of the interface in the bottom graph.

A.4 Full Lockages

To conclude this appendix, simulations of full lockages are presented in Figure A.15 to A.18. There are ten full lockage cycles per tidal cycle (as shown in Figure 3.2, reproduced in Figure 3.25) with a single ship being transported in each levelling phase. To show this, Figures A.15 and A.16 show single lockages for respectively high - and low tide, followed by simulations of 5 lockages during high - and low tide. The lockage phases per lockage cycle are divided by the vertically loosely dotted lines, whereas full lockage cycles are divided by the vertically dashed lines.

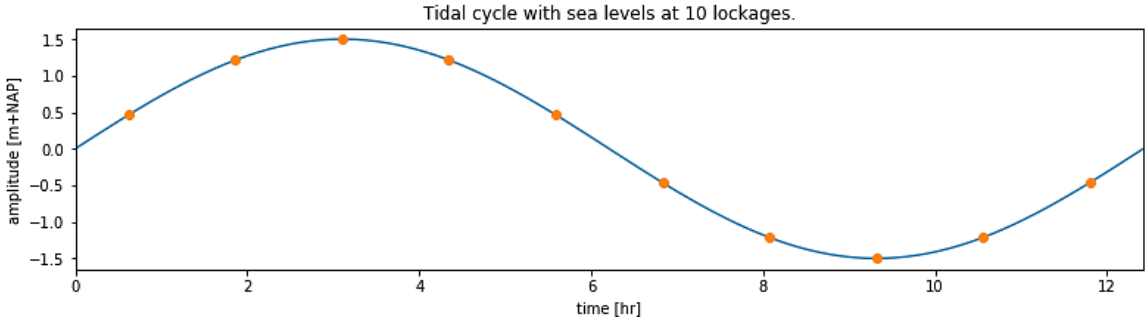

Figure A.14: Tidal cycle discretized in several lockages equally far apart. The orange dots represent the water levels for consecutive lockages.

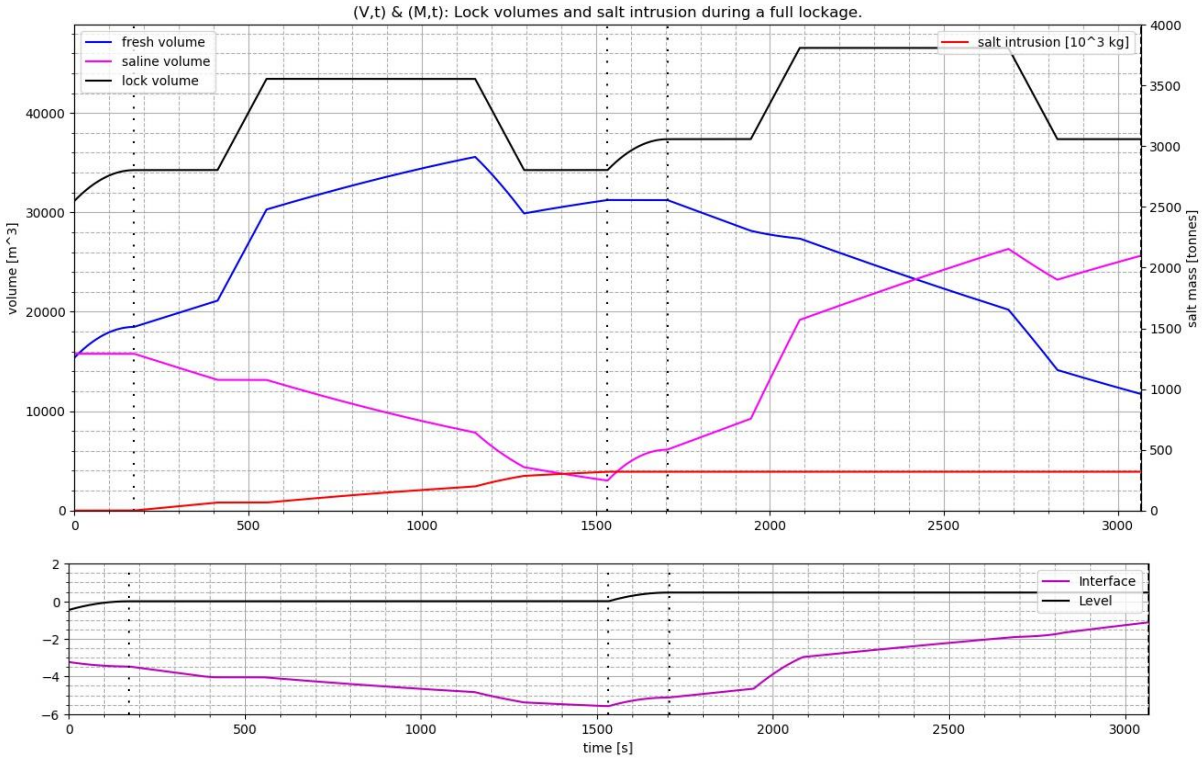

Figure A.15: Computation of a full lockage with vessel class CEMT: VIa during high tide.

All previously explained lockage phases are carried out successively in Figures A.15 and A.16. Differences between high - and low tide are not directly visible from these figures: both figures show the same general trend in the courses of lock volumes. To magnify the differences between the tidal situations the individual lockage cycles will be carried out successively according to Figure A.14.

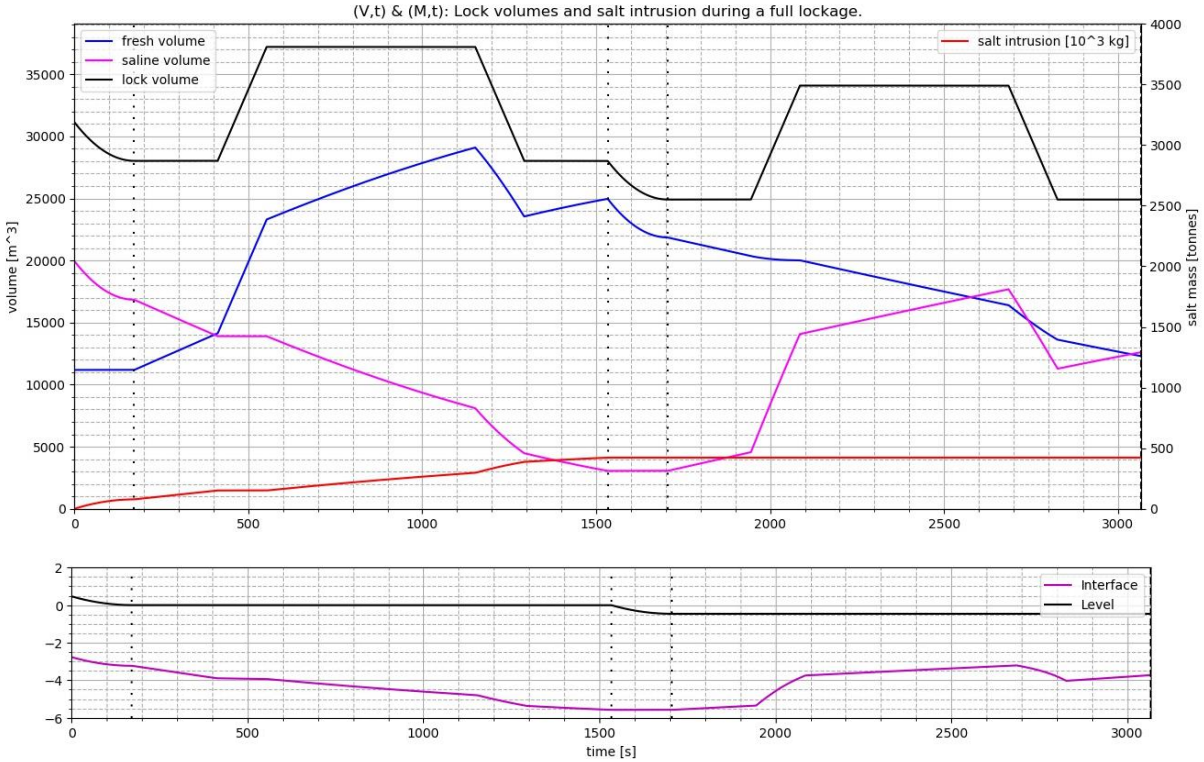

Figure A.16: Computation of a full lockage with vessel class CEMT: VIa during low tide.

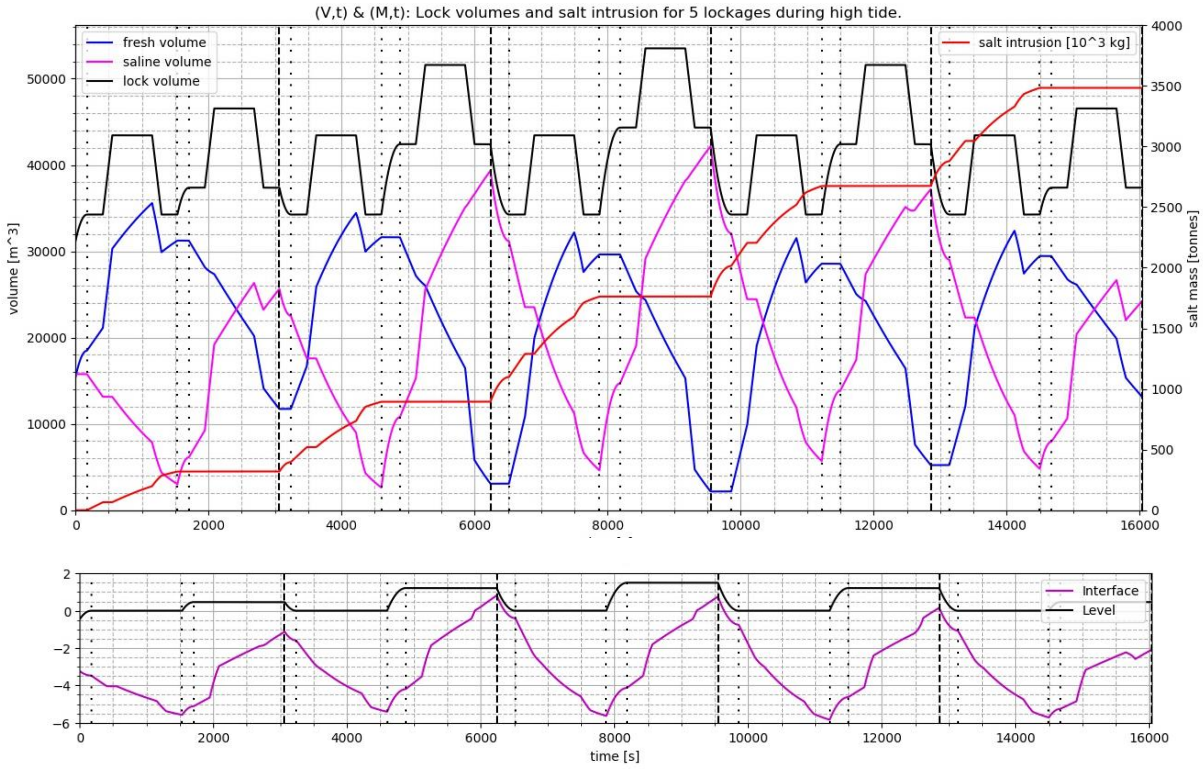

Figure A.17: Computation of 5 full lockages with vessel class CEMT: VIa during high tide.

Figures A.17 and A.18 show five lockages during high and low tide respectively. After five lockages, a periodic equilibrium can already be seen.

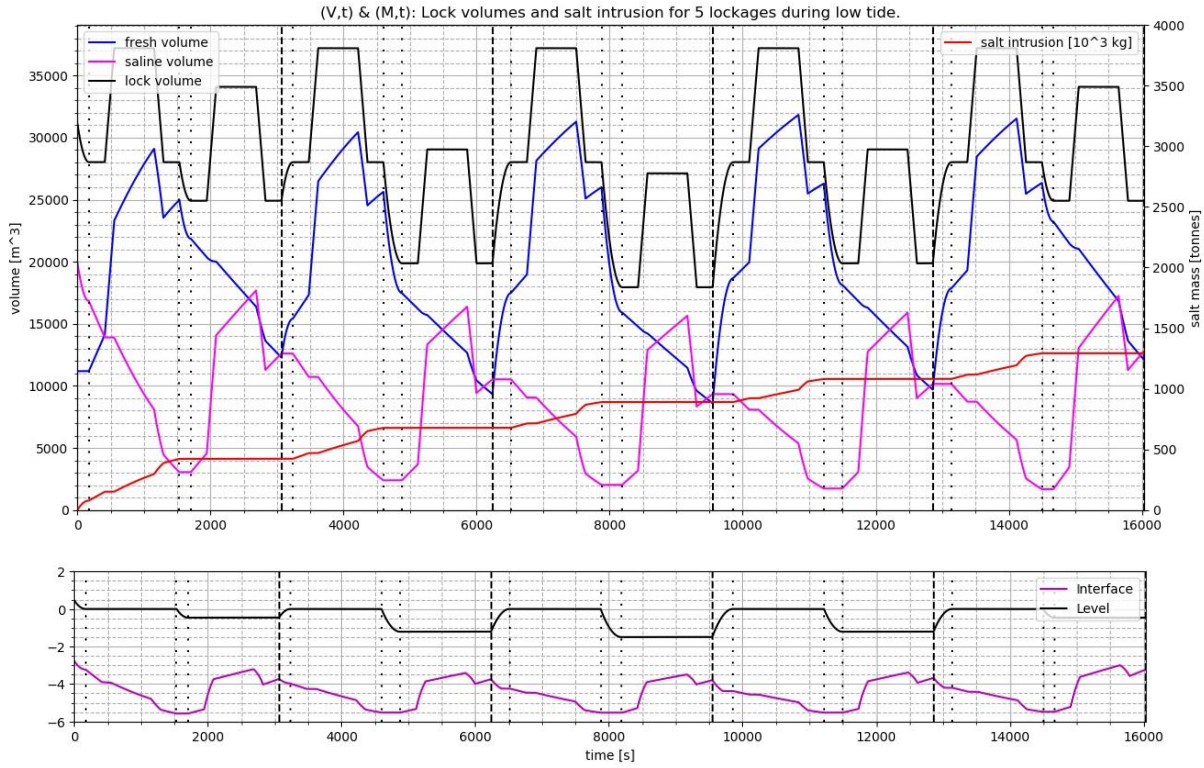

Figure A.18: Computation of 5 full lockages with vessel class CEMT: VIa during low tide.

B Schijf's Diagram

The following appendix presents the use of Schijf's diagram to determine return current speeds and depressions that occur during ship movements according to an example. It is mentioned several times throughout this study that the ships in the conceptual model are assumed to be travelling at about 60% of the limiting speed. This limiting speed can too be determined from Schijf's diagram and will be explained in this section as well. Table B.1 shows the parameters of the example which will be covered. Ship class CEMT: VIa and the dimensions of the Krammer Locks are used. No subscripts denote lock dimensions, where the subscript *s* denotes ship dimensions. A_C and A_s are the cross-sectional area of the lock and ship respectively. Schijf's diagram is shown in Figure B.1.

For the determination of the return current speed, an assumption is required regarding the sailing speed. In this study, a sailing velocity of 60% of the limiting speed is used in the conceptual model. The 60% is determined by adjusting the limiting speed to observations of lockages at the Krammer locks by the author, of which two pictures are included in the end of the appendix. It was observed and estimated by eye that the average sailing speed of the ships was approximately 1 meter per second.

Table B.1: Parameters for the example of applying Schijf's diagram.

Parameter	Value
l [m]	*280,0*
w [m]	*24,0*
d [m]	*6,0*
V [m³]	*40320*
l_s [m]	*135,0*
w_s [m]	*17,0*
d_s [m]	*4,0*
V_s [m³]	*9180*
u_s/u_L [m/s]	*0,6*

The determination process starts with finding the ratio of the cross-sectional areas of the ship over the lock. This point is then to be marked on the top axis of Schijf's diagram, shown in Figure B.1.

$$\frac{A_s}{A_c} = \frac{w_s d_s}{wd} = \frac{68}{144} = .472 \qquad (B.1)$$

Next, a vertical line is to be drawn from this point to the bottom graph. This then shows the limiting velocity u_L on the bottom graph, given in $u_s/\sqrt{gh}$. The limiting velocity then follows as:

$$u_L = 0{,}21\sqrt{gh} \qquad (B.2)$$

From $(B.2)$, the limiting velocity is 1,61 meters per second. The assumption of the sailing speed (the ships sail with 60% of the limiting speed) then follows from the observations at the Krammer locks ($u_s = 1\ m/s$) and the limiting speed according $(B.3)$.

$$\frac{u_s}{u_L} \approx 0{,}6 \qquad (B.3)$$

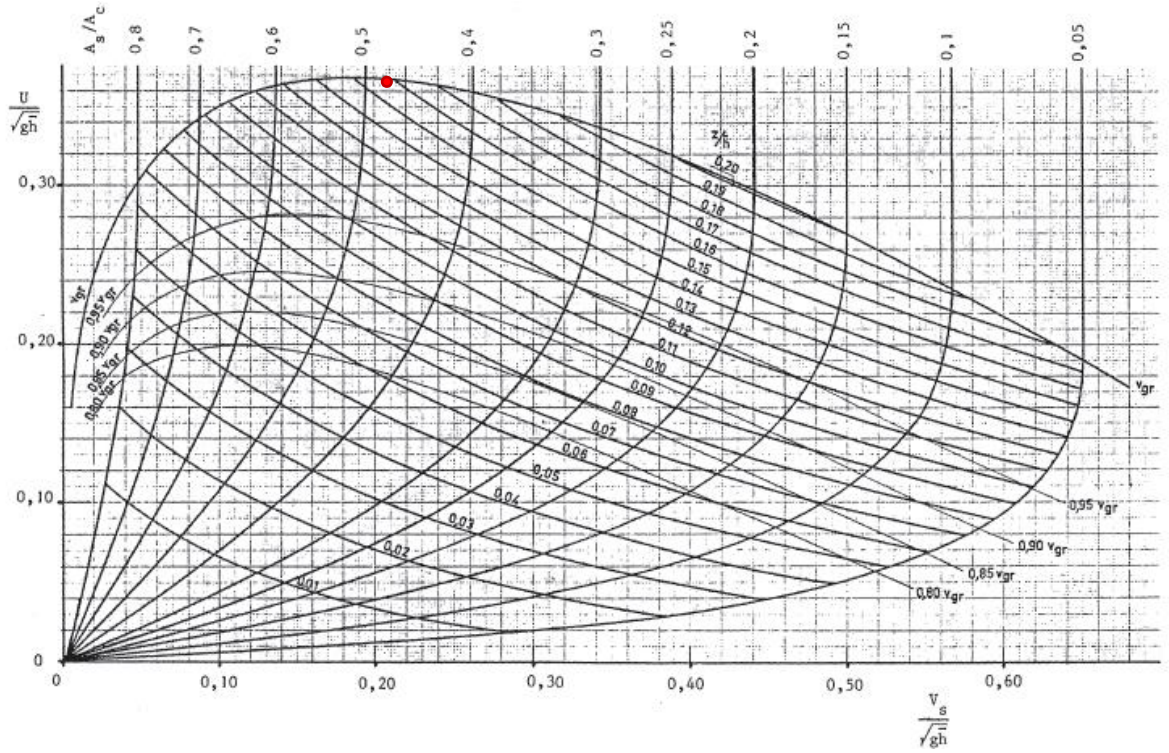

Figure B.1: Diagram of Schijf. Taken from a memo from Van Hattum & Blankenvoort in 1998 [17].

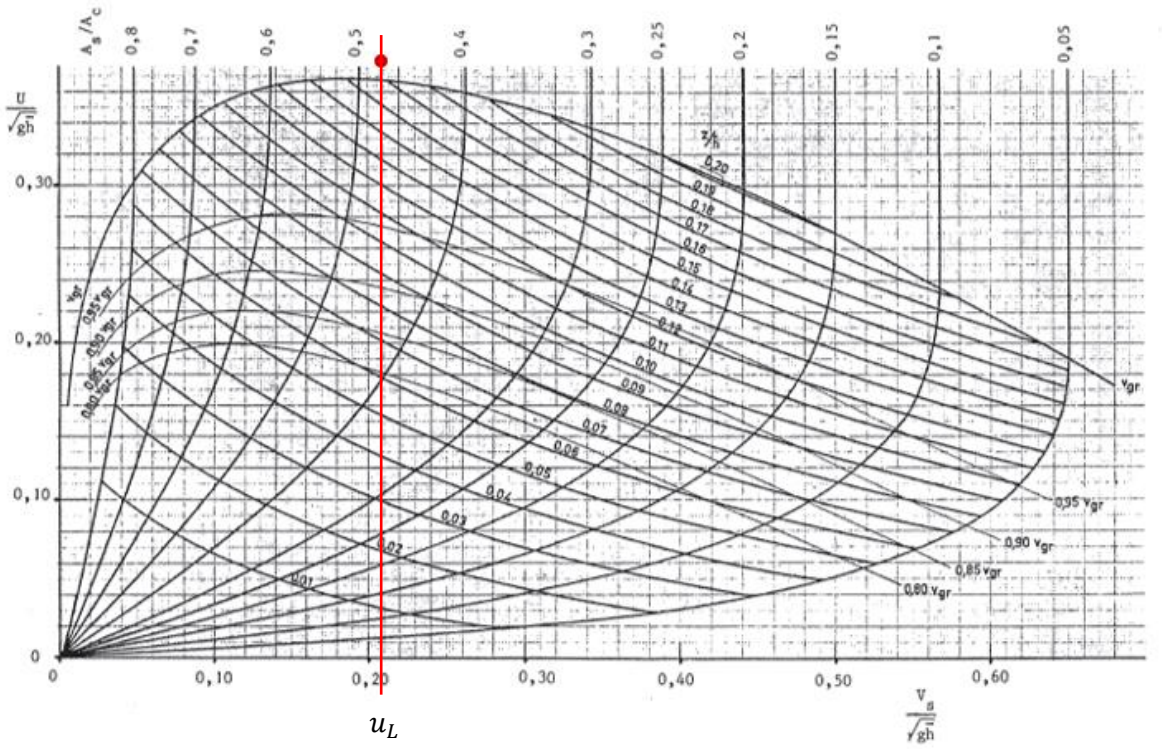

Figure B.2: Diagram of Schijf, with the limiting velocity (u_L) shown on the lower horizontal axis.

From $(B.2)$ and $(B.3)$, the velocity of the ship can be determined based on $\sqrt{gh}$, which is added to Figure B.3 by a second red line.

$$u_s = 0{,}126\sqrt{gh} \qquad (B.4)$$

Throughout the diagram, horizontally curved lines are drawn with subscripts v_{gr} to $0{,}8v_{gr}$ which represent the assumption of sailing speed expressed in the limiting speed (*gr* from 'grens', translated 'limit'.) Because no line is present for the $0{,}6v_{gr}$ sailing speed, this is added in Figure B.3 in green by hand.

The next step in the determination of the return current velocity is found by drawing a line from the original red dot which denotes the value of A_s/A_c parallel to the vertically curved lines to the origin of the axis system, which is added in blue in Figure B.4. The return current velocity follows then from the vertical projection of the intersection point of this line with the previously drawn green line.

$$u_{primary} = 0{,}12\sqrt{gh} \qquad (B.4)$$

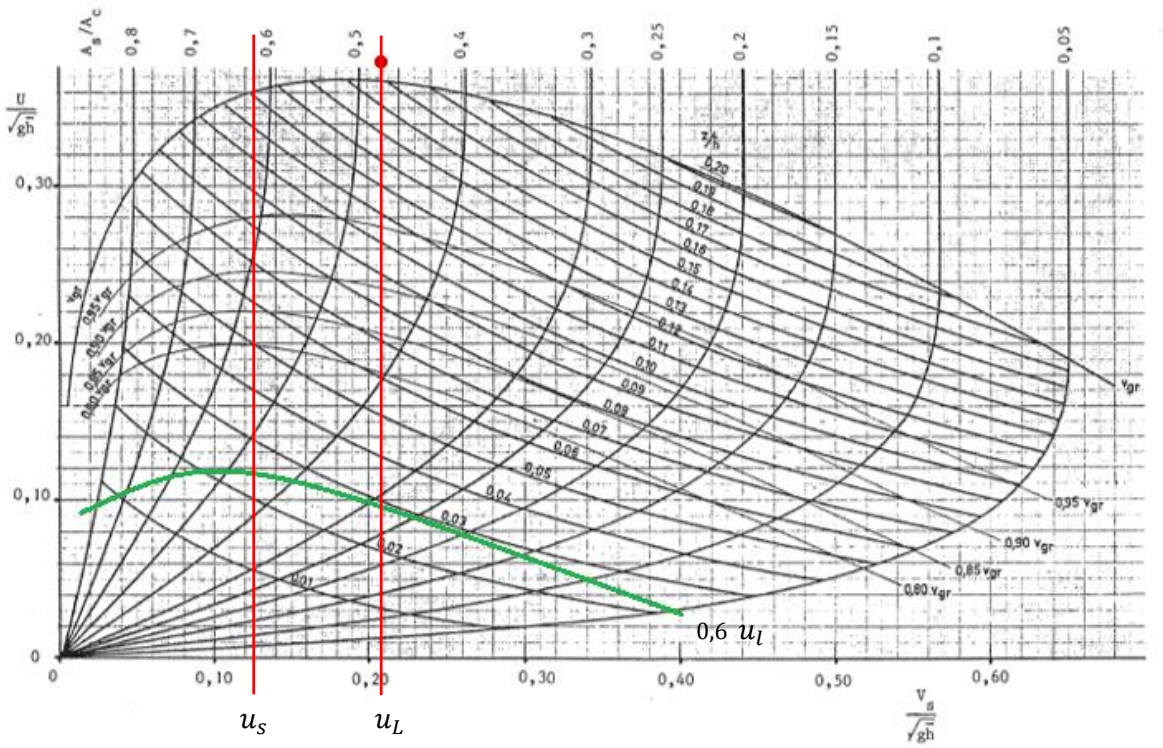

*Figure B.3: Diagram of Schijf. The green line is added and represents the assumption of the sailing speed (0,6*u_L (v_{gr} in drawing)).*

The final step in the determination process is finding the depression. This is obtained by drawing a line from the found intersection point (*blue* point Figure B.4) parallel to the horizontally, concavely shaped curved lines denoted by z/h. This line is added to the figure in Figure B.5. According Schijf's diagram, a depression is present of 2,5% relative to the water depth.

$$z = 0{,}025h \qquad (B.5)$$

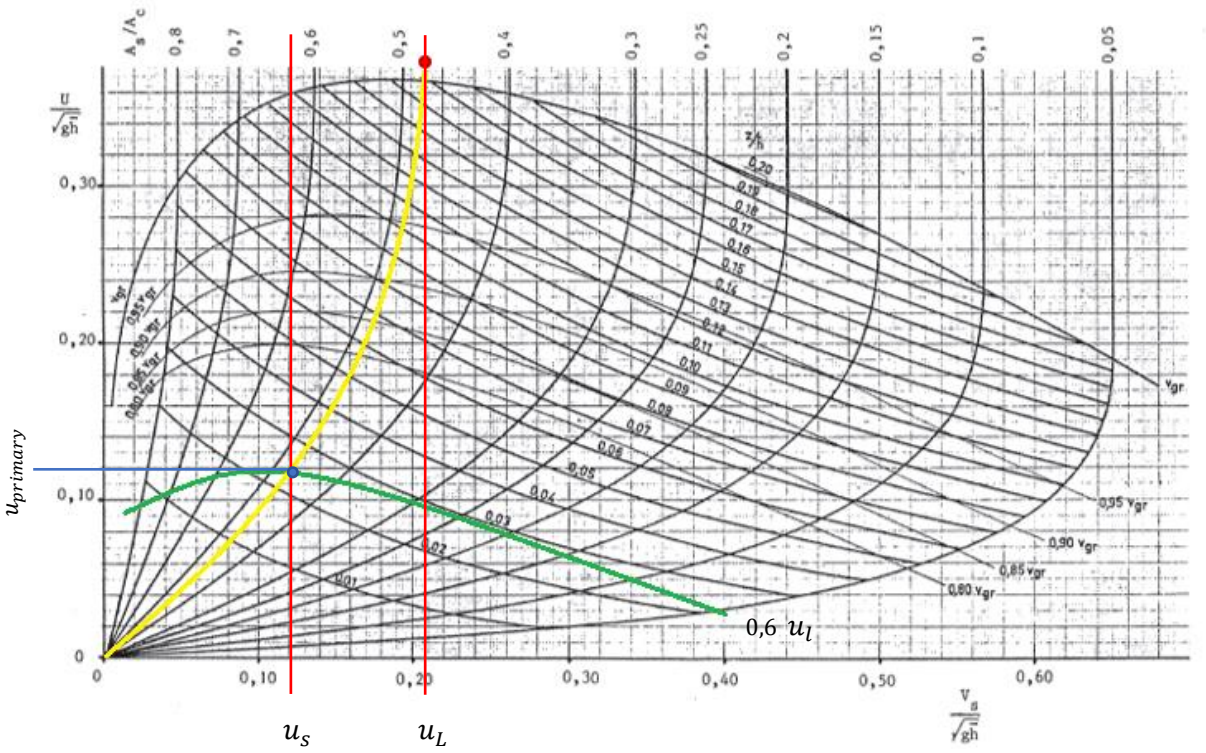

Figure B.4: Diagram of Schijf. The yellow line runs parallel to the other vertically curved lines to the origin of the axis system. The return current velocity follows from the intersection of the yellow and green lines.

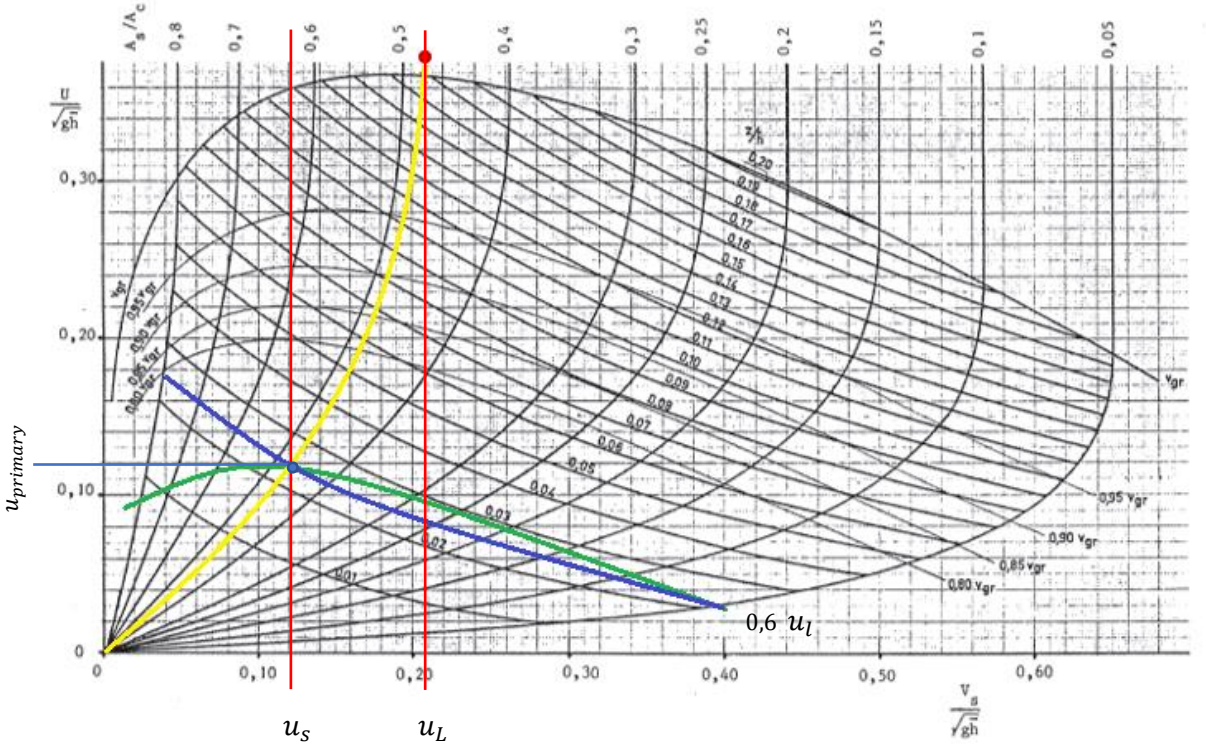

Figure B.5: Diagram of Schijf. The blue line is drawn parallel to the horizontally curved lines denoting the depression (z/h), which amounts to 0,025.

Figure B.6: Incoming vessel at the Krammer locks.

Figure B.7: Incoming vessel at the Krammer locks.

C Sensitivity Analysis Graphs

In the last appendix, the graphs of the sensitivity analysis from section 5.1.3 are presented. These have been grouped in the Appendix to overload the reader with less relevant graphs in Chapter 5 but are included nonetheless because they may be important to the reader.

The following figures are attached in this appendix, whereby figures C.1 to C.5 deal with the analysis of the door-open time (t_{door}/t_{LE}), C.6 to C.13 with the waiting time t_{wait}/t_{LE}, and C.14 to C.20 deal with the relative contributions from the ZSF with respect to the $2L\Delta t$ assumptions.

Figures C.1 & C.2: Simulations with $2L\Delta t$ assumptions and varying t_{wait}/t_{LE} for t_{door}/t_{LE} = 1/3, and 2/3.

Figures C.3 - C.5: Simulations with ZSF assumptions and varying t_{wait}/t_{LE} for t_{door}/t_{LE} = 0, 1/3, and 2/3.

Figures C.6 - C.9: Simulations with $2L\Delta t$ assumptions, $t_{door}/t_{LE} = 0$, and varying CEMT classes for t_{wait}/t_{LE} = 0, 1/3, 2/3, and 1.

Figures C.10 - C.13: Simulations with ZSF assumptions, $t_{door}/t_{LE} = 0$, and varying CEMT classes for t_{wait}/t_{LE} = 0, 1/3, 2/3, and 1.

Door-open time (t_{door}/t_{LE})

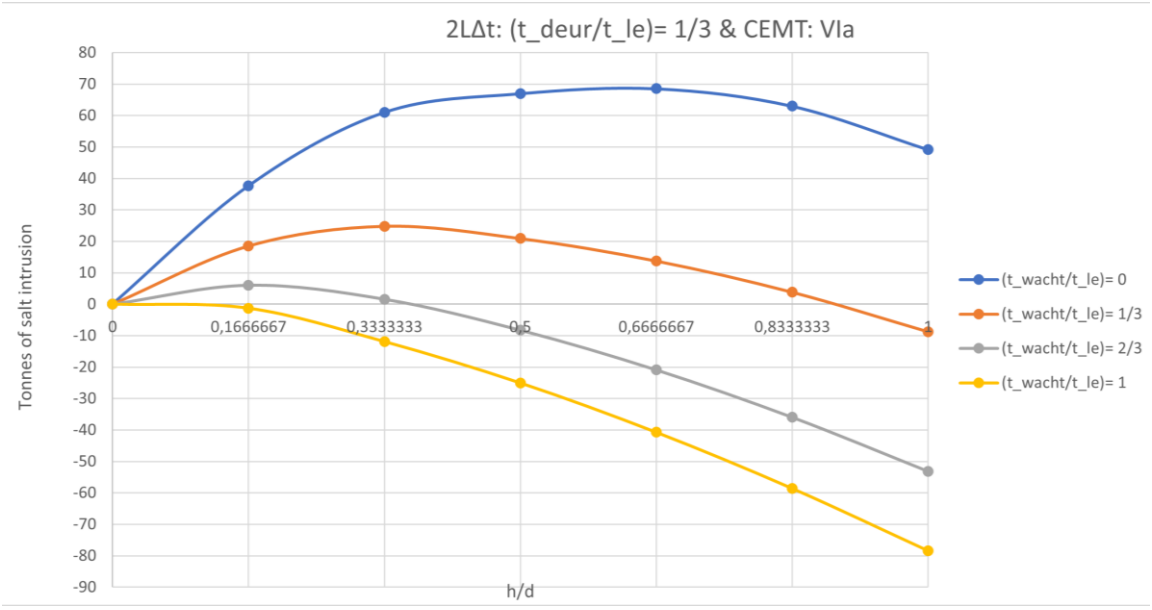

Figure C.1: Simulations with $2L\Delta t$ assumptions, t_{door}/t_{le}= 1/3, and different t_{wait}/t_{le} between ship movements.

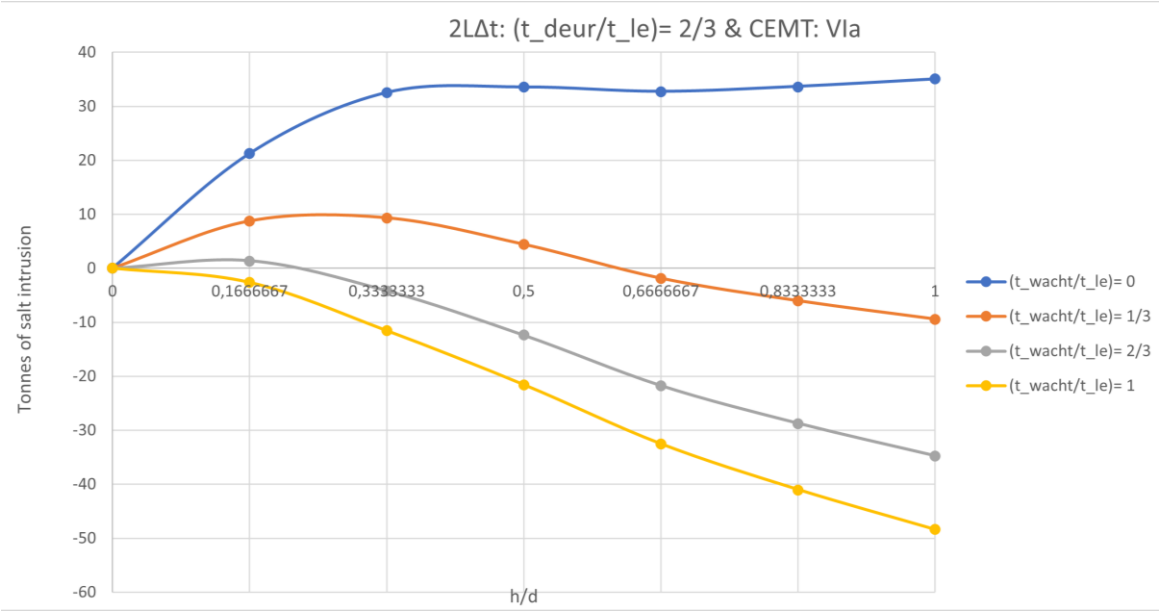

Figure C.2: Simulations with 2LΔt assumptions, t_{door}/t_{le}= 2/3, and different t_{wait}/t_{le} between ship movements.

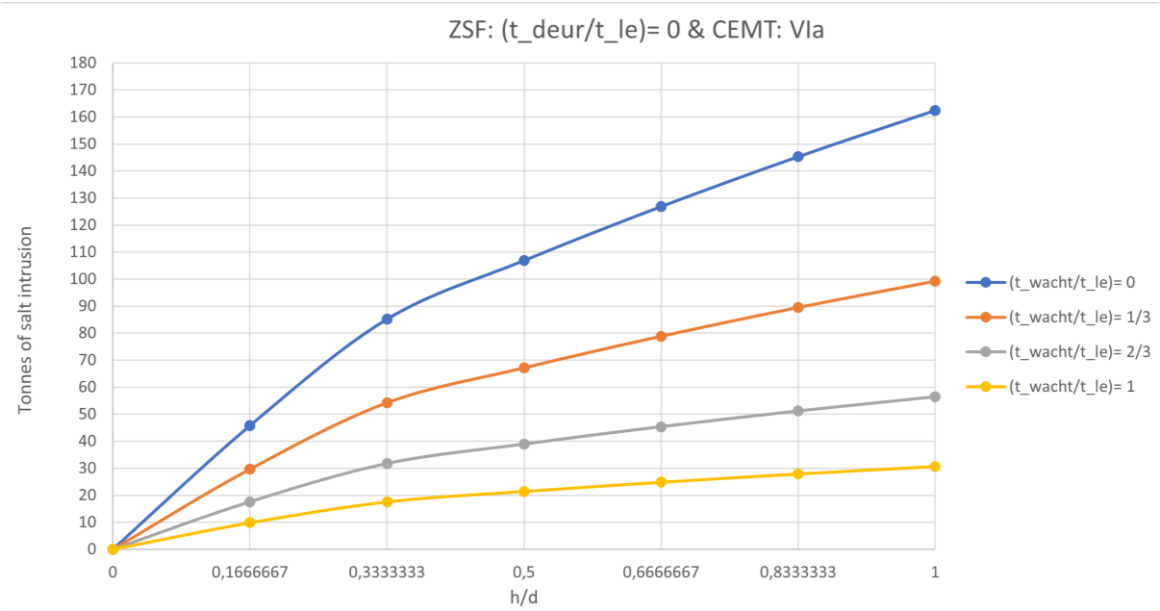

Figure C.3: Simulations with ZSF assumptions, t_{door}/t_{le}= 0, and different t_{wait}/t_{le} between ship movements.

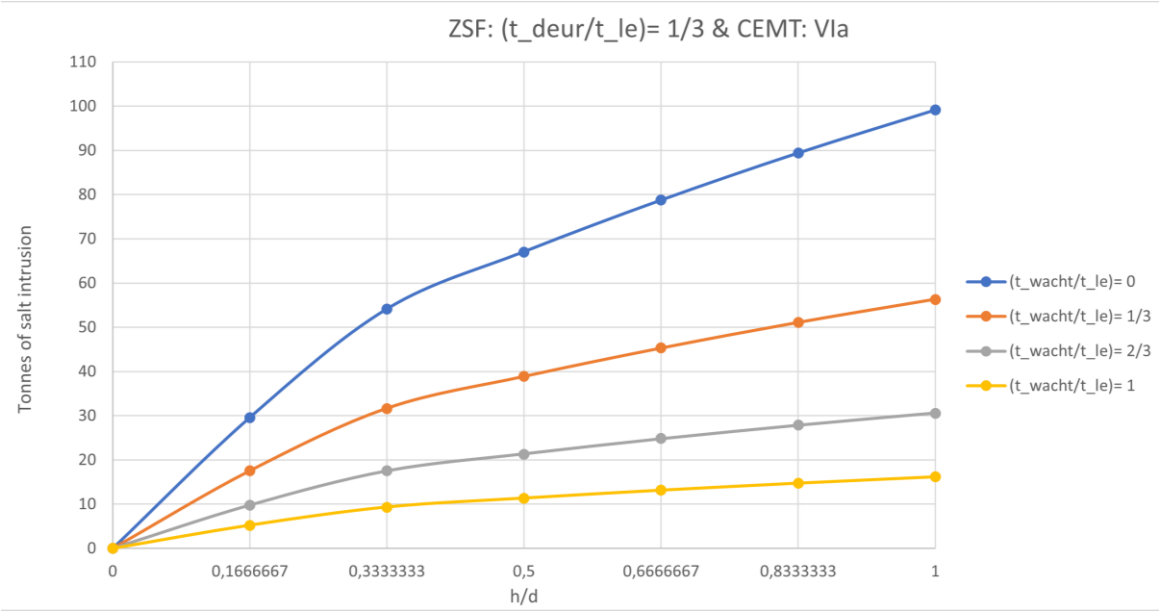

Figure C.4: Simulations with ZSF assumptions, t_{door}/t_{le}= 1/3, and different t_{wait}/t_{le} between ship movements.

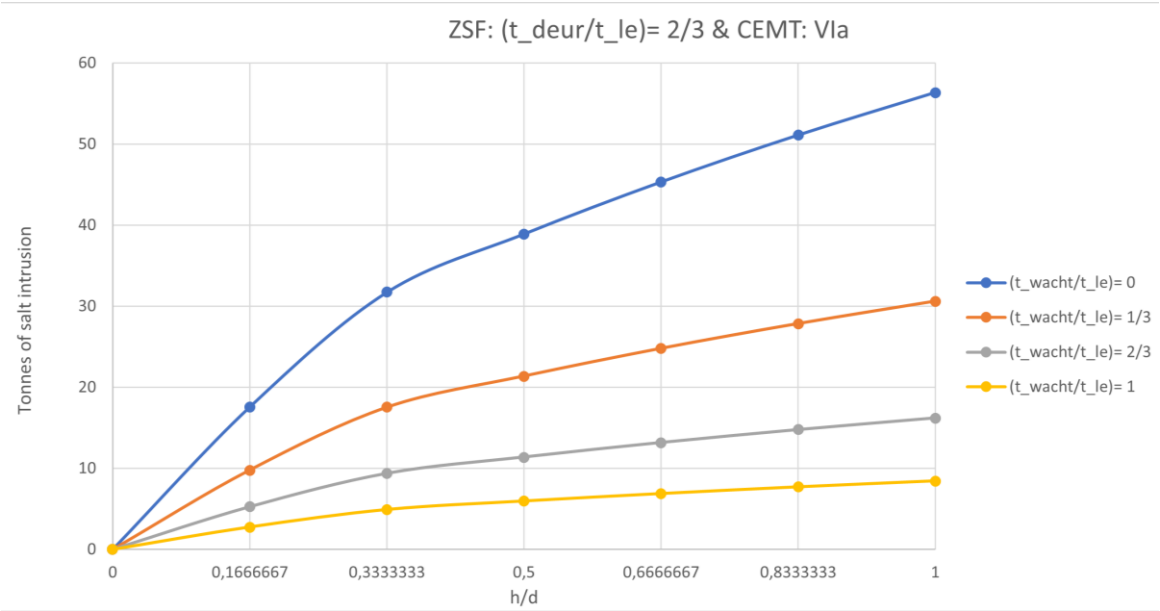

Figure C.5: Simulations with ZSF assumptions, t_{door}/t_{le}= 2/3, and different t_{wait}/t_{le} between ship movements.

Waiting time (t_{wait}/t_{LE})

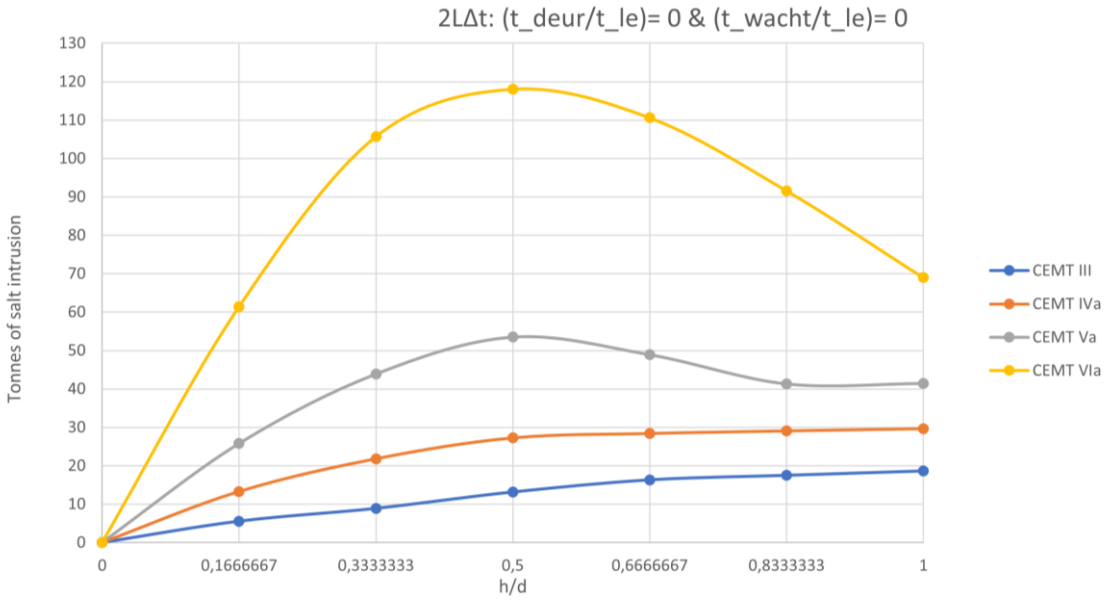

Figure C.6: Simulations with 2LΔt assumptions, t_{door}/t_{le}= 0, t_{wait}/t_{le}= 0, and different shipping classes.

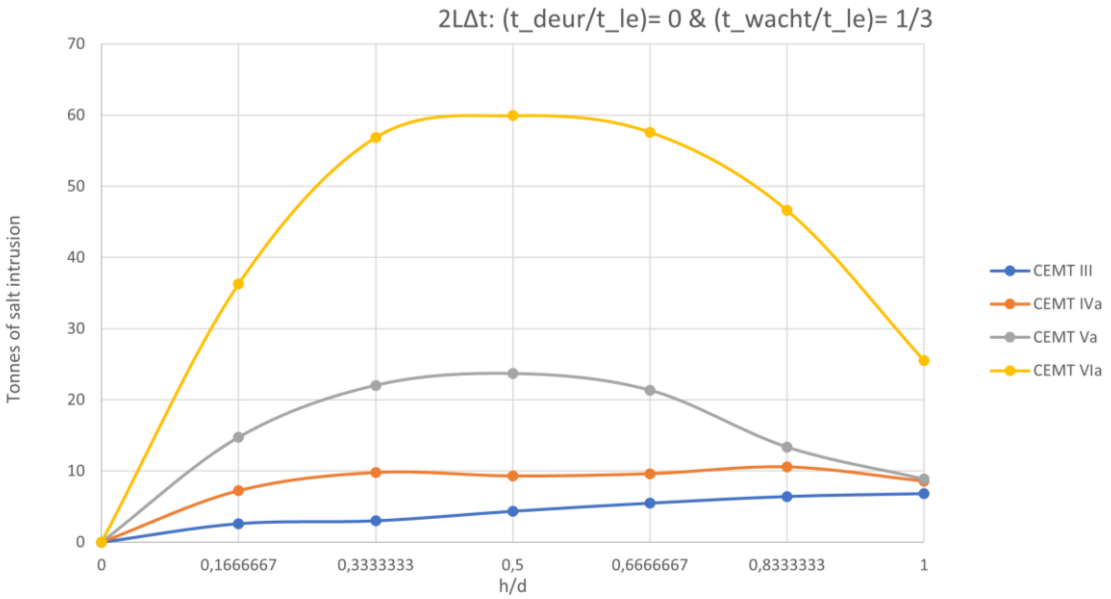

Figure C.7: Simulations with 2LΔt assumptions, t_{door}/t_{le}= 0, t_{wait}/t_{le}= 1/3, and different shipping classes.

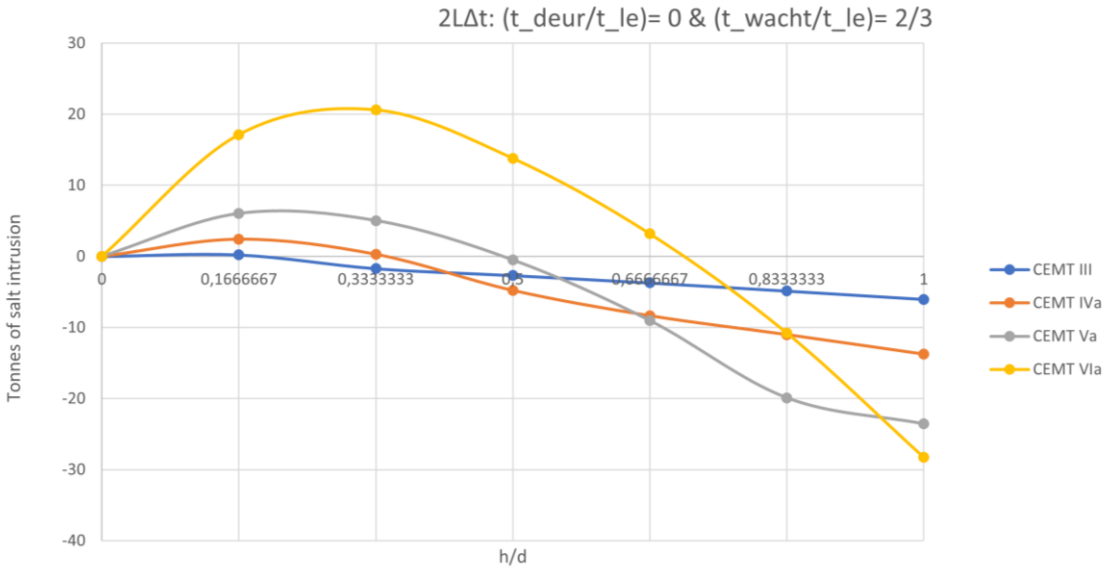

Figure C.8: Simulations with 2LΔt assumptions, t_{door}/t_{le}= 0, t_{wait}/t_{le}= 2/3, and different shipping classes.

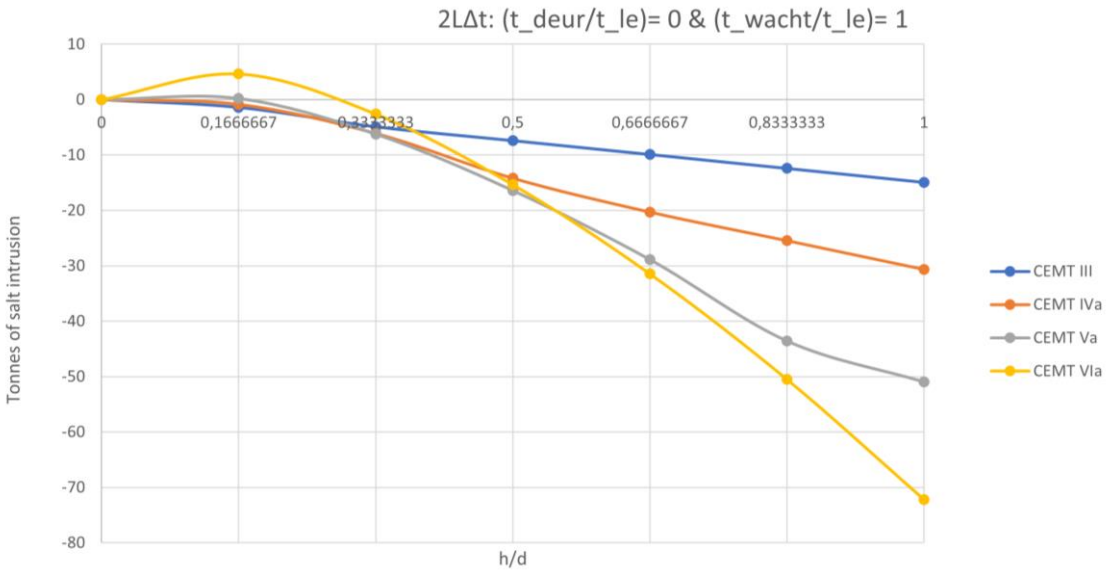

Figure C.9: Simulations with 2LΔt assumptions, t_{door}/t_{le}= 0, t_{wait}/t_{le}= 1, and different shipping classes.

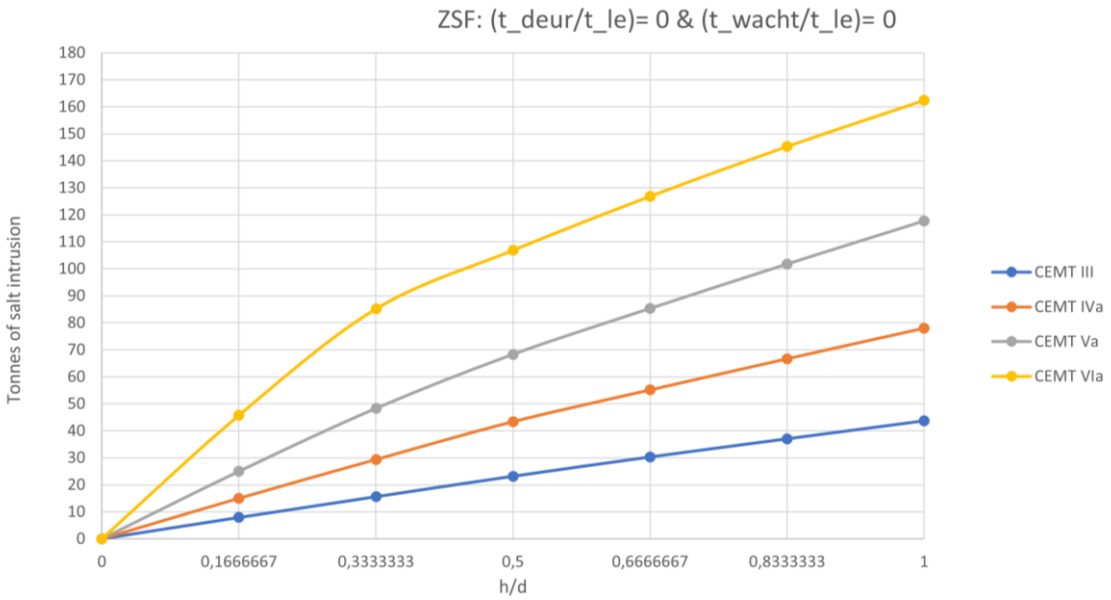

Figure C.10: Simulations with ZSF assumptions, t_{door}/t_{le}= 0, t_{wait}/t_{le}= 0, and different shipping classes.

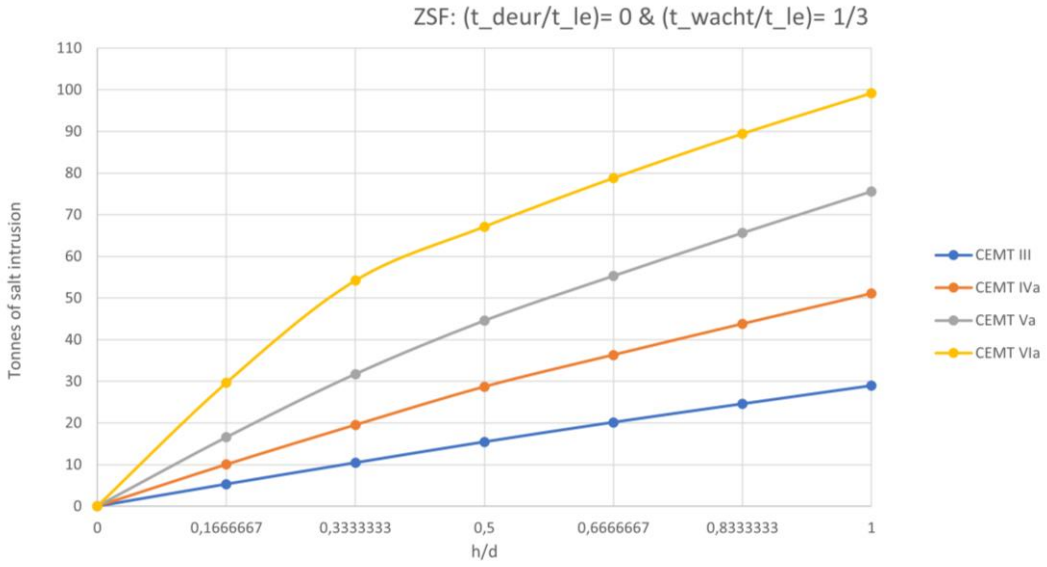

Figure C.11: Simulations with ZSF assumptions, t_{door}/t_{le}= 0, t_{wait}/t_{le}= 1/3, and different shipping classes.

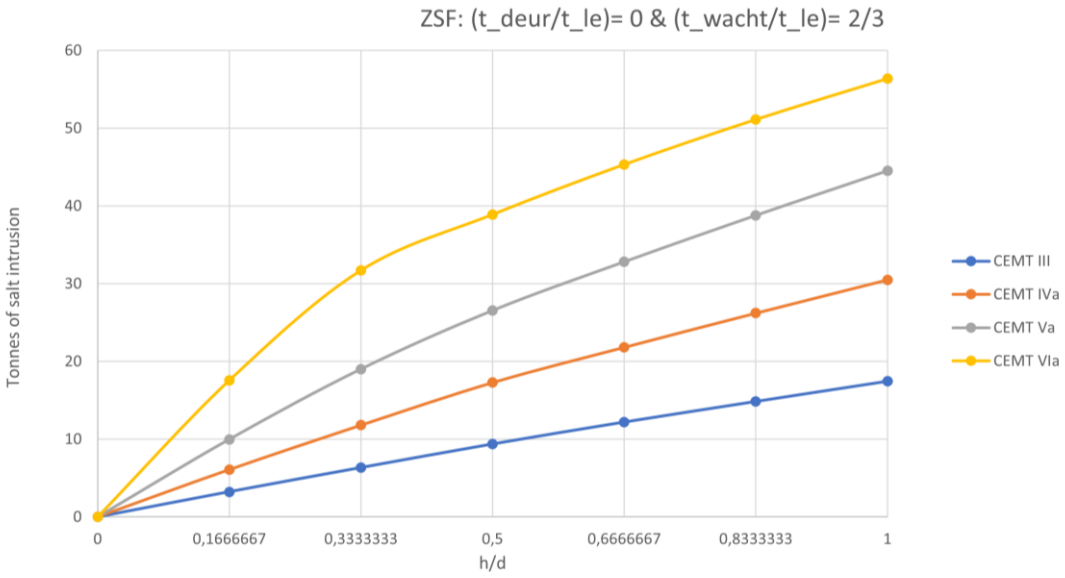

Figure C.12: Simulations with ZSF assumptions, t_{door}/t_{le}= 0, t_{wait}/t_{le}= 2/3, and different shipping classes.

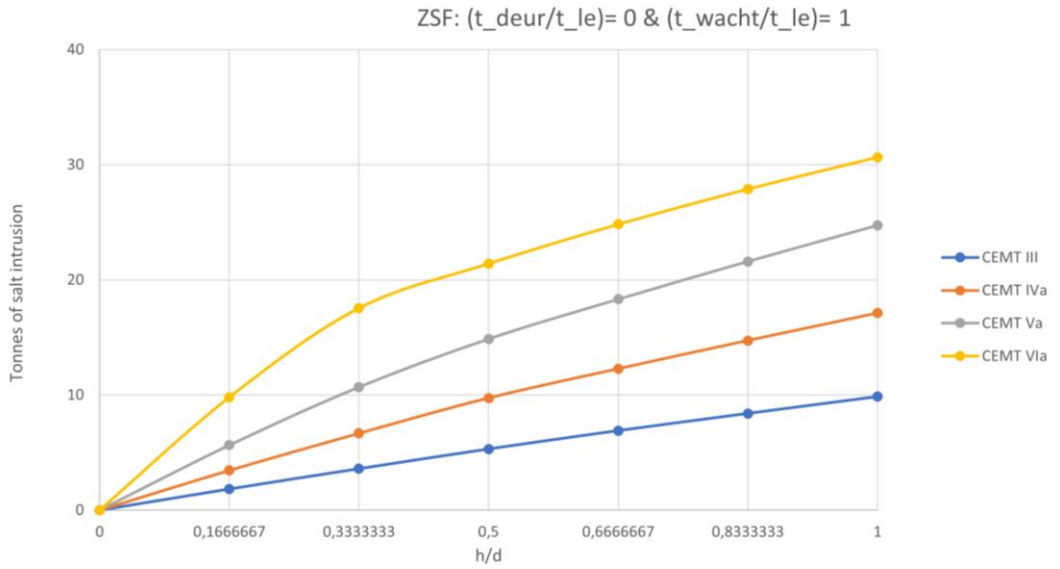

Figure C.13: Simulations with ZSF assumptions, t_{door}/t_{le}= 0, t_{wait}/t_{le}= 1, and different shipping classes.